IN-71
3460

NASA Contractor Report 177565

A Study of Rotor Broadband Noise Mechanisms and Helicopter Tail Rotor Noise

Shau-Tak Rudy Chou

(NASA-CR-177565) A STUDY OF ROTOR BROADBAND NOISE MECHANISMS AND HELICOPTER TAIL ROTOR NOISE (Cornell Univ.) 188 p CSCL 20A
N91-21829
Unclas
G3/71 0003460

CONTRACT NAG2-379
August 1990

NASA
National Aeronautics and
Space Administration

NASA Contractor Report 177565

A Study of Rotor Broadband Noise Mechanisms and Helicopter Tail Rotor Noise

Shau-Tak Rudy Chou
Cornell University, Ithaca, New York

Prepared for
Ames Research Center
CONTRACT NAG2-379
August 1990

National Aeronautics and
Space Administration

Ames Research Center
Moffett Field, California 94035-1000

TABLE OF CONTENTS

LIST OF FIGURES

ACKNOWLEDGEMENTS

I owe a special debt of gratitude to Professor A. R. George, who suggested the thesis topic and served as the chairman of my special committee during the course of this research. His encouragement, guidance, and suggestions will always be remembered and appreciated. Special thanks are also due to Professors F. C. Gouldin and M. C. Leu, who acted as my special committee members.

The financial support from NASA Langley Research Center, Aeroacoustics Branch (Dr. F. Farassat, Technical Monitor) and from NASA Ames Research Center, Full-Scale Aerodynamics Research Division (Dr. C. A. Smith, Technical Monitor) are gratefully acknowledged. I would also like to thank Dr. W. Johnson of NASA Ames Research Center for his helpful discussions and for providing the CAMRAD code to this research.

I would like to thank my friends and colleagues for their valuable friendship, advice, and encouragement. Thanks are also due to Miss Noel Van Ness for proofreading this thesis. Lastly, but certainly not least, very special thanks are given to my mother for her love and continuous encouragement, without which this thesis would never have been completed.

A STUDY OF ROTOR BROADBAND NOISE MECHANISMS AND HELICOPTER TAIL ROTOR NOISE

Shau-Tak Rudy Chou, Ph.D.
Cornell University, 1987

A study is made of the relative problems of rotor broadband noise mechanisms and the helicopter tail rotor noise. The rotor broadband noise mechanisms considered in the present study are (1) lift fluctuation due to turbulence ingestion, (2) boundary layer/trailing edge interaction, (3) tip vortex formation, and (4) turbulent vortex shedding from blunt trailing edge. Predictions are compared to available experimental data and show good agreement. The study shows that inflow turbulence is the most important broadband noise source for typical helicopters' main rotors at low- and mid-frequencies. Trailing edge noise and tip vortex noise are found to be important at high frequencies; they are very sensitive to the rotor blades' angle of attack. Trailing edge thickness noise is also very important; it generates a large spectrum hump, and is very sensitive to any change of the trailing edge thickness.

Due to the size difference, isolated helicopter tail rotor broadband noise is not important compared to the much louder main rotor broadband noise. However, the inflow turbulence noise from a tail rotor can be very significant because it is operating in a highly turbulent environment, ingesting wakes from upstream components of the helicopter. Our study indicates that the main rotor turbulent wake is the most important source of tail rotor broadband noise. Tail rotor harmonic noise due to nonuniform inflow resulting from various upstream disturbances (e.g. main rotor, fuselage, engine exhaust, and main rotor hub) is also investigated. The harmonic noise due to the main rotor mean wake is found to be very important.

Finally, the tail rotor harmonic noise due to ingestion of main rotor tip vortices is studied. The CAMRAD code is used to find the main rotor tip vortex trajectories; then, using the near-normal blade-vortex interaction model of Amiet, the noise radiation is calculated. Tail rotor position is found to be very important as it directly affects the geometry of the interactions. The tail rotor phasing is also found to be important in case of commensurate tail and main rotor RPM's.

Chapter I

INTRODUCTION

> In those days, the world teemed; the people multiplied, the world bellowed like a wild bull, and the great god was aroused by the clamour. Enlil heard the clamour and he said to the gods in council, "The uproar of mankind is intolerable and sleep is no longer possible by reason of the babble." So the gods agreed to exterminate mankind. (From a translation by N. K. Sandars of The Epic of Gilgamesh, a Babylonian story believed to be the forerunner of the flood story in the Bible.)

In recent years, helicopters have been proved to be a convenient and reliable means of transportation. Their ability to land, take off, and maneuver in areas inaccessible to fixed wing airplanes has been successfully used in rescue work and inter-city commuter applications. However, the increasing use of helicopters in both civilian and military applications has raised attention to the noise they generate. In civilian applications, the high noise level has prejudiced the very operation which helicopters are uniquely fitted to perform - inter-city transportation. In military applications, the far-field noise provides unnecessary early warning of the approach of helicopters to their potential enemies. The internal noise problems are also significant, causing helicopters to be unattractive to prospective civilian passengers and, in the military field, internal noise levels often substantially exceed the acceptable limits (Lowson and Ollerhead, 1969).

In this thesis, chapter II will review and derive basic governing equations of aeroacoustics. Chapter III will investigate mechanisms that generate rotor broadband noise; various analyses will be extended or developed and they will be shown to be capable of predicting rotor noise spectra. Chapter IV will study the harmonic and broadband noise from helicopter tail rotors using existing aerodynamic and acoustic analyses. Chapter V will examine the interaction between helicopter tail rotor and main rotor tip vortices and the noise it generates.

The primary noise sources for a typical helicopter are the main and tail rotors, engine(s), and gearbox. According to the origins of these noise sources, they can be divided into those generated aerodynamically (i.e. noise from main and tail rotors) and those generated mechanically (engine and gearbox noise). Cox and Lynn (1962) found that at moderate distance from a typical helicopter, the various noise sources can be listed according to their order of importance:

(1) blade slap (when it occurs)
(2) tail rotor rotational noise
(3) main rotor broadband noise
(4) main rotor rotational noise
(5) gearbox noise
(6) turbine engine noise
(7) other sources

In general, the relative importance of these mechanisms depends upon the particular helicopter design and the operating conditions.

The main rotor impulsive noise (i.e. blade slap) is the most important helicopter noise source when it occurs. However, in the case of modern helicopters, main rotor impulsive noise sometimes is not as significant due to careful design. This often leaves the rotational noise from the tail rotor and the broadband noise from main and tail rotors as the most important noise sources on helicopters. In the present study, we will focus our attention on these particular aerodynamic noise sources.

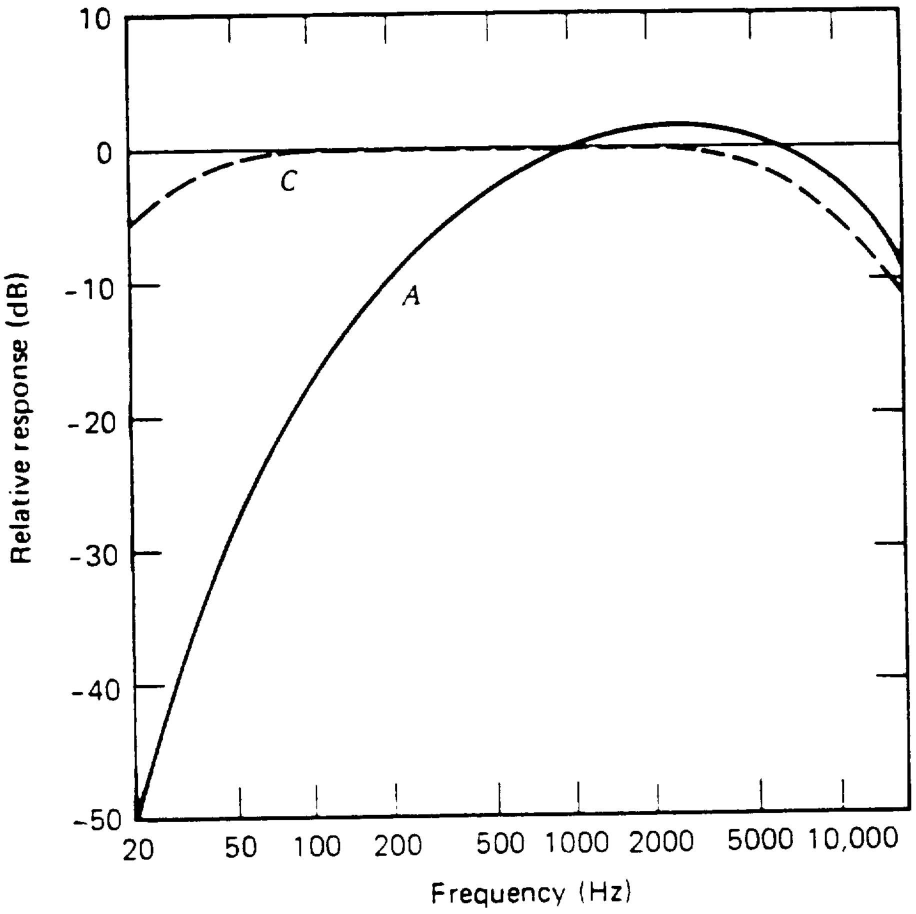

Figure 1.1: Filter Characteristics for A-Weighted Sound Level.

The frequencies of interest in the present study are mainly determined by human annoyance (or detection in some cases). The common measures of annoyance, such as the perceived noise level (PNdB) or A-weighted sound level (dBA), account for the fact that humans find low frequencies, say below a few hundred Hertz, much less annoying. The filter characteristics for A-weighted sound level are shown in Figure 1.1. On the other hand, if long distance propagation is a factor for the rotor in question, then high frequencies can be attenuated significantly by molecular absorption. For example, after propagation over one kilometer, sound waves with frequencies above a few thousand Hertz are attenuated drastically (George, 1978). Thus frequencies in the range from approximately one hundred to several thousand Hertz are of primary interest.

Figure 1.2 shows a typical acoustic time history of a helicopter in flight. Two distinctive signal patterns are apparent: the first is periodic impulses with fundamental frequency originating from the blade passing frequency, and the second is essentially a random background signal. After Fourier analysis, the difference between two types of signals becomes even wider. The periodic impulses generate a line spectrum at the fundamental frequency (i.e. blade passing frequency) and its harmonics; the random signal leads to a continuous but possibly peaked broadband spectrum. A typical helicopter noise spectrum is given in Figure 1.3. Generally speaking, the periodic impulses are more distinct during high speed forward flight and are due to the effects of the blade steady loading, due to volume displacement effects, due to the periodic blade-vortex interactions,

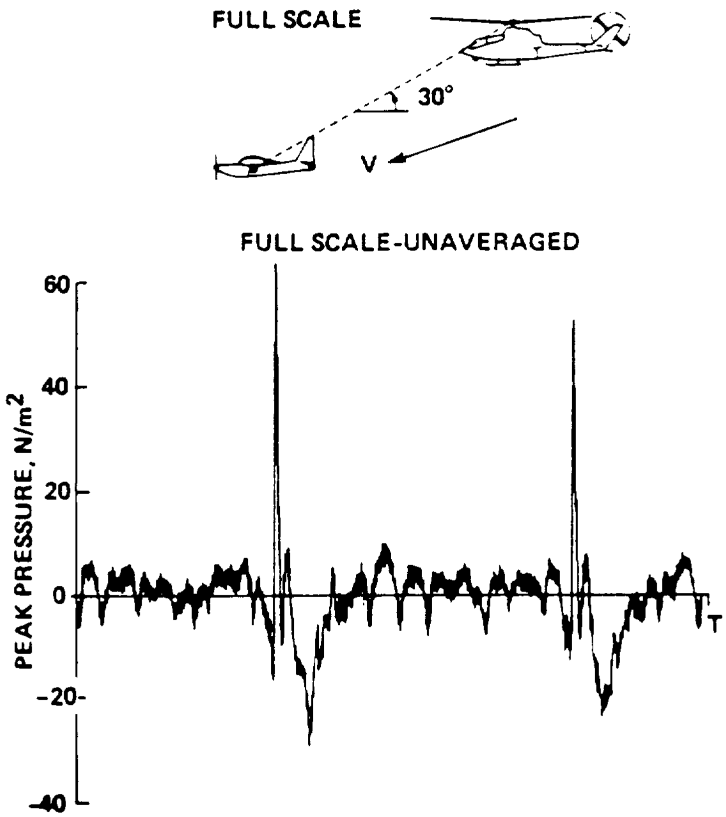

Figure 1.2: Measured Pressure-Time History for a UH-1H in 60 Knot Partial-Power Descent (400 ft/min Rate of Descent), $\phi = -30^{\circ}$, from Schmitz and Yu (1983).

and due to other periodic blade loading variations. On the other hand, the random background signal is generally due to various blade-turbulence interaction effects. They can be the primary noise sources in the absence of extensive impulsive noise, as in the hover case. A series of hover spectra are given in Figure 1.4.

Despite extensive research over the past fifty years, and particularly over the last fifteen years, the relative importances of various rotor aerodynamic noise mechanisms are only now becoming understood. The accuracies of the existing analyses are also hard to

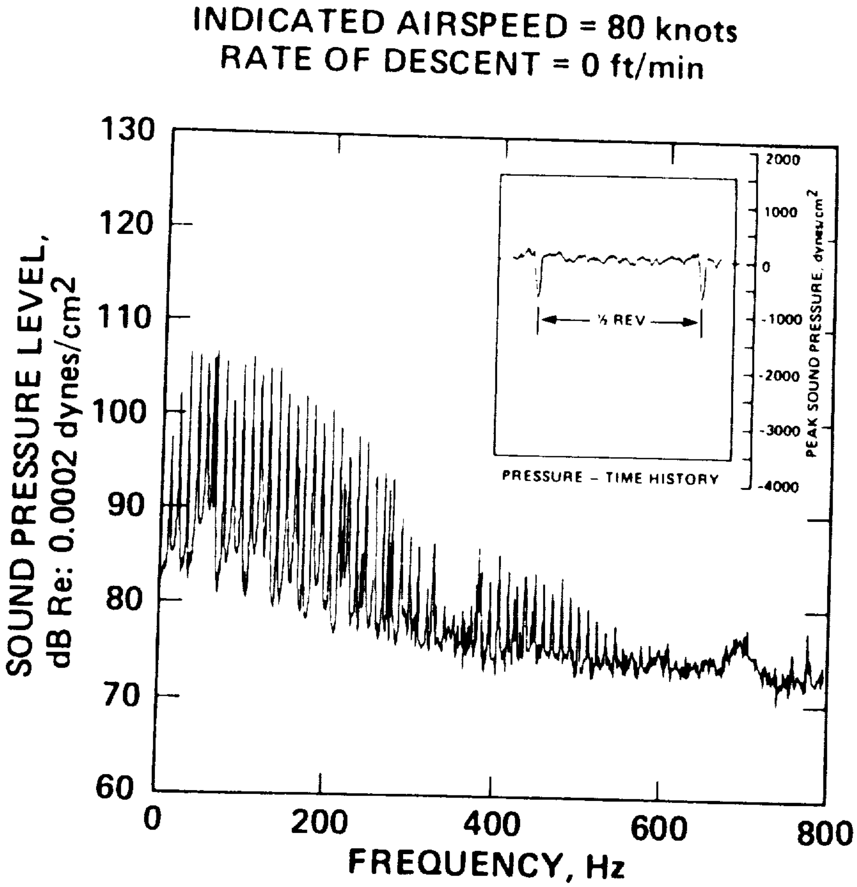

Figure 1.3: In-Plane UH-1H Acoustic Power Spectrum for 80 Knot Level Flight, from Schmitz and Yu (1983).

document. The primary reason for these difficulties is that there are a large number of noise mechanisms on rotors which can be important in different parts of the acoustic spectrum, depending upon the rotors' parameters and their operating environment. The wide variety of source mechanisms is due to various aeroacoustic effects: boundary layers, separated flow, and inflow turbulence; high Mach numbers, including nonlinear effects; blade-vortex interactions; non-uniform inflow; etc. (George, 1978). These mechanisms have been postulated and studied both analytically and experimentally to access their

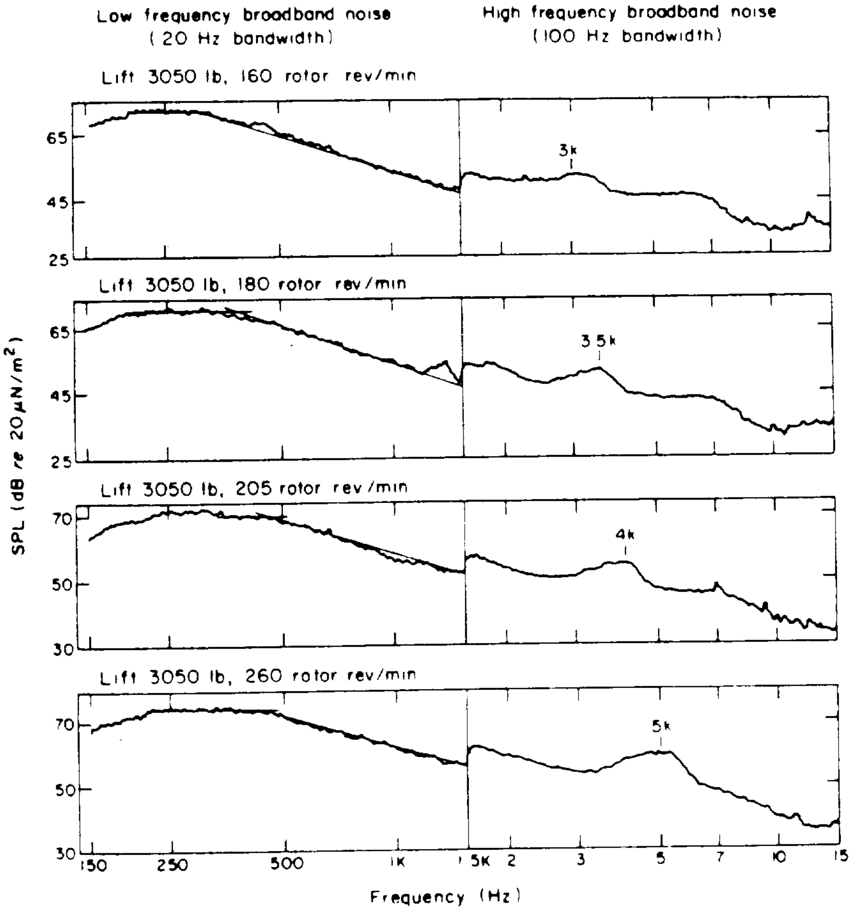

Figure 1.4: Broadband Noise Spectra, Full Scale S-55 Rotor, $\phi = -75^{\circ}$, from Leverton (1973).

possible significance as noise sources. In general, the mechanisms each affect different parts of the acoustic spectrum. Moreover, on craft with either tandem or main and tail rotors, many of these mechanisms can interact with each other and between rotors. Thus, in many cases, it is not clear which mechanisms are dominant in many operating conditions for full scale helicopters, propellers, etc. A brief summary of the various noise generating mechanisms will be given in the remainder of this chapter where emphasis will be put on explaining the physical phenomena rather than on deriving the theory. The mechanisms will be analyzed in the later chapters.

Discrete frequency noise (sometimes called rotational or harmonic noise) is caused by steady or harmonically varying forces, volume displacements, or nonuniform inflows. At low to moderate blade tip Mach number these can be due to the basic blade rotation and forward flight of a helicopter or to the steady inflow variations. These mechanisms have been analyzed by a number of researchers (Gutin, 1936; Deming, 1938; Hubbard, 1953; Lowson, 1969; and Wright, 1969).

The first theoretical model of rotor noise was developed by Gutin (1937) who recognized that steady aerodynamic forces on a propeller blade act as acoustic dipoles. His analysis showed that the first few noise harmonics are related to the steady thrust and drag (torque) forces acting on a propeller blade.

For many years "Gutin noise" formed the sole basis for rotor noise prediction. Since the discrete noise spectrum due to steady loadings decays very rapidly with frequency, the steady loading noise is generally restricted to the first dozen or so harmonics of the blade passing frequency. Thus it is not usually of importance to helicopter main rotors or large wind turbines as these frequencies generally lie in the frequency range below 100 Hertz where human ears are not very sensitive. These low order harmonics are, however, very important to high speed propellers or tail rotors.

Since the rapidly decaying steady loading noise severely underestimates the harmonics at high frequencies, it was felt that sizable unsteady loading fluctuations due to steady but spatially nonuniform inflow to the rotor generate noise at high frequencies. This problem was formulated and solved by Lowson and Ollerhead (1969) and Wright (1969) who analyzed the noise radiation due to azimuthally varying blade loadings which are steady in time. They found that the higher loading harmonics of rotor blades are extremely important to the high frequency discrete frequency noise. In fact, at high frequencies the sound generated by even very small loading harmonics dominates that generated by the steady loading noise analyzed by Gutin.

Impulsive noise (sometimes called blade slap) consists of nearly distinct repeated pulses at blade passing frequency. It is a special type of rotational noise. When an impulsive acoustic time history is Fourier analyzed, the repeated pulses will yield discrete or harmonic spectra, but their particular identity is due to their impulsive time histories and origins. These pulses are caused by particular events at certain blade azimuth angles such as main rotor blade-vortex interactions or high speed noise due to local transonic blade motion toward the observer (say Mach number greater than approximately 0.75). These noise mechanisms have been analyzed by Widnall (1971), Ffowcs Williams and Hawkings (1969a), Farassat (1975, 1980, 1983, 1984), Hanson (1979), Yu and Schmitz (1980), George and Chang (1983c, 1984b), and George and Lyrintzis (1986). Impulsive noise is unquestionably the most important noise source on helicopters or wind turbines when it exists. However, a prime goal of aeroacoustic rotor design or operation is to avoid impulsive noise generation by controlling the blade-vortex interactions and by avoiding high tip Mach number. This often leaves broadband noise as the important controlling noise in many situations where relative tip speeds are low and blade-vortex interactions are not intense.

Broadband noise is characterized by a continuous (although sometimes humped or peaked) spectrum and is caused by disturbances which are not precisely repeated at each blade revolution but are basically random in nature. These random disturbances are generally due to some sort of turbulence/rotor blade interactions. The turbulence can either be that already existing in the surrounding atmosphere or can be generated by the blades' motions. Recent reviews of broadband noise research may be found in the works of George and Chou (1983a, 1984a) and Schlinker and Brooks (1982).

Opinions regarding the origin of broadband noise vary somewhat among investigators. Part of the reason for this variation is that broadband noise actually has several origins, although they are all related to the random loading/surface pressure fluctuations on rotor blade due to interactions with turbulence. Several possible causes have been proposed and investigated. Figures 1.5 and 1.6 give the sketches of the aerodynamic aspects of some of the mechanisms.

One of the sources of the random part of the rotor broadband noise is the fluctuating loading associated with the encounter of the ambient turbulence (Sharland, 1964). When a rotor blade is moving in turbulent flow, the local incidence angle is determined by the resultant of the mean velocity and the instantaneous turbulent velocity. These random fluctuations in incidence angle lead to unsteady loading fluctuations on the rotor blade and subsequently

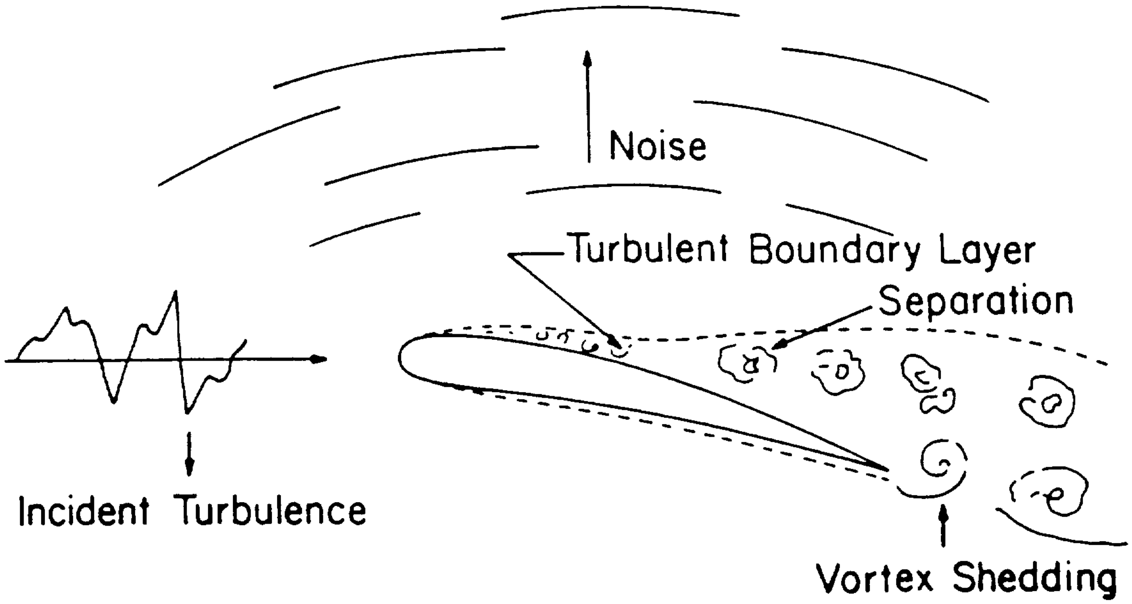

Figure 1.5: Broadband Noise Sources of a Stationary Airfoil.

generate noise. This mechanism is particularly important in the low- to mid-frequency range. The incident turbulence may be that already existing in the atmosphere, or it may be generated by the recirculation wake due to ground effect, or it may be from the turbulent wake of the preceding blades.

Another type of random force fluctuations on surfaces in a moving fluid is the surface pressure field arising from an attached turbulent boundary layer (Sharland, 1964). The problem regarding the sound generation from boundary layer turbulence was solved by Powell (1959). He used the "reflection principle" to show that the major surface

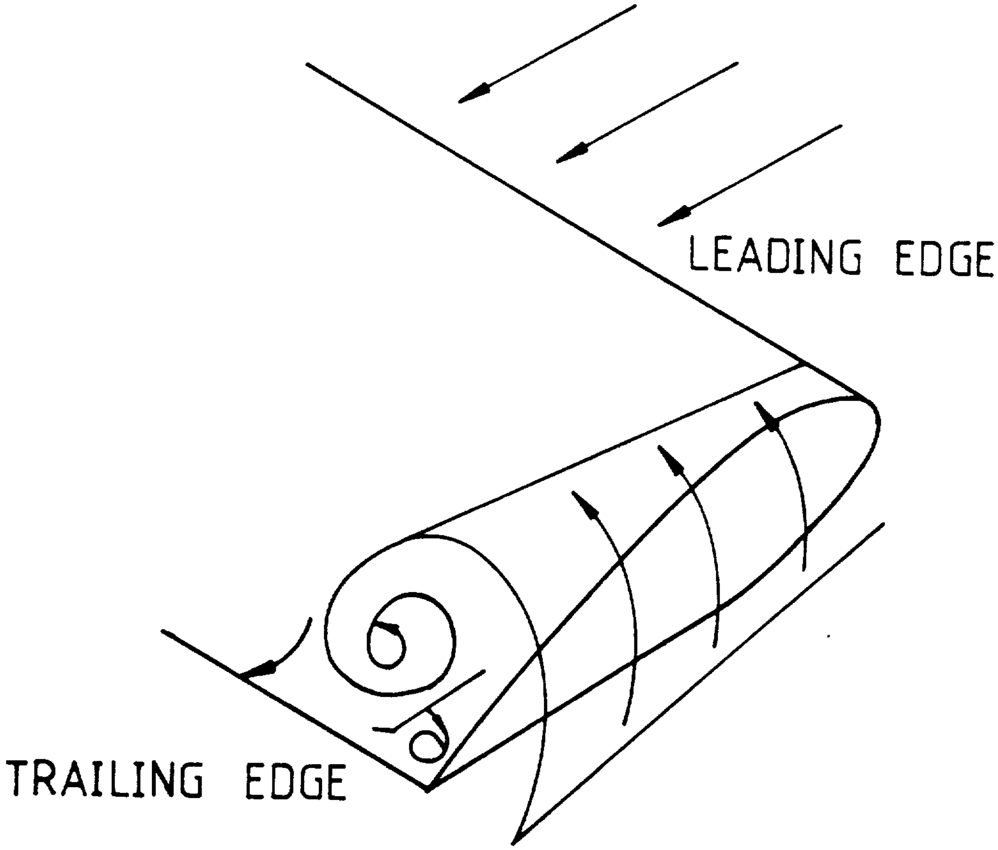

Figure 1.6: Vortex Formation on the Tip of a Rotor Blade.

dipoles vanish on an infinite, flat, and rigid surface. This leaves only the viscous dipoles with their axes lying on the surface remain effective. Since such viscous stresses can only become significant at low Reynolds numbers, direct radiation from the turbulent boundary layer is generally not important. However, Hayden (1972) suggested that, providing the acoustic wavelength is much smaller than the blade chord, pressure fluctuations in the turbulent boundary layer can interact with a sharp trailing edge to produce significant noise radiation.

Force fluctuations can also appear when there is vorticity shed from the rear of a moving body. A classical example of this is the "Karman Vortex Street" occuring behind a circular cylinder in certain Reynolds number ranges. Although the shape of rotor blades is different from that of a circular cylinder, similar pressure fluctuations which are associated with nearly periodic vortex shedding occuring in the laminar boundary layer Reynolds number range. The nearly periodic nature of the force fluctuations gives rise to a continuous but peaked spectrum, this is often identified as "vortex noise" or "high-frequency broadband noise" (Paterson, et al., 1973). However, this phenomenon generally does not exist in full-scale rotors as the flows around the blades are usually turbulent.

The importance of turbulence in blade tip flows was also suggested by several investigators. Lowson's experiments (1972) on low speed axial flow fans indicated that tip shape has a significant influence on the high frequency broadband noise. He suggested that this can be traced to the breakdown of the tip vortex, which induces high intensity turbulent flow over the outer portion of the rotor blades.

A similar mechanism of turbulent vortex shedding from blunt trailing edges has been identified by Brooks and Hodgson (1980). Unlike laminar vortex shedding, the vortices shed from the trailing edges are essentially random, although some correlation exists between the pressure fluctuations and the free stream velocity and the thickness of the trailing edges.

Other sources of broadband noise from rotor blades can be due to turbulence in locally stalled regions (Paterson, et al., 1975). This phenomenon can be associated with either high angle of attack or close encounter with a vortex shed from previous blade. Presently, there is no analytical model available for either the local separation or the noise radiation.

Most of the discussions above are concerned with the noise generated from helicopter main rotors. Despite its smaller size compared to the main rotor, the tail rotor's importance on the overall noise should not be underestimated. It has been known for some time that the tail rotor is an important source of helicopter noise. Although perhaps an exaggeration, Lynn et al. (1970) reported: "For nearly all flight conditions the tail rotor is the predominant noise source for single rotor helicopters." Similarly, Leverton (1977, 1980), Balcerak (1976), Levine (1976), and Pegg and Shidler (1978), in their analytical and experimental studies on tail rotor noise, have all emphasized the importance of tail rotor noise due to interaction with the wakes of main rotor and other upstream objects.

Tail rotor rotational noise is of particular importance since tail rotors are often operated at higher speeds than main rotors. The rotational noise of a typical helicopter tail rotor lies in the 100 to 1,000 Hertz range, a range which is extremely important to audibility and annoyance. Tail rotor broadband noise is also very important due to the highly turbulent inflow which originates from various aerodynamic wake effects.

As mentioned previously, the added difficulty involved in the study of tail rotor noise is the complexity of the inflow. The inflow field of the tail rotor is very difficult to predict, it consists of a number of components: the overall main rotor wake, the main rotor tip vortices, the wakes of fuselage and main rotor hub, and the engine exhaust flow. These components affect both the mean flow and the turbulence properties as seen by the tail rotors. The overall main rotor mean wake can be calculated by several methods but it has a fairly minor influence on the tail rotor noise, because it leads primarily to low order loading noise harmonics. On the other hand, the concentrated main rotor tip vortices are quite localized and will lead to more annoying, higher frequency noise. The trajectories of the main rotor tip vortices are difficult to predict; they follow initially helicoidal paths which are perturbed by: (1) the roll-up of the vortex wake into a horseshoe vortex system; (2) the self-induced instabilities of the vortex trajectories; (3) and the action of the pre-existing atmospheric turbulence. The actual structures of the vortices are also not known except that they are generally turbulent. They can contain axial velocities in their cores which are very important to the unsteady loading fluctuations on the tail rotor blades. Also under certain conditions the main rotor tip vortices are found to be "diffuse" or "burst" (the "vortex breakdown" phenomenon). When this occurs, the vortices become more spread out and turbulent. This strongly affects the characteristics of both the mean and turbulent inflow seen by the tail rotor.

In the present study, we limit our attention to the aerodynamic noise generation from helicopter rotors. In particular, the broadband noise from main and tail rotors, and the harmonic noise from tail rotors due to wakes from main rotor, hub, fuselage, and engine exhaust are studied thoroughly.

Chapter II treats the general problem of aerodynamic noise generation. Various forms of governing equations are derived and their solutions discussed. For the simplified cases, the sound field from moving acoustic point singularities (in both straight-line and circular motion) is discussed. Finally, several approaches for predicting rotor noise are reviewed to conclude this chapter.

Chapter III addresses part of the helicopter noise problem - broadband noise, particularly those from helicopter main rotors. It reviews previous broadband noise analyses and describes the extensions we make in the present study. For inflow turbulence noise, we extend the analysis of George and Kim (1976) to allow the use of von Karman spectrum. For boundary layer/trailing edge noise, the present study extend the analysis of Kim and George (1980) to include the effect of rotor blades' angle of attack. We also extend the analysis of George et al. (1980) for the tip vortex formation noise; a 3-dimensional normalized surface pressure spectrum is obtained. We also study the noise due to turbulent vortex-shedding from blunt trailing edges and develop an analysis to predict it analytically. Calculations based on various analyses of broadband noise mechanisms are compared to each other and to available experiments. The aims of this chapter are to help understand which broadband noise mechanisms are important under which circumstances, to identify a number of satisfactory, existing, and well-documented experimental measurements, and to evaluate the various analytical approaches. It is shown that several satisfactory analytical approaches are available and their limitations are delineated. These analyses can show which mechanisms are important in which cases and are able to predict absolute spectra to within about 5 dB for clean experiments.

Chapter IV describes results from a comparative study of helicopter tail rotor noise. With components including the wakes of the main rotor, the main rotor hub, the main rotor shaft, the fuselage boundary layer, the fuselage separation, and the engine exhaust, tail rotor inflow is very complex and turbulent. This leads to higher than normal noise radiation considering the tail rotor's size. The primary harmonic noise source we focus on in this chapter is the interaction between the tail rotor and the main rotor mean wake. For the broadband noise, the intensities and length scales for turbulence generated by various upstream disturbances are estimated and the resulting noise from a typical tail rotor is calculated and discussed.

In chapter V, we focus on the harmonic noise generated from tail rotor blades chopping the main rotor tip vortices. The analysis of Amiet (1984, 1986a) for near-normal blade-vortex interaction is reviewed. The details of a complicated simulation we devised for the present study are outlined. Results of the noise calculations for full-scale and model-scale UH-1 helicopters are discussed to conclude this chapter.

The summary and conclusions drawn from the present research are given in Chapter VI.

Chapter II

BASIC AEROACOUSTIC FORMULATION

This chapter reviews the basic theory of aerodynamic noise generation. Emphasis is placed on the mathematic modelling of the sound fields generated by given noise sources rather than on the physical modelling of the aerodynamic noise sources, which will be discussed in later chapters. Various forms of the governing equations will be derived and the general solutions will also be discussed. To conclude this chapter, several approaches developed previously to apply the basic acoustic equations to rotor noise prediction are reviewed and discussed.

2.1 CLASSICAL THEORY

The theory of sound received its fair share of attention during the advance of modern science. The fundamentals of acoustic theory had been set down well before the end of nineteenth century (Rayleigh, 1896). These fundamentals were applied to the studies of a number of harmonic phenomena, e.g. tuning forks, organ pipes, and church bells, etc. Basically, the main interests of the classical acoustic theory were the production and propagation of small disturbances in the pressure (or density) caused by stationary sources in an unbounded, stationary medium. Rayleigh's basic theory has been used by a number of researchers through a wide span of time. This not only gives witness to the correctness of the works of Rayleigh but also indicates that acoustics has, in its fundamentals, changed far less since Rayleigh's time than other disciplines in science.

For the basic theory of aerodynamic sound, the main facts that needed to be recalled from the classical acoustic theory are the elementary solutions of the equation of motion, namely, sources (monopoles), and dipoles (Rayleigh, 1896; Morse, 1948). The classical theory of acoustics correctly identified that sound can be generated by the injections of either mass or momentum into the acoustic medium.

For a point monopole (injection of mass), it is the variation of mass outflow from the source that generates sound (in the present study, we generally call source of this type monopoles rather than sources as in classical acoustics). Assume new fluid is introduced at a rate Q(t), we may call its time derivative $\dot{Q}(t)$ the strength of the monopole, since the pressure fluctuation at a distance r away from the monopole can be expressed by

$$p = \tilde{p} - p_0 = \frac{\dot{Q}(t - \frac{r}{c_0})}{4\pi r} \tag{2.1}$$

where p is the pressure perturbation ($\equiv \tilde{p} - p_0$). Notice that p is proportional to the value of $\dot{Q}$ at the retarded time ($\tau \equiv t - r/c_0$), i.e. at the instant when a wave travelling at speed of sound c_0 had to be launched in order to reach the observer at the current time t.

The next simplest elementary solution is a dipole, where sound is generated by the injection of momentum. In other word, the acoustic dipole is equivalent to a concentrated point force, varying in magnitude or direction or both. The strength of a dipole is the force itself. The pressure fluctuation seen by an observer at $\mathbf{x} = (x_1, x_2, x_3)$ relative to the dipole F_i can be expressed by

$$p = -\frac{\partial}{\partial x_i}\left[\frac{F_i(t - \frac{r}{c_0})}{4\pi r}\right] \tag{2.2}$$

where $r = |\mathbf{x}|$. It should be noted that the dipole strength, as a vector, has direction as well as magnitude.

Gutin (1936) was the first to consider flow-generated acoustics in his pioneering study of propeller noise. He applied the results of Lamb (1932) on the acoustic field of a concentrated force (i.e. dipole) to the problem of sound radiation from a stationary propeller. Yet, it was not until Lighthill (1952) introduced the acoustic analogy, then a general theory of modern aeroacoustics began to emerge. Lighthill's acoustic analogy will be derived and discussed in the following section.

2.2 GOVERNING EQUATIONS FOR MODERN AEROACOUSTICS

In this section, we will derive, review and discuss the generalized Lighthill's equation and an extension to it by Ffowcs Williams and Hawkings (1969a).

2.2.1 Generalized Lighthill's Equation

Modern aeroacoustics owes its major development to Lighthill (1952), who first considered turbulent flow as a source of sound. Originally Lighthill's theory was introduced to calculate the sound radiation from a relatively small turbulent flow region embedded in an unbounded homogeneous fluid at rest, where the speed of sound c_0 and the density of the undisturbed fluid ρ_0 are constants. Away from the small region of turbulence, the density fluctuation ρ ($\equiv \tilde{\rho} - \rho_0$) can be considered small and varying isentropically, hence it satisfies the homogeneous wave equation

$$\frac{\partial^2 \rho}{\partial t^2} - c_0^2 \frac{\partial^2 \rho}{\partial x_i^2} = 0 \tag{2.3}$$

The pressure fluctuation p ($\equiv \tilde{p} - p_0$) can be expressed in terms of the density fluctuation ρ according to the isentropic relationship

$$\tilde{p} - p_0 = c_0^2 (\tilde{\rho} - \rho_0) \tag{2.4}$$

Lighthill's analogy can be derived from the equations of mass and momentum conservation, if they are arranged in a form similar to equation (2.3). We start the derivation of the Lighthill's equation by writing down the continuity equation (in Cartesian tensor notation)

$$\frac{\partial \tilde{\rho}}{\partial t} + \frac{\partial}{\partial x_i} (\tilde{\rho} u_i) = Q \tag{2.5}$$

where Q is the rate of introduction of mass per unit volume. The momentum equation can also be written in the same fashion as

$$\frac{\partial}{\partial t} (\tilde{\rho} u_i) + \frac{\partial}{\partial x_i} (\tilde{\rho} u_i u_j) = \frac{\partial \sigma_{ij}}{\partial x_j} + F_i \tag{2.6}$$

where F_i is the external force per unit volume acting on the fluid, and σ_{ij} is the stress tensor given by

$$\sigma_{ij} = - \mathcal{P}\delta_{ij} + \mu \left(\frac{\partial u_i}{\partial x_j} + \frac{\partial u_j}{\partial x_i} - \frac{2}{3} \delta_{ij} \frac{\partial u_k}{\partial x_k} \right)$$

where $\mathcal{P}$ is the hydrostatic pressure (assuming Stokes' hypothesis holds). Eliminating $\tilde{\rho} u_i$ between equations (2.5) and (2.6) gives

$$\frac{\partial^2 \rho}{\partial t^2} = \frac{\partial Q}{\partial t} - \frac{\partial F_i}{\partial x_i} + \frac{\partial^2}{\partial x_i \partial x_j} (\tilde{\rho} u_i u_j - \sigma_{ij}) \qquad (2.7)$$

Substracting $\partial^2(c_0^2 \rho \delta_{ij})/\partial x_i \partial x_j$ from both sides of equation (2.7), Lighthill obtained an inhomogeneous wave equation which is later refered to as the Lighthill's equation (or the Lighthill acoustic analogy):

$$\frac{\partial^2 \rho}{\partial t^2} - c_0^2 \frac{\partial^2 \rho}{\partial x_i^2} = \frac{\partial Q}{\partial t} - \frac{\partial F_i}{\partial x_i} + \frac{\partial^2 T_{ij}}{\partial x_i \partial x_j} \qquad (2.8)$$

where T_{ij} is the Lighthill's stress tensor defined by

$$\begin{aligned} T_{ij} &= \tilde{\rho} u_i u_j - \sigma_{ij} - c_0^2 \rho \delta_{ij} \\ &= \tilde{\rho} u_i u_j + \delta_{ij}(p - c_0^2 \rho) - \mu \left(\frac{\partial u_i}{\partial x_j} + \frac{\partial u_j}{\partial x_i} - \frac{2}{3}(\frac{\partial u_k}{\partial x_k}) \delta_{ij} \right) \qquad (2.9) \end{aligned}$$

The three terms which appear on the right hand side of equation (2.8) are generally recognized as monopole, dipole, and quadrupole, respectively.

From equation (2.9), one can easily see that the quadrupole sources represented by Lighthill's stress tensor T_{ij}, actually consist of three different mechanisms: the first term $\tilde{\rho}u_i u_j$ represents the direct convection of the momentum component $\tilde{\rho}u_i$ by the velocity component u_j, the second term $\delta_{ij}(p - c_0^2 \rho)$ represents the effects of any change in entropy, and the last term simply represents the viscous stress effects (for an ideal fluid, this represents the convection of momentum by the motions of molecules relative to the flow velocity u_i).

In Lighthill's original paper, T_{ij} was approximated by $\rho_0 u_i u_j$ for turbulent flow at small Mach number assuming the density fluctuation ρ is much smaller than ρ_0; under this condition, the flow can be considered to be isentropic (i.e. $p - c_0^2 \rho = 0$), thus the second term in equation (2.9) can be dropped. Also the viscous effects will be small compared to the inertial effects (assuming Re >> 1), hence the third term in equation (2.9) can also be dropped.

In addition, Lighthill assumed that neither mass sources nor external forces are found in the acoustic medium (thus $Q = F_i = 0$). Thus the original Lighthill equation was given by

$$\frac{\partial^2 \rho}{\partial t^2} - c_0^2 \frac{\partial^2 \rho}{\partial x_i^2} = \frac{\partial^2 T_{ij}}{\partial x_i \partial x_j}$$

Clearly, the Lighthill equation (2.8) is an exact equation. No assumption was made during its derivation from the continuity and momentum equations. Also it should be noted that the Lighthill equation applies only to fluid without internal solid boundary. The theory for sound generated aerodynamically with the presence of internal solid boundaries was later developed by Curle (1955) and Ffowcs Williams and Hawkings (1969a), this is the subject we will discuss in the following section.

2.2.2 Theory for Flows with Internal Boundaries

From the previous section, we had shown that the problem of aerodynamic sound can be posed as an acoustic analogy in which the turbulence provides a quadrupole distribution in an ideal acoustic medium at rest. However, Lighthill's general theory did not consider the general effects of any internal solid surface that might be present. The first attempt to extend Lighthill's general theory was done by Curle (1955). Curle considered two effects introduced by the solid boundaries: (1) the reflection and diffraction of sound wave at the solid boundaries, and (2) the pressure dipole distribution on solid boundaries (it is the limiting case of Lighthill's quadrupole distributions). Curle showed that the effect of the solid boundaries upon the sound field is equivalent to a surface dipole distribution, each representing the force that solid surfaces applied to the fluid.

In the hydrodynamic sense, a full representation of any solid surfaces lying within the fluid should consist of distributions of sources and surface forces. Thus, later Lighthill (1962) further suggested that the sound field should be described by surface distributions of monopoles, dipoles, and distributions of quadrupoles in the space exterior to the solid boundaries. In this section, our review will closely follow the study of Ffowcs Williams and Hawkings (1969a).

It is quite clear that the theory of aerodynamic sound is built upon the equations of mass and momentum conservation of a compressible fluid, and results in an inhomogeneous wave equation governing the production and propagation of sound waves. These equations are generally valid only in the region exterior to any closed internal surfaces that may be presented. Such a situation is essentially inhomogeneous in space, in that these equations are valid in the volume outside the surfaces, but are meanless elsewhere. However, the spatial homogeneity can be restored by considering the following problem. First the closed solid surfaces are replaced with their corresponding mathematical surfaces, thus instead of having solid surfaces embedded in the fluid, the fluid is petitioned into several regions. The motion of the fluid on and outside the mathematical surfaces is defined to be completely identical with the real motion, whereas the interior flow can be specified arbitrarily. The interior motion is usually assumed to be very simple, and consequently does not match the exterior flow at the boundaries. Mass and momentum sources then have to be introduced to maintain these discontinuities, and these ultimately act as sound generators.

Consider an unbounded fluid with a moving solid surface embedded. Replacing the moving solid surface by an equivalent mathematical surface

$$f(\mathbf{x},t) = 0 \tag{2.10}$$

$f > 0$ represents the volume exterior to the surface, and $f < 0$ denotes the region enclosed by the surface $f = 0$. Let $\mathbf{v}$ be the velocity of the solid surface f, and $\mathbf{n}$ be the outward normal on surface $f = 0$. Assume that in the region inside $f = 0$ the fluid is at rest (i.e. $u_i = 0$), with density ρ_0 and pressure p_0. These values of density and pressure are those which would be found in the real fluid were it at rest. Also assumed is that the surface is impermeable, i.e. $u_i = v_i$ on the surface $f = 0$. The continuity and momentum equations can then be written as (Ffowcs Williams and Hawkings, 1969a)

$$\frac{\partial \rho}{\partial t} + \frac{\partial}{\partial x_i} (\tilde{\rho} u_i) = \rho_0 \, v_i \, \delta(f) \, \frac{\partial f}{\partial x_i}$$

$$\frac{\partial}{\partial t} (\tilde{\rho} u_i) + \frac{\partial}{\partial x_i} (\tilde{\rho} u_i u_j) = \frac{\partial \sigma_{ij}}{\partial x_j} - \sigma_{ij} \, \delta(f) \, \frac{\partial f}{\partial x_j} \tag{2.11}$$

Similar to what we have done in the previous section, ρu_i is eliminated from the equations. Thus we obtain the Ffowcs Williams and Hawkings' equation

$$\frac{\partial^2 \rho}{\partial t^2} - c_0^2 \frac{\partial^2 \rho}{\partial x_i^2} = \frac{\partial^2 T_{ij}}{\partial x_i \partial x_j} + \frac{\partial}{\partial x_i}\left(\sigma_{ij} \delta(f) \frac{\partial f}{\partial x_j}\right) + \frac{\partial}{\partial t}\left(\rho_0 v_i \delta(f) \frac{\partial f}{\partial x_i}\right) \tag{2.12}$$

It should be noted that the Lighthill's stress tensor T_{ij} is zero for fluid inside surface f.

Equation (2.12) shows that, in general, sound can be regarded as generated by three source distributions. The first is a distribution of quadrupoles of strength T_{ij}, distributed throughout the region exterior to the solid surfaces (Lighthill, 1952). This is supplemented by surface distributions of dipoles of strength $\sigma_{ij}n_j$ (Curle, 1955). If the solid surfaces are moving, the sound field will be further enhanced by a distribution of monopoles of strength $\rho_0 v_i n_i$ to represent the volume displacement effects of moving solid surfaces (Ffowcs Williams and Hawkings, 1969a).

It should be noted that equation (2.12) remains valid even when there are shock discontinuities embedded in the flow field. The shock surfaces can be treated just like solid surfaces by replacing them with the corresponding mathematical surfaces; since the mass and momentum fluxes are continuous across shock, no distribution of monopole or dipole is needed on the shock surface. But the distribution of T_{ij} will now contains discontinuities other than at physical boundaries.

2.3 GENERAL SOLUTION TO THE GOVERNING EQUATIONS

No matter what form of governing equation is chosen, we generally have a nonhomogeneous wave equation to solve. Consider a general expression for such type of partial differential equation

$$\frac{\partial^2 \rho}{\partial t^2} - c_0^2 \frac{\partial^2 \rho}{\partial x_i^2} = g(\mathbf{x},t) \tag{2.13}$$

where $g(\mathbf{x},t)$ represents the forcing terms which are the linear combination of monopoles, dipoles, and quadrupoles. Refer to the right hand side of equation (2.8) for details.

The most straightforward way to solve a nonhomogeneous wave equation is by using the Green's function method. The Green function of wave equation is essentially the solution for a nonhomogeneous wave equation with an unit impulse as its forcing term. Let $\mathbf{y} = (y_1, y_2, y_3)$ be the source coordinates where an impulse of unit strength is applied at the instance when $t = \tau$. The Green's function of wave equation $G(\mathbf{x},t;\mathbf{y},\tau)$ satisfies

$$\frac{\partial^2 G}{\partial t^2} - c_0^2 \frac{\partial^2 G}{\partial x_i^2} = \delta(\mathbf{x}-\mathbf{y}) \cdot \delta(t-\tau) \tag{2.14}$$

G must also satisfy the causality conditions for hyperbolic equations, i.e.

$$G = \frac{\partial G}{\partial t} = 0; \qquad \text{for } t < \tau \tag{2.15}$$

G can be solved by first finding the Laplace transformation of (2.14) with respect to time, solving the resultant equation by use of the properties of spherical symmetry, and then inverting the transformation to find the solution (Carrier and Pearson, 1976)

$$G = \frac{\delta(\tau - t + r/c_0)}{4\pi c_0^2 r} \tag{2.16}$$

where $r = |\mathbf{x}-\mathbf{y}|$. The formal solution of (2.13) can then be expressed in the following integral form

$$\rho = \frac{1}{4\pi c_0^2} \int_V dV \int_{-\infty}^{+\infty} g \cdot \frac{\delta(\tau - t + r/c_0)}{r} \, d\tau \tag{2.17}$$

Equation (2.17) can be integrated by using the property of the Dirac delta function

$$\int_{-\infty}^{+\infty} f(\mathbf{x},t)\, \delta(t-\tau)\, dt = f(\mathbf{x},\tau) \tag{2.18}$$

By first carrying out the integration in (2.17) over time (τ) using (2.18), we can have

$$\rho = \frac{1}{4\pi c_0^2} \int_V \left[\frac{g}{r} \right] dV \tag{2.19}$$

where the square bracket indicates that g and r are evaluated at the retarded time τ ($= t - r/c_0$) for each point in the volumetric integration.

Replacing g in equation (2.19) with the right-hand side of the Ffowcs Williams and Hawkings' equation (2.12), its solution can be found as

$$\begin{aligned} 4\pi c_0^2 \rho = {} & \frac{\partial^2}{\partial x_i \partial x_j} \int_V \left[\frac{T_{ij}}{r|1-M_r|} \right] dV(\eta) + \frac{\partial}{\partial x_i} \int_S \left[\frac{\sigma_{ij} n_j}{r|1-M_r|} \right] dS(\eta) \\ & + \frac{\partial}{\partial t} \int_S \left[\frac{\rho_0 v_n}{r|1-M_r|} \right] dS(\eta) \end{aligned} \tag{2.20}$$

where v_n is the normal component of the velocity of the solid surfaces S, V represents the volume exterior to S, and M_r is the component of M in the radiation direction. Note that the terms in the right-hand side of (2.20) are integrated with respect to the Lagrangian coordinates η which move with the acoustic sources. The second and the third terms on the right-hand side of (2.20) are linear, they are generally well defined and comparably easy to evaluate (surface integrals). However, the proper treatment of the quadrupole term requires integration over a volume that is large enough to enclose all nonlinear effects. The computation will clearly be very lengthy. Fortunately in most low speed cases, quadrupoles are not as efficient sources as monopoles and dipoles, i.e. the quadrupole terms are often negligible.

2.4 SOUND FIELD OF MOVING SINGULARITIES

According to Lighthill (1962), the sound field for a point force in uniform rectilinear motion can be given by

$$\rho = \left[\frac{z_i - y_i}{4\pi c_0^3 r^2 (1-M_r)^2} \frac{\partial F_i}{\partial t} \right] \qquad (2.21)$$

where z_i and y_i are the Cartesian coordinates of observer and source respectively. This equation implies that if the force is constant no sound will be radiated. However, it is generally known that sound can also be generated by the convection of constant forces. The uniform rectilinear motion assumption made in equation (2.21) is sufficiently restrictive to remove some of the terms giving rise to the radiated sound. This effect has been studied by Lowson (1965); in this section our discussion will closely follow his derivation.

2.4.1 Sound Field for a Point Force in Motion

Consider a point force in arbitrary motion. It can be expressed in terms of the product of **F** and a Dirac delta function $\delta(\mathbf{y})$. **F** gives magnitude as well as direction of the point force, and it can be regarded as a function of time only. $\delta = \delta(\mathbf{y})$ gives the position of the moving point force. Since the point force is moving, **y** is also a function of time.

By putting $g = -\partial F_i/\partial x_i$ into equation (2.19), the sound field of a moving point force (dipole) can be written as

$$\rho = -\frac{1}{4\pi c_0^2}\int_V \left[\frac{1}{r}\frac{\partial(F_i\delta)}{\partial x_i}\right] dV \qquad (2.22)$$

The proper evaluation of (2.22) depends critically on the treatment of the square brackets, which requires the evaluation of its contents at the retarded time τ ($= t - r/c_0$).

Let us consider any function $f(\mathbf{x},t)$. The chain Rule shows that

$$\frac{\partial}{\partial x_i}[f] = \left[\frac{\partial f}{\partial x_i} + \frac{(z_i-y_i)}{c_0 r}\frac{\partial f}{\partial t}\right] \qquad (2.23)$$

For a moving singularity, we have

$$\frac{\partial \delta}{\partial t} = -\frac{\partial \delta}{\partial x_i}\frac{\partial y_i}{\partial t} \qquad (2.24)$$

where y_i is the component of $\mathbf{y}$ in the i direction. From (2.23) and (2.24), with some arrangements, we have

$$\left[\frac{\partial \delta}{\partial t} \right] = \left[- \frac{c_0 M_i}{1 - M_r} \right] \frac{\partial}{\partial x_i} [\delta] \tag{2.25}$$

where M_r is the component of the instantaneous convection Mach number in the direction $\mathbf{r}$ toward the observer. M_r can be written as

$$M_r = \frac{(z_i - y_i) M_i}{r}$$

where M_i is the component of the instantaneous convection Mach number in the i direction.

Using (2.23) and (2.25), after some mathematical manipulations, equation (2.22) can be rewritten as

$$\rho = \frac{1}{4\pi c_0^2} \int_V \left\{ [F_i] \frac{\partial}{\partial x_i} \left[\frac{1}{r} \right] + \left[\frac{(z_i - y_i)}{c_o r^2} \frac{\partial F_i}{\partial t} \right] + \frac{\partial}{\partial x_j} \left[\frac{(z_i - y_i) F_i M_j}{r^2 (1 - M_r)} \right] \right\} [\delta] \, dV \tag{2.26}$$

where $[\delta] = \delta(\mathbf{z} - \mathbf{y}(t - r/c_0))$. To evaluate the integral of $[\delta]$, the variable in the integrand is changed from $\mathbf{y}$ to η

$$\eta = \mathbf{z} - \mathbf{y}(t - r/c_0)$$

Thus the integration can be evaluated directly, yielding

$$\rho = \frac{1}{4\pi c_0^2\,[1-M_r]}\left\{ [F_i]\,\frac{\partial}{\partial x_i}\left[\frac{1}{r}\right] + \left[\frac{(z_i-y_i)}{c_0 r^2}\,\frac{\partial F_i}{\partial t}\right] + \frac{\partial}{\partial x_j}\left[\frac{(z_i-y_i)F_iM_j}{r^2(1-M_r)}\right]\right\} \tag{2.27}$$

where all quantities are evaluated on the path of the singularity. Using (2.23) on the last term of (2.27), retaining only the radiative terms, we have

$$\rho = \frac{1}{4\pi c_0^2\,[1-M_r]}\left\{ [F_i]\,\frac{\partial}{\partial x_i}\left[\frac{1}{r}\right] + \left[\frac{(z_i-y_i)}{c_0 r^2}\,\frac{\partial F_i}{\partial t}\right] + \frac{\partial}{\partial x_j}\left[\frac{(z_i-y_i)F_iM_j}{r^2(1-M_r)}\right]\right\} \tag{2.28}$$

Thus, the radiative terms of (2.28) can be given as (Lowson, 1965):

$$\rho = \left[\frac{(z_i-y_i)}{4\pi(1-M_r)^2 c_0^3 r^2}\left\{\frac{\partial F_i}{\partial t} + \frac{F_i}{1-M_r}\,\frac{\partial M_r}{\partial t}\right\}\right] \tag{2.29}$$

where $\partial M_r/\partial t$ is the component of acceleration in the **r** direction.

$$\frac{\partial M_r}{\partial t} = \frac{(z_i-y_i)}{r}\,\frac{\partial M_i}{\partial t}$$

The second term in (2.29) will vanish if the convection velocity is constant, and the result reduces to the same as given by Lighthill, i.e. equation (2.21). It should be noted that if the force is accelerating, the second term will give rise to the sound radiation even when the force is constant. We can also write down the near field term, which can be given as (Lowson, 1965):

$$\rho = \left[\frac{1}{4\pi c_0^2 (1-M_r)^2 r^2} \left\{ \frac{F_i(z_i - y_i)}{r} \frac{(1-M^2)}{(1-M_r)} - F_i M_i \right\} \right] \tag{2.30}$$

Note that the near field solution shows no dependence on the acceleration.

2.4.2 Sound Fields for Moving Monopoles

The classical solution for a monopole with constant convection velocity can be written as (Lighthill, 1962)

$$\rho = \left[\frac{1}{4\pi c_0^2 r (1-M_r)} \frac{\partial Q}{\partial t} \right] \tag{2.31}$$

Just as we have done for the moving dipole, the far field solution for a moving monopole can be written as (Lowson, 1965)

$$\rho = \left[\frac{1}{4\pi c_0^2 (1-M_r)^2 r} \left\{ \frac{\partial Q}{\partial t} + \frac{Q(\partial M_r/\partial t)}{1-M_r} \right\} \right] \tag{2.32}$$

The near field solution can also be found as (Lowson, 1965)

$$\rho = \left[\frac{Q(M_r - M^2)}{4\pi c_0^2 (1-M_r)^3 r^2} \right] \tag{2.33}$$

For a monopole with constant convection velocity, the second term in (2.32) vanishes. However, this is different from the classical result (2.31) by a factor of $(1-M_r)$. To clarify this, we rewrite equation (2.32) as

$$\rho = \left[\frac{\partial Q/\partial t}{4\pi c_0^2(1-M_r)r} + \frac{z_i-y_i}{4\pi c_0^2(1-M_r)^2r^2} \left\{ \frac{\partial QM_i}{\partial t} + \frac{QM_i}{1-M_r}\frac{\partial M_r}{\partial t} \right\} \right] \tag{2.34}$$

We can now see that the sound field of an arbitrarily moving monopole is actually caused by three different mechanisms: (1) pure monopole effect of the rate of introduction of mass, this yields the same result as the classical solution, (2) dipole effect of the convected momentum, and (3) quadrupole effect of acceleration.

2.5 SOUND FIELD OF SINGULARITIES IN CIRCULAR MOTION

The theory of the far field solution for rotating singularities was studied by Ffowcs Williams and Hawkings (1969b). In this section, their results will be reviewed. Unlike the method we discussed in section 2.4, which deals with the solution in time domain, Ffowcs Williams and Hawkings solve the problem in frequency domain.

From the discussions in previous section, the solution of (2.13) can be written in real time form as

$$\rho(\mathbf{x},t) = \frac{1}{4\pi c_0^2 r} \int_V g(\mathbf{y},t-r/c_0)\, d\mathbf{y} \tag{2.35}$$

alternatively it can be written in spectral form as

$$\rho(\mathbf{x},f) = \frac{e^{-2\pi i f r/c_0}}{4\pi c_0^2 r}\, g(-\frac{f}{c_0}\mathbf{r},f) \tag{2.36}$$

where $\mathbf{r}$ is the unit vector in the radiation direction. The solution in spectral form $\rho(\mathbf{x},f)$ is the generalized Fourier transform of $\rho(\mathbf{x},t)$ and can be written as

$$\rho(\mathbf{x},f) = \int_{-\infty}^{+\infty} \rho(\mathbf{x},t)\ e^{-2\pi ift}\ dt$$

$g(\mathbf{k},f)$ is the wave number, frequency spectral component of the source field, it is the four-dimensional Fourier transform of $g(\mathbf{x},t)$

$$g(\mathbf{k},f) = \iint_{-\infty}^{+\infty} g(\mathbf{x},t)\ e^{-2\pi i\mathbf{k}\cdot\mathbf{x}}\ e^{-2\pi ift}\ d\mathbf{x}dt \tag{2.37}$$

In terms of the spectral components of the multipole strength of equation (2.8), this can be written as

$$g(\mathbf{k},f) = S(\mathbf{k},f) + 2\pi ik_iD_i(\mathbf{k},f) - (2\pi)^2k_ik_jT_{ij}(\mathbf{k},f)$$

The particular component of $g(\mathbf{k},f)$ that generates acoustic waves at frequency f, propagating in the direction $\mathbf{r}$, is

$$g(-\frac{f}{c_0}\mathbf{r},f) = S(-\frac{f}{c_0}\mathbf{r},f) - 2\pi i\frac{f}{c_0}r_i\ D_i(-\frac{f}{c_0}\mathbf{r},f)$$
$$- (2\pi)^2\frac{f^2}{c_0^2}r_ir_j\ T_{ij}(-\frac{f}{c_0}\mathbf{r},f) \tag{2.38}$$

where r_i is the component of the unit vector $\mathbf{r}$ in the direction i.

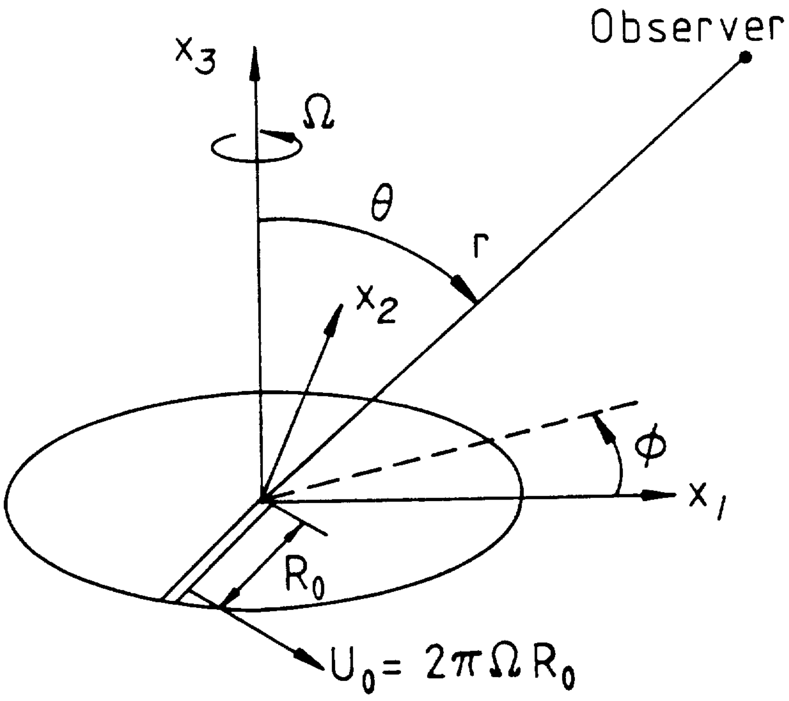

Figure 2.1: Sketch of the Rotating Acoustic Singularities.

Consider concentrated acoustic sources rotating in the $x_3 = 0$ plane at radius R with rotational frequency Ω. The acoustic sources can be written symbolically as

$$g(\mathbf{x},t) = q(\phi,t)\cdot\delta(\mathbf{x}-\mathbf{R})$$

where $q(\phi,t)$ is the time dependent strength of source which occupied angular position ϕ from the x axis at time $t = 0$, and **R** is the position vector of that source at time t. Refer to Figure 2.1 for the geometry. Putting this into equation (2.37), the four-dimensional Fourier transform of the source density becomes

$$g(\mathbf{k},f) = \int_{-\infty}^{+\infty} q(\phi,t)\ e^{-2\pi i\mathbf{k}\cdot\mathbf{R}}\ e^{-2\pi ift}\ dt$$

Again $q(\phi,t)$ may be expressed in terms of its generalized Fourier transform as

$$q(\phi,t) = \int_{-\infty}^{+\infty} q(\phi,\alpha)\ e^{2\pi i\alpha t}\ d\alpha$$

and the radiating component of the source spectrum becomes

$$g(-\frac{f}{c_0}\mathbf{r},f) = \iint_{-\infty}^{+\infty} q(\phi,\alpha)e^{-2\pi it(f-\alpha)}e^{2\pi ifR\sin\theta\cos(2\pi\Omega t+\phi)}dt d\alpha \qquad (2.39)$$

In (2.39), $\mathbf{r}.\mathbf{R}$ is equal to $R\sin\theta\cos(2\pi\Omega t+\phi)$, and θ is the angle at which the wave is propagating relative to the rotor axis x_3 (which is $\theta = 0^o$).

To evaluate equation (2.39), the integration with respect to time is performed first, yielding

$$g(-\frac{f}{c_0}\mathbf{r},f) = \int_{-\infty}^{+\infty}\sum_{n=-\infty}^{n=+\infty} q(\phi,\alpha)\ e^{-in\pi/2}\ e^{i\phi(f-\alpha)/\Omega}\ J_n(-\frac{2\pi fR\sin\theta}{c_0})$$
$$\cdot\ \delta(\frac{f-\alpha}{\Omega} - n)\ \frac{d\alpha}{\Omega}$$
$$= \sum_{n=-\infty}^{n=+\infty} q(\phi,f-n\Omega)\ e^{-in(\pi/2-\phi)}\ J_n(-\frac{2\pi fR\sin\theta}{c_0}) \qquad (2.40)$$

where J_n is the Bessel function of the first kind (subscript n denotes the order of the Bessel function). The infinite summation over the Bessel function is due to the Doppler effect of rotating singularities.

Consider the three different source components: monopoles, dipoles, and quadrupoles. Their spectra can be written as $s(\phi,\alpha)$, $d_i(\phi,\alpha)$, and $t_{ij}(\phi,\alpha)$ respectively. By equations (2.40) and (2.36), the far field general solution for ρ in spectral form can be expressed as

$$\rho(\mathbf{x},f) = \frac{e^{-2\pi i f r/c_0}}{4\pi c_0^2} \sum_{n=-\infty}^{n=+\infty} \left\{ \left[s(\phi,f-n\Omega) - \frac{2\pi i f}{c_0} r_i d_i(\phi,f-n\Omega) - (2\pi)^2 \frac{f^2}{c_0^2} r_i r_j t_{ij}(\phi,f-n\Omega) \right] \cdot e^{-in(\pi/2-\phi)} J_n\left(-\frac{2\pi f R \sin\theta}{c_0}\right) \right\} \qquad (2.41)$$

To make equation (2.41) practically useful, one must find the power spectral density relations to predict statistics of the radiation field in terms of statistics of the sources' strength. This is done by multiplying both sides of equation (2.41) by their conjugates, averaging, and normalizing by a factor common to both sides whose magnitude need not be considered and can be taken as unity. Since our present study is dealing primarily with dipole radiation, we limit the discussion to this particular case. Equation (2.41) reduces to

$$\rho(\mathbf{x},f) = -\frac{e^{-2\pi i f r/c_0}}{2c_0^3 r} \, i f r_i \sum_{n=-\infty}^{n=+\infty} d_i(\phi, f-n\Omega) J_n\left(-\frac{2\pi f R \sin\theta}{c_0}\right) \tag{2.42}$$

This equation will be used to develop a formula relating the power spectral density of a time-dependent dipole strength to the power spectral density of the density fluctuation in the far field radiation field, $\Theta(\mathbf{x},f)$

$$\Theta(\mathbf{x},f) = \frac{f^2}{4c_0^6 r^2} \sum_{n=-\infty}^{n=+\infty} \sum_{m=-\infty}^{m=+\infty} \overline{d_r(\phi, f-n\Omega) d_r(\phi, -f+m\Omega)} \, e^{-i(n-m)(\pi/2-\phi)}$$
$$\cdot J_n\left(-\frac{2\pi f R \sin\theta}{c_0}\right) J_m\left(-\frac{2\pi f R \sin\theta}{c_0}\right) \tag{2.43}$$

Here d_r has been written for the dipole component in the particular radiation direction $r_i d_i$. If we assume that all Fourier elements are uncorrelated unless they are conjugates, and this is so in a stationary field, we can have

$$\begin{aligned} \overline{d_r(\phi,\alpha) d_r(\phi,\beta)} &= D_r(\phi,\alpha); \qquad \text{if } \alpha = -\beta \\ &= 0; \qquad \text{if } \alpha \neq -\beta \end{aligned} \tag{2.44}$$

Furthermore, we can neglect the dependence of D_r on α without losing any generality, since $\Theta(\mathbf{x},f)$ is the averaged quantity over one revolution period. Thus the double sum in equation (2.43) can be reduced to a single summation over n:

$$\Theta(\mathbf{x},f) = \frac{f^2}{4c_0^6 r^2} \sum_{n=-\infty}^{n=+\infty} D_r(f-n\Omega) J_n^2(-\frac{2\pi f R \sin\theta}{c_0}) \qquad (2.45)$$

where D_r is the power spectral density of the dipole strength in the radiation direction.

The spectra for pressure fluctuation $p(\mathbf{x},f)$ can be obtained from the spectral for density fluctuation $\rho(\mathbf{x},f)$ in conjunction with the isentropic relation given in equation (2.4):

$$p(\mathbf{x},f) = c_0^2\ \rho(\mathbf{x},f)$$

Thus, the power spectral density of the pressure fluctuation $<S(\mathbf{x},f)>$ can also be found as

$$<S(\mathbf{x},f)> = \Theta(\mathbf{x},f)\ c_0^4 / \rho_0 c_0$$

$$= \frac{f^2}{4\rho_0 c_0^3 r^2} \sum_{n=-\infty}^{n=+\infty} D_r(f-n\Omega) J_n^2(-\frac{2\pi f R \sin\theta}{c_0}) \qquad (2.46)$$

This is the primary result of this section. It is extremely useful in the prediction of high frequency broadband rotor noise. The only term that remains unknown is D_r, the power spectral density of the dipole strength in the radiation direction. It can be found from the unsteady airfoil response or surface pressure fluctuations due to various blade-turbulence interactions and will be discussed in detail in Chapter III.

2.6 APPROACHES TO THE PREDICTION OF BROADBAND ROTOR NOISE

In analyzing the broadband rotor noise problems, several approaches have been applied so far by previous researchers. They are:

(1) Treat the general case of unsteady forces distributed in space following equation (2.8) with specialization to rotating blades.

(2) Approximate the distributed blade unsteady forces as rotating point forces (i.e. dipoles) using the method we just discussed in section 2.5 (Ffowcs Williams and Hawkings, 1969b).

(3) Find the acoustic radiation from an airfoil segment in linear motion, and then approximate a rotating blade section by a sequence of airfoil straight line motions.

An example of the first type of approach is the analysis of Homicz and George (1974). The second type of approach has been used by George and co-workers on the study of a number of broadband rotor noise mechanisms (George and Kim, 1976; Kim and George, 1980; George, Najjar, and Kim, 1980; Chou and George, 1985). Examples on the third approach are the analyses of Amiet (Amiet, 1976; Schlinker and Amiet, 1981). A brief review of some of the representative analyses is given below.

2.6.1 The General Approach

The analysis of the sound generated by the unsteady forces due to turbulence injection into subsonic unducted rotors began with the quite general analysis of Homicz and George (1974). In their analysis, they found that the far field sound from arbitrarily-varying forces on a plane S (e.g. a rotor disk) can be expressed as

$$<S(\mathbf{x},f)> = \frac{f^2}{4\rho_0 c_0^3} \frac{x_i x_j}{r^4} \int_S <P_{L_i L_j}(\eta, -\frac{f}{c_0}\mathbf{n}_0, f)> dS \qquad (2.47)$$

where $<P_{L_i L_j}(\mathbf{x},\mathbf{k},f)>$ is the generalized averaged three-dimensional cross-spectral density of the forces L_i (e.g. rotor loads) per unit area on the plane S (assume to be $x_3 = 0$), and $\mathbf{n}_0$ is the unit vector along the observer's direction. Refer to Figure 2.2 for the geometry of the analysis.

It should be emphasized that $P_{L_i L_j}$ is the load spectrum as measured in coordinates fixed with respect to the observer, not moving with the blades. Thus blade-to-blade correlation can be treated rigorously.

2.6.2 The Rotating Dipole Approach

The analysis of George and Kim (1977) was developed for the high frequency inflow turbulence noise prediction. Their analysis is based on the second approach mentioned previously.

By using the rotating dipole theory of Ffowcs Williams and Hawkings (1969b), they assumed the fluctuating forces rotate in a circle and their components in the observer's direction are

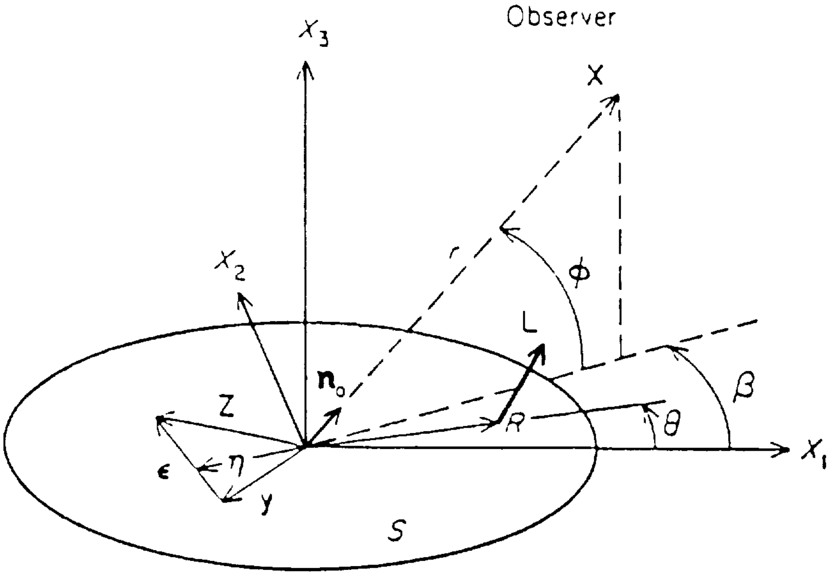

Figure 2.2: Plane Rotor Geometry and Coordinates System.

statistically stationary. This effectively restricts the analysis to forces that are normal to the rotor plane (fluctuating lifts) and thus does not account for the smaller fluctuating drag forces which can be significant for observers in the rotor plane. Also, since only dipole forces are assumed, the analysis does not account for the detailed radiation directivity of the blade elements. The assumptions of circular motion also does not allow accurate treatment of the helicopter forward-flight cases. Fortunately, these restrictions are not very important except for observers within about 15 degrees to the rotor plane or for rotor advance ratios greater than about 0.4.

This approach was later used by George and co-workers on other rotor broadband mechanisms including boundary layer/trailing edge noise (Kim and George, 1980), tip vortex formation noise (George, Najjar, and Kim, 1980), and turbulent vortex shedding noise from blunt trailing edges (Chou and George, 1985). This approach generally gives a reasonably simple equation and can be evaluated quite easily, even at high frequencies.

2.6.3 The Computational Approach

The rotor noise prediction methods of Amiet (Amiet, 1976; Schlinker and Amiet, 1981) can be classified as the third approach we mentioned in the beginning of this section. His analysis is a semi-analytical, semi-computational approach. The circular motion of a rotor section is approximated by a sequence of an airfoil segment's linear motions. The noise spectrum of an operating rotor can thus be obtained by summing and averaging the noise spectrum of a number of individual blade linear motions over one revolution. A schematic sketch of this approach is given in Figure 2.3.

Amiet's method has the advantage of being able to account for the full range of wavelength-to-chord ratios and thus accurately predict the directivity of the sound radiation. In addition, it is very easy to account for the effect of forward flight. The equation is simple and is very efficient to compute.

In this chapter, we have reviewed the analytical tool for calculating the far field noise from given sources. The rest of this thesis will deal with the physical modelling of various rotor aerodynamic noise sources.

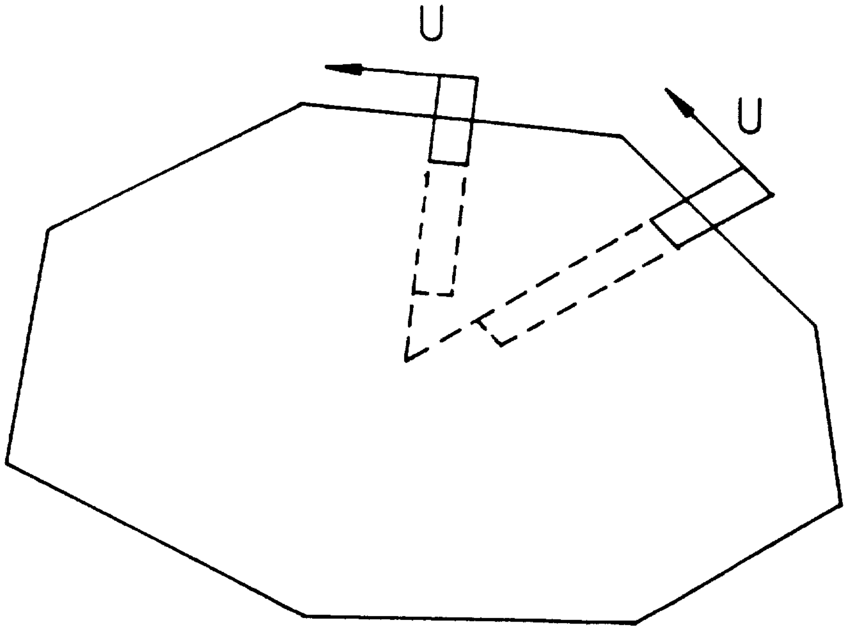

Figure 2.3: Schematic Sketch of Amiet's Method.

Chapter III

ROTOR BROADBAND NOISE MECHANISMS

In the present chapter, various "first-principles" analyses of rotor broadband noise are reviewed and extended; new analyses are developed. Emphasis is placed on the physical modelling of various broadband noise mechanisms. The results are used in association with the basic acoustic analysis given in chapter II to predict the absolute noise spectra. These analyses are not based on empirical correlation equations and do not require the determination of empirical constants for different families of rotors. To determine the relative importance of various mechanisms for different rotor parameters and for different operating conditions, computations are made for many rotors. The results are then compared to each other and to selected experimental data.

3.1 REVIEW OF PREVIOUS RESEARCH

Broadband rotor noise had been studied extensively for almost two decades. Historically, the first broadband noise prediction methods were based on empirical correlation of overall sound pressure level (OASPL), e.g. Widnall (1969). Very early investigators identified broadband noise with some sort of vortex shedding from rotor blades (similar to that from circular cylinders), hence the early name "vortex noise" was used. Actually most broadband noise is due to unsteady loading and surface pressure fluctuations induced by turbulent flows.

Vortex shedding remains as one noise source; it was found that in the atypical case of laminar flow, the laminar boundary layers on blades can indeed shed nearly regular vortices from trailing edges and thus radiate a narrow peaked broadband sound, this was refered to as "high frequency broadband noise" by several investigators (Paterson et al., 1973; Aravamudan et al., 1979a). This mechanism is not important for most full scale rotors since the flows around them are generally turbulent. Possible exceptions are helicopter tail rotors and small axial flow fans. Even in these cases it can be eliminated easily by tripping the boundary layers (Aravamudan et al., 1979a, 1979b).

Reviews of recent broadband rotor noise research can be found in the work by Schlinker and Brooks (1982), or by George and Chou (1983a, 1984a).

3.1.1 Inflow Turbulence Noise

Inflow turbulence noise originates from unsteady loading (particularly lift) fluctuations when rotor blades encounter turbulence. The noise produced can be broadband, or, if turbulent eddies are chopped by more than one blade, the noise can be narrow-bank random, i.e. spectrum humped or peaked around harmonics of the blade passage frequency.

3.1.1.1 Analysis of Homicz and George

The analysis of the sound generated by unsteady loading fluctuations due to turbulence ingestion began with the quite general analysis of Homicz and George (1974). They treated the general case of unsteady forces distributed in space, following the Lighthill equation of aeroacoustics with specialization to rotating blades. Refer to Section 2.6 for the acoustic result of their analysis.

Homicz and George then applied this acoustic result, i.e. equation (2.47), to the unsteady loading (lift) fluctuations on rotating blade. The unsteady loadings were obtained from an approximate compressible aerodynamic analysis for an inflow of homogeneous isotropic turbulence. The noise spectrum they obtained can be written as

$$<S_1(\mathbf{x},f)> = \frac{f^2 M_t^2}{\Omega \rho_0 c_0^3} \frac{16\pi^4 B^2 M_0^4}{1-M_0^2} \left(\frac{bc}{rR_0} \right)^2 \left(\frac{\Omega\Lambda}{V_c} \right)^3 \int_{\xi_{min}}^{+\infty} d\xi \; \xi \sum_{n=n_1}^{n_2} \sum_{l=-\infty}^{+\infty} \cdot E_{int} E_\ell E_{turb} \qquad (3.1)$$

$$\xi_{min} = \frac{\left| \frac{f}{\Omega} - nB \right|}{(V_c/\Lambda\Omega)} , \qquad n_{1,2} = \frac{\frac{f}{\Omega} \mp \left(\frac{V_c}{\Lambda\Omega} \right)\xi}{B}$$

where

$$E_{int} \simeq \sin^2\phi \; J^2_{nB-1}\left(M_0 \frac{f}{\Omega} \cos\phi\right)$$

$$E_\ell = J_1^2\left(\frac{M_0}{M_c} \left(\left(\frac{V_c \xi}{\Lambda\Omega}\right)^2 - \left(\frac{f}{\Omega} - nB\right)^2\right)^{1/2}\right)$$

$$E_{turb} = \frac{\left(\frac{V_c}{\Lambda\Omega}\right)^2 \xi^2 - \left(\frac{f}{\Omega} - nB\right)^2}{(1 + 4\pi^2\xi^2)^3}$$

where M_0, M_c, and M_t are the rotational, convective, and turbulence Mach numbers, and $\xi = k\Lambda$ is the dimensionless turbulence wave number. R_0 represents the effective radius of the equivalent rotating point dipole. The notation nB denotes the nearest blade passing harmonics to f/Ω.

It should be noted that while equation (3.1) was derived for inflow turbulence defined by Dryden spectrum, other homogeneous and isotropic spectra can also be handled, since the integration over ξ must be done numerically in any event. (In such cases, E_{turb} will have to be modified.)

To account for the effect of compressibility in the unsteady aerodynamic analysis, Homicz and George found that an additional multiplicative factor should be added to the integrand in equation (3.1), which is

$$E_{aero} = \frac{J_0^2\left(\frac{M_0^2 \bar{k}_t}{1-M_0^2}\right) + J_1^2\left(\frac{M_0^2 \bar{k}_t}{1-M_0^2}\right)}{1 + \frac{2\pi}{1-M_0^2}\bar{k}_t} \qquad (3.2)$$

where

$$\bar{k}_t = \left(\bar{k}_c^2 + \bar{k}_s^2\right)^{1/2}$$

and $\bar{k}_c$ and $\bar{k}_s$ are the averaged reduced aerodynamic frequencies along the chord and the span directions over one blade revolution.

Equation (3.1) was derived assuming uniform spanwise source strength. This is obviously not the case if the turbulent wavelength is smaller than the blade span. In order to account for this effect, Homicz and George (1974) suggested that another multiplicative factor should be added to the integrand in equation (3.1):

$$E_{span} = (1 + \bar{k}_c b/\pi c)^{-1} \tag{3.3}$$

It should be pointed out that the analysis of Homicz and George uses coordinates fixed with respect to space rather than to the rotor blade. This allows rigorous treatments of the blade-to-blade correlation. Such correlation explains the humped or peaked nature of the low frequency part of the spectrum as being due to the large scale components of the turbulence inflow. These large scale components give nearly periodic (i.e. modulated) disturbances as they are swept through the rotor plane; this leads to a nearly periodic but finite bandwidth sound. The most important parameter affecting the shape and magnitude of the acoustic spectrum is shown to be the ratio of the time taken by the rotor to complete one revolution ($1/\Omega$) to the time needed to convect one integral length scale of turbulence through the rotor disk (Λ/V_c).

This analysis is not well suited for high frequencies, where the complexity of combining equations (3.1), (3.2), and (3.3) requires prohibitly large CPU times for the calculations. Thus, high frequency analyses were developed later by George and Kim (1976) and by Amiet (1976).

3.1.1.2 High Frequency Analysis of George and Kim

In order to predict the high frequency noise efficiently, George and Kim (1976) treated the same problem in a different fashion. They approximated the distributed blade forces as rotating concentrated forces (dipoles), and used the result of Ffowcs Williams and Hawkings (1969a) to get the noise radiation. The result of their analysis can be written as

$$<S_1(\mathbf{x},f)> = \frac{Bf^2}{4\rho_0 c_0^3 r^2} \sum_{n=-\infty}^{n=\infty} \sin^2\phi \; \Phi_{\ell\ell}(|f-n\Omega|) \; J_n^2(M_0 \frac{f}{\Omega} \cos\phi) \tag{3.4}$$

where

$$\Phi_{\ell\ell}(f) = \frac{24\pi^5\Lambda^4 w^2 \rho_0^2 Q^2 b^2 c^2}{(U+fb)\;(1-M_0^2)} \int_0^\infty dk_2 \frac{x^2\left\{J_0^2\left(\frac{M_0^2\pi c}{1-M_0^2}\,x\right)+J_1^2\left(\frac{M_0^2\pi c}{1-M_0^2}\,x\right)\right\}}{\left(1+\frac{2\pi^2 c}{1-M_0^2}\,x\right)\left(1+4\pi^2\Lambda^2x^2\right)^{5/2}}$$

$$x^2 = \frac{f^2}{U^2} + k_2^2$$

$$Q = \rho_0 \, U^2 \,/\, 2$$

It should be noted that ϕ is the observer elevation angle measured from the rotor plane, as shown in Figure 2.2. Equation (3.4) completely neglects any effect on blade-to-blade correlation, and is only valid at high frequencies. This analysis also assumes that the force components in the observer's direction are statistically stationary. This effectively restricts the analysis to the forces normal to the rotor plane (i.e. lift) and thus does not allow accounting for detailed radiation directivity nor for the much smaller torque forces which can be significant for observers near the plane of rotation. The assumption of circular motion also does not allow accurate treatment of forward-flight helicopter cases. However, these are not important restrictions except for within about 15° of the rotor plane, or for advance ratios greater than about 0.4 (George and Chou, 1983a, 1984a).

This formulation can be evaluated quite efficiently since the integration inside the summation is evaluated semi-analytically. Details on the numerical approach are given by George and Kim (1976).

The original analysis was specially derived for turbulence defined by a Dryden spectrum. Other homogeneous, isotropic turbulence models can also be handled by modifying $\Phi_{\ell\ell}$, the power spectral density of the lift on rotor blade. But, the equation is then more difficult to evaluate compared to the original equation, which can be evaluated quite efficiently.

3.1.1.3 Analytical-Computational Analysis of Amiet

The analysis of Amiet (1976) is based on a different concept. Initially, Amiet analyzed the radiation of sound from a stationary, non-rotating airfoil in a uniform mean flow containing turbulence (Amiet, 1975; Paterson and Amiet, 1977). Amiet's analysis can handle a full range of wavelength-to-chord ratios, and can accurately predict the directivity of the sound radiation (which becomes multi-lobed at intermediate wavelength-to-chord ratios). Figure 3.1 shows several representative directivity patterns (Kaji, 1975). The result is given by Amiet as

$$<S_1(\mathbf{x},f)> = \left(\frac{\pi f z \rho_0 c}{c_0 r^2} \right)^2 \frac{Ub}{4} \int_{-\infty}^{+\infty} \frac{2\sin^2\left[\frac{b}{2}(k_y + \frac{\omega b}{c_0 \sigma}) \right]}{\left(k_y + \frac{\omega y}{c_0 \sigma} \right)^2 \pi b} \, |\mathcal{L}(x,K_x,k_y)| \cdot \Phi_{ww}(K_x,k_y)\, dk_y \tag{3.5}$$

where

$$\omega = 2\pi f$$

$$K_x = -\,\omega/U$$

$$\mathcal{L}(x,k_x,k_y) = \int_{-c/2}^{c/2} g(x_0,k_x,k_y)\; e^{-i\omega x_0 (M - x/\sigma)/c_0 \beta^2}\, dx_0$$

Refer to Amiet's original paper (1975) for details of this analysis.

Later, Amiet used this result to synthesize the average noise radiation from the rotating blade by numerically summing and averaging

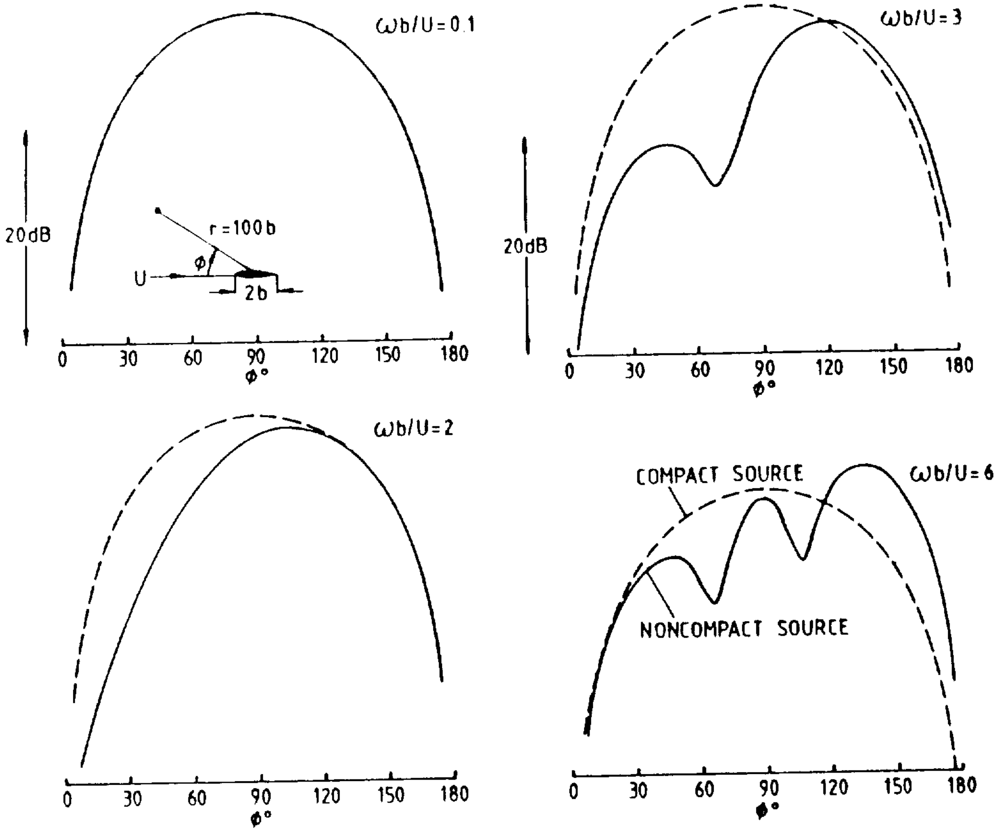

Figure 3.1: Comparison of Directivity Patterns of Radiated Sound Predicted by Compact and Non-Compact Sources, $M = 0.5$, from Kaji (1975).

the radiation from a sequence of blade linear motions which approximate the circular (or epicycloidal) motion of a rotating blade. Refer to Figure 2.3 for sketch of Amiet's approach.

The analysis of Amiet includes both low- and high-frequency response functions in addition to source non-compactness and compressibility effects. Amiet's method has the advantage of being able to treat forward-flight easily and of being based on a more exact model of sound radiation directivity. However, when one sums and averages the multi-lobed radiation pattern over one revolution of the rotor blades, the pattern is smoothed out to a pattern which, except when the observer is very close to the rotor plane, is quite close to the results of the approximation of George and Kim (1976).

3.1.2 In-Plane Broadband Noise Due to Turbulence

The analyses described in the previous section considered lift fluctuations due to turbulence ingestion as the primary source. They tend to under-predict the noise perceived by an observer in the plane of the rotor, where the smaller drag dipoles and other in-plane sources become dominant.

Consider an in-plane fluctuating force D (e.g. drag). According to elementary acoustics, the sound field can be written as

$$p(\mathbf{x},t) = \frac{1}{4\pi}\frac{\partial}{\partial x_\beta}\int\left[\frac{D_\beta}{r(1-M_r)}\right]d\Sigma \qquad (3.6)$$

where $\beta = 1,2$ are the two in-plane directions and Σ is the mean blade planform. Unfortunately, it is very difficult to obtain the correct distribution for the high frequency drag force component, even if the viscous effects are neglected. This distribution for the high frequency drag force component depends directly upon the full pressure distribution over the blade surface. The finite-thickness and the three-dimensional effects must be retained in calculating such detailed pressure distribution. In other word, simple aerodynamic response theory will not give the information we need for evaluating the in-plane broadband noise due to fluctuating drag dipoles.

Consider a thin airfoil embedded in turbulent flow. In order to satisfy the unsteady boundary condition (including velocity perturbations due to turbulence) at the airfoil surface, an additional monopole distribution should be added. Hawkings (1978) showed that for a thin symmetric airfoil in incompressible flow, the sound generated due to the in-plane components of the velocity perturbation w_β can be given as

$$p(\mathbf{x},t) = \frac{1}{4\pi} \frac{\partial^2}{\partial t \partial x_\beta} \int \left[\frac{\rho_0 h w_\beta}{r(1-M_r)} \right] d\Sigma \tag{3.7}$$

where β is again confined to the two in-plane directions. This mechanism is refered to as "unsteady thickness noise", and it has been shown to be a major in-plane rotor broadband noise source (Glegg, 1986). Note that this is the direct analog of thickness noise with the blade speed U replaced by the unsteady gust velocity w_β. The main feature of this equation, however, is that it essentially represents an in-plane quadrupole field (because of the double derivative outside the integral).

Unsteady thickness noise is different from the noise generated by fluctuating drag dipoles. However, a simple dimensional analysis shows that unsteady thickness noise can be significantly higher than drag noise at high frequencies. A drag dipole typically has a local source strength of the order of $0.1\rho Uw$ (U is the typical blade speed), whereas the quadrupole source is of order of $0.1\rho cw$ (c is the blade's chord). However, this has to be multiplied by the frequency f, because of the additional time derivative outside the integral.

Hence, the ratio of the unsteady thickness noise to the drag noise is of the order of fc/U. Clearly at high frequencies, the unsteady thickness noise will be much more important.

Hawkings' unsteady thickness noise analysis can be applied to the rotor broadband noise problem with an approach similar to Amiet's inflow turbulence noise analysis (1976). The sound field from an airfoil in linear motion must first be determined if this approach is to be used.

Consider a symmetric airfoil whose surface is defined by

$$y = \tau_c \left[b_0\left(\frac{x}{c}\right)^{1/2} + a_1\left(\frac{x}{c}\right) + a_2\left(\frac{x}{c}\right)^2 + a_3\left(\frac{x}{c}\right)^3 + a_4\left(\frac{x}{c}\right)^4 \right]$$

Then the unsteady thickness noise can be given as (Glegg, 1986)

$$<S_1(\mathbf{x},f)> = \left(\frac{f}{2rc_0} \right)^2 \rho_0^2 \ c^2 \ b \ U \ \pi^2 \left(\frac{4w^2}{9\pi k_e^2} \left(\frac{k_e U}{\omega} \right)^{8/3} \right)$$

$$\cdot \left\{ |\chi_3|^2 \left(\frac{x_3}{r}\right)^2 + |\chi_1|^2 \left(\left(\frac{x_2}{r}\right)^2 \left[(1-M_r)^2 + \frac{3}{8} \right] + \frac{3}{8}\left(\frac{x_1}{r}\right)^2 \right) \right\} \qquad (3.8)$$

where

$$\chi_\beta = \frac{-i\omega}{U} \ 2\tau_c \left(\frac{b_0\pi^{1/2}}{2(-iK)^{3/2}} + \frac{a_1}{(-iK)^2} + \frac{4a_2}{(-iK)^3} + \frac{18a_3}{(-iK)^4} + \frac{96a_4}{(-iK)^5} \right)$$

$$|\chi_3|^2 = 1/2\pi\tilde{\omega}; \qquad \text{if } \lambda > c/4(1-M_r)$$

$$1/\pi^2\tilde{\omega}^2; \qquad \text{if } \lambda < c/4(1-M_r)$$

$$K = (k_1 - \omega x_1/c_0 r)c = \omega c/U$$

$$\tilde{\omega} = k_1 c/2 = \omega c(1-M_r)/2U$$

This analysis was derived with inflow turbulence defined by Karman spectrum. To find the noise due to this source, the sound spectrum is summed and averaged over one blade revolution.

3.1.3 Boundary Layer/Trailing Edge Noise

Noise can also be produced by the self-generated turbulence in a blade's boundary layer passing its trailing edge. This phenomenon was recognized as far back as 1959 (Powell, 1959). Various investigators looked at very simplified models for this noise, but these early models were not complete and were useful only as bases for empirical correlations. Fink (1978), for example, used such a correlation to predict the on-axis noise of a rotor due to boundary layer/trailing edge interaction. Complete "first-principles" analyses of rotor trailing edge noise were developed more recently by Kim and George (1980) and by Schlinker and Amiet (1981).

The analytical problem of sound radiating from the effect of turbulence being convected past a non-rotating blade's trailing edge has been studied intensively since about 1970. A variety of model problems were studied (see the review of Howe, 1978), but these studies primarily resulted in scaling laws which require empirical constants be determined. There remained a number of questions regarding the details of the modelling and the effects of the Kutta condition. Alternatively, Amiet developed a method which is based on solving the problem of a statistically stationary pressure field being convected past a trailing edge (Amiet, 1976, 1978). Amiet's analysis requires that only the surface pressure spectrum in the boundary layers be determined experimentally. Amiet's analysis has been compared to the experimental findings of Brooks (1981) and found to be consistent.

3.1.3.1 Analysis of Kim and George

In 1980, Kim and George constructed an analysis of boundary layer noise from rotors by using the blade forces from Amiet's aerodynamic model in the same manner as they did earlier for the inflow turbulence noise. Thus, their analysis is again restricted to angles not too close to the rotor plane and to the low advance ratios which are found in helicopter forward flight. Again this is a high-frequency analysis, and it neglects blade-to-blade correlation. Their final result can be written as

$$<S_1(\mathbf{x},f)> = \frac{Bf^2 b^2 U_c^2 \sin^2\phi}{2\pi\rho_0 c_0^3 r^2} \sum_{n=-\infty}^{n=\infty} \frac{F_g(|f-n\Omega|) S_{pp}(|f-n\Omega|)}{(1+\frac{b}{\ell_2(|f-n\Omega|)})(f-n\Omega)^2}$$

$$\cdot\ J_n^2(M_0 \frac{f}{\Omega} \cos\phi) \qquad (3.9)$$

where

$$F_g = F^2 + G^2$$

$$F = \left(\frac{\mu+M\mu+K_1}{\mu+M\mu}\right)^{1/2} [(c_1+s_1)\cos 2K_1+(c_1-s_1)\sin 2K_1)]+1-(c_2+s_2)$$

$$G = \left(\frac{\mu+M\mu+K_1}{\mu+M\mu}\right)^{1/2} [(c_1-s_1)\cos 2K_1-(c_1+s_1)\sin 2K_1)]-(c_2-s_2)$$

$$c_1 - is_1 = E^*(2\mu(1+M)$$

$$c_2 - is_2 = E^*(2(\mu+\mu M+K_1))$$

$$K_1 = \omega c/2U_c$$

$$\mu = MK/\beta^2$$

$$\ell_2(f) \simeq 2.1U_c/2\pi f$$

and the surface pressure spectrum S_{pp} can be given as (assuming flat plate boundary layer)

$$S_{pp}(f) = Q^2 \frac{\delta^*}{U} \frac{2 \times 10^{-5}}{(1 + \tilde{\omega} + 0.217\tilde{\omega}^2 + 0.00562\tilde{\omega}^4)} \quad , \; 0.1 < \tilde{\omega} < 10$$

$$\tilde{\omega} = 2\pi f\delta^*/U$$

$$\delta^* = 0.047 \; c \; Re^{-1/5}$$

3.1.3.2 Analysis of Schlinker and Amiet

Similar to his treatment to the inflow turbulence noise, Amiet first analyzed the sound field of turbulence past an airfoil's trailing edge (Amiet, 1976, 1978). He found that the sound field due to self-generated turbulence past the trailing edge of an airfoil in linear motion can be written as

$$\langle S_1(\mathbf{x},f)\rangle = \left(\frac{k_x Mcz}{4\pi\sigma^2} \right)^2 \frac{b}{4\pi} \left| \mathcal{L}(x,k_x,\lambda,k_y) \right|^2 \ell_2(f) \; S_{pp}(f) \qquad (3.10)$$

where S_{pp} and ℓ_2 are defined in the previous section. Refer to Amiet's paper (1976) for details of this analysis.

Schlinker and Amiet (1981) used the same numerical summing and averaging method that Amiet used for the inflow turbulence noise (1976) to treat the rotor trailing edge noise problem. Again, the simple rotating dipole method of Kim and George (1980) gives essentially the same results as Amiet's method except within about 15°

of the rotor plane, where additional source terms should be included in both methods.

3.1.4 Tip-Vortex Formation Noise

Another source of broadband noise on airfoils or rotors is that due to tip vortex formation. Similar to the boundary layer/trailing edge noise discussed in the previous section, it is generated due to surface pressure fluctuations beneath a highly turbulent tip vortex. Kendall (1978), Ahtye et al. (1979), and Fink and Bailey (1980) experimentally observed localized noise sources at wing and flap tips. Changes in noise from variations in rotor tip shape were experimentally observed some time ago by Lowson et al. (1972), although these effects may have been due to blade loading changes. George et al. (1980) identified this effect with the turbulence in the vortex formation and local separation region over the blade tip interacting with the trailing edge.

The model starts with the experimental observations of separation on the suction side of blade or rotor tips due to the boundary layer being swept around the tip by the pressure gradient. This separated vortex flow is similar to the flow over the top surfaces of a sharp-edged delta wing in subsonic flow.

Figures 3.2, 3.3, and 1.6 show the sketches of delta wing and wing/rotor tip vortex flows. It is generally known that these leading edge vortices are quite turbulent. Large fluctuating pressures have been measured on the surfaces of delta wings underneath these vortices. George et al. (1980, 1983b) used the pressure fluctuation

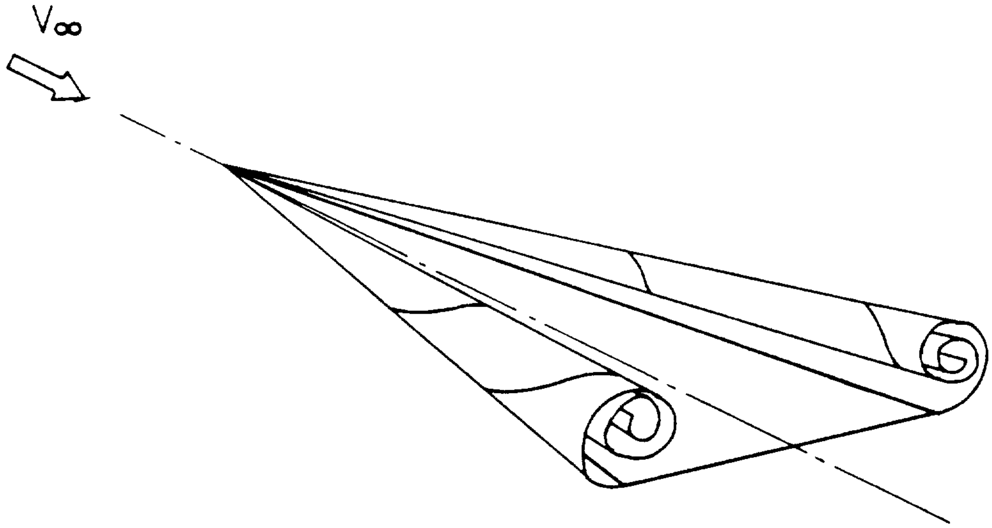

Figure 3.2: Vortex Formation on a Lifting Delta Wing.

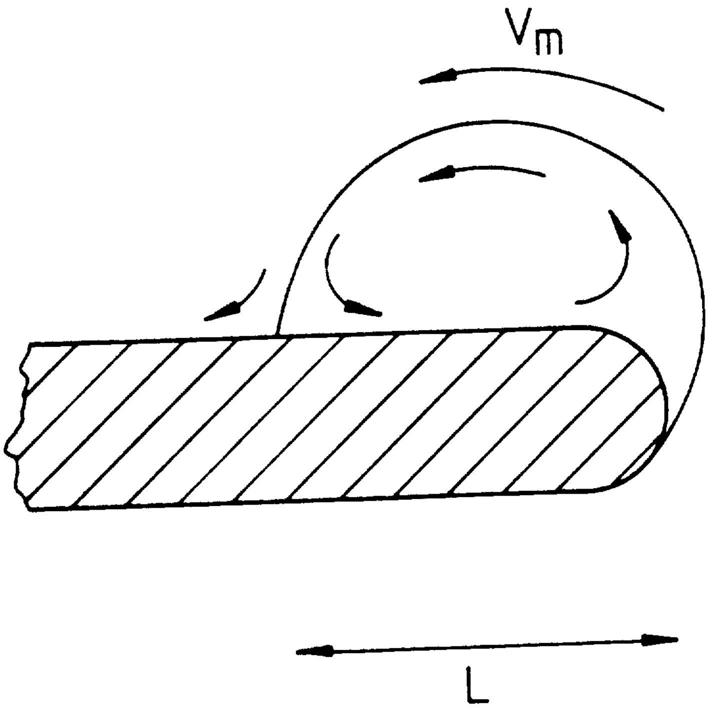

Figure 3.3: Sketch of 2-Dimensional Tip Flow Model.

data from 2-dimensional flows, and data on the geometry and velocities associated with wing and rotor tip flows to estimate the separated turbulent pressure spectrum being convected past the trailing edge.

This surface pressure information was used to predict the resulting radiated sound in a manner similar to George and Kim's treatment of inflow turbulence and boundary layer trailing edge noise. This tip vortex noise is shown to increase with blade loading, as had been experimentally observed in many cases. The original analysis gives the far field sound spectrum as

$$<S_1(\mathbf{x},f)> = \frac{Bf^2L^2U_c^2\sin^2\phi}{8\pi\rho_0 c_0^3 r^2} \sum_{n=-\infty}^{n=\infty} \frac{F_g(|f-n\Omega|)S_{pp}(|f-n\Omega|)}{\left(1+\frac{b}{\ell_2(|f-n\Omega|)}\right)(f-n\Omega)^2} \cdot J_n^2\left(M_0 \frac{f}{\Omega}\cos\phi\right) \qquad (3.11)$$

where

$$S_{pp}(f) = (0.5\rho_0 V_m^2)^2 \, L \, S_1(\tilde{\omega}) \; / \; V_m$$

$$\tilde{\omega} = fL/V_m$$

V_m is the maximum circumferential velocity in the vortex core, L is the size of the tip vortex separation region. $S_1(\tilde{\omega})$ is the normalized spectrum for the fluctuating surface pressure, which can be approximated by

$$
\begin{array}{ll}
S_1(\tilde{\omega}) = 0; & \text{for } \tilde{\omega} < 0.1375 \\
\qquad 5.9703\times10^{-3}\tilde{\omega}-3.5673\times10^{-4}; & \text{for } 0.1375 < \tilde{\omega} < 0.387 \\
\qquad 3.144\times10^{-3}\sin(3.2388\tilde{\omega}-0.5506); & \text{for } 0.3872 < \tilde{\omega} < 0.793 \\
\qquad 1/(93.035+557.09\tilde{\omega}); & \text{for } 0.7935 < \tilde{\omega} < 1.060 \\
\qquad 1/(-258.896+1964.19\tilde{\omega}-2416.78\tilde{\omega}^2+1288.94\tilde{\omega}^3-100.862\tilde{\omega}^4); & \\
 & \text{for } 1.0605 < \tilde{\omega}
\end{array}
$$

Note that equation (3.11) is essentially the same formulation as the trailing edge noise analysis of Kim and George (1980); the only differences being the surface pressure spectrum used and a slightly different coefficient. (Also this mechanism occurs only at the tip region of a rotor blade).

3.2 INFLOW TURBULENCE NOISE

It can be seen from Section 3.1 that the accuracies of the predictions of inflow turbulence noise depend upon how the inflow turbulence is described. To describe the inflow turbulence properly, one has to specify the turbulent intensity, the length scale, and the spectral shape.

There are several equations available for describing turbulent spectra, e.g. Dryden spectrum, von Karman spectrum, and "mild knee" spectrum, etc. As pointed out by Houbolt (1973), nonhomogeneity can also change the spectral shape. Consider the time history shown in Figure 3.4. If the signals in two periods (a and b) were analyzed separately, spectral curves a and b would result, each of which would be represented well by the von Karman spectrum. Analysis of the combined record, however, leads to the composite spectrum shown. This composite spectrum exhibits a "mild knee" variation, as contrasted to the sharper distinct knee of the Karman spectrum.

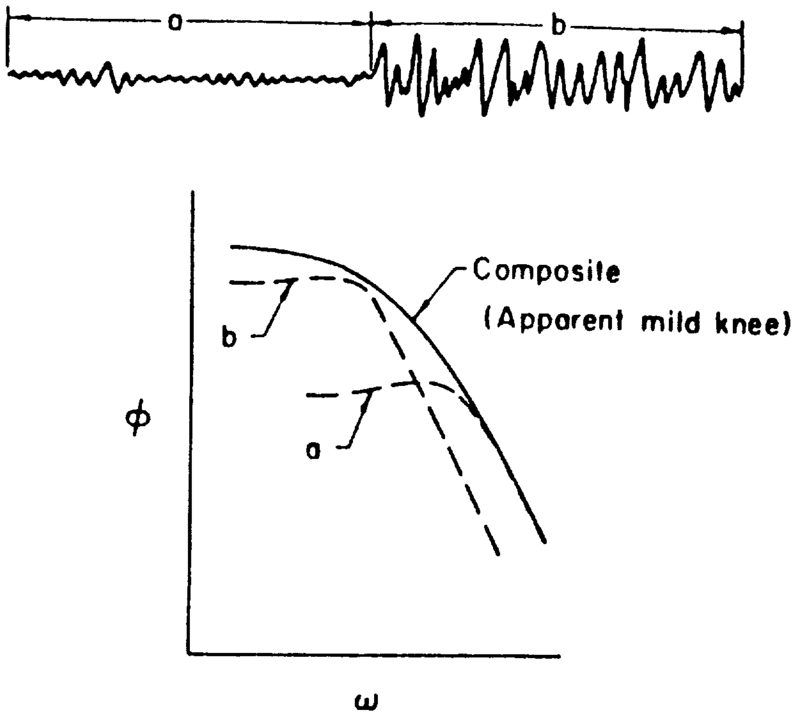

Figure 3.4: Effect of Non-Homogeneity on Turbulent Spectral Shape, from Houbolt (1973).

Also consider the data shown in Figure 3.5. To fit the same data, the von Karman spectrum yields a length scale of 700 ft, while the mild knee expression indicates a scale of 2100 ft. When one applies the two different spectra to the inflow turbulence noise calculation, the results can be quite different.

In the present study, we will limit out discussion to the Dryden spectrum and the von Karman spectrum only.

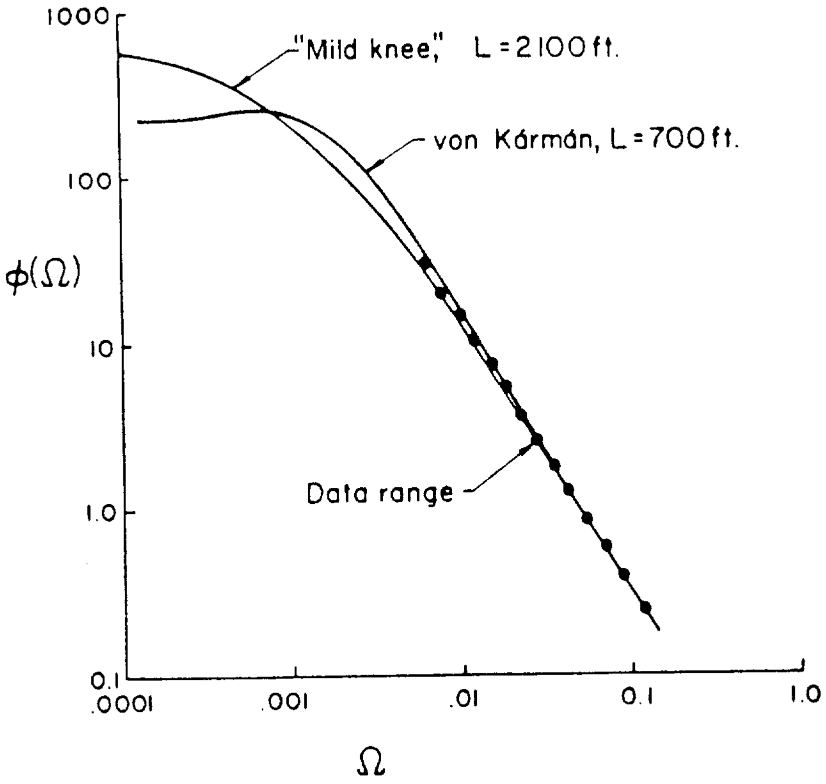

Figure 3.5: Influence of Spectral Equations on Deduced Λ Values, from Houbolt (1973).

3.2.1 Dryden Spectrum and Karman Spectrum

The Dryden spectrum has been used by George and co-workers in inflow turbulence noise calculation (Homicz and George, 1974; George and Kim, 1976). The spectrum can be written as

$$\Phi_{ww}(k) = 64\,\pi^3\,w^2\,\Lambda^5\,\frac{k_1^2 + k_2^2}{(1 + 4\pi^2\Lambda^2k^2)^3} \qquad (3.12)$$

where Λ is the turbulence length scale in m, and w is the turbulent intensity in m/sec. Although it is fairly accurate at low frequencies, the Dryden spectrum is not a very good model for high frequencies.

The Karman spectrum has been used by Amiet in his inflow turbulence analysis (1976). This model represents a more realistic energy distribution at high frequencies. With some rearrangements, the von Karman spectrum can be written in a form similar to the Dryden spectrum, i.e. equation (3.12):

$$\Phi_{ww}(k) = \frac{55}{36\pi^4}\left[\frac{\Gamma(1/3)}{\Gamma(5/6)}\right]^4 w^2\Lambda^5 \frac{k_1^2 + k_2^2}{\left\{1 + \left[\frac{\Gamma(1/3)}{\Gamma(5/6)\sqrt{\pi}}\right]^2\Lambda^2k^2\right\}^{17/6}} \qquad (3.13)$$

or, one can plug in the numerical values for Gamma functions and get

$$\Phi_{ww}(k) = 0.4976\ w^2\ \Lambda^5 \frac{k_1^2 + k_2^2}{(1 + 1.7929\Lambda^2k^2)^{17/6}}$$

Figure 3.6 shows a comparison of the two spectra. At high frequency, i.e. $k >> 1$, the Dryden spectrum has a k^{-4} behavior, but the von Karman spectrum decays with a slower rate ($k^{-11/3}$). At low frequencies, i.e. $k << 1$, although both spectra have the same k^2 slope, their absolute values are quite different.

As will be shown later in this chapter, for full scale helicopter rotors and wind turbines, the Karman spectrum yields better comparisons between the experiments and the predictions than the Dryden spectrum. On the other hand, for small scale tests, namely those tests involving model rotor testing in wind tunnels, calculations made with the Dryden spectrum are more accurate than those using the Karman spectrum. More attention has to be devoted to

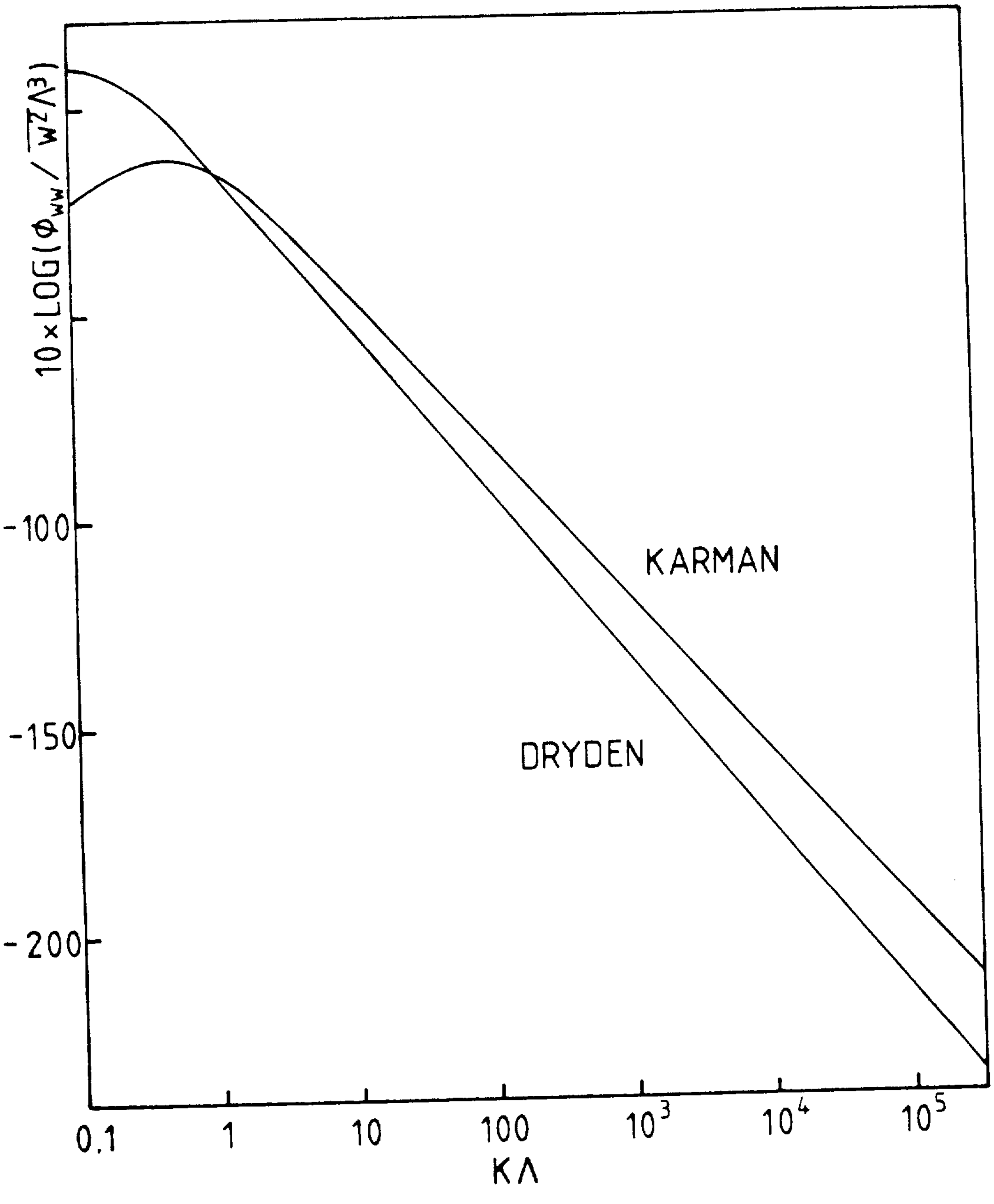

Figure 3.6: Comparison of von Karman Spectrum and Dryden Spectrum.

turbulence spectral modeling equations to clear up the uncertainty of which model should be used.

When turbulence is drawn to the rotor disk, severe distortion can occur to the ingesting flow. Amiet has studied the change of turbulent spectrum due to the mean flow contraction using a rapid distortion theory (Simonich et al., 1986a, 1986b; Amiet et al., 1986b). The mean flow contraction produces a nonisotropic turbulence field at the rotor disk. For hover and low speed vertical ascent, the inflow distortion results in an increased noise of 10 dB at low frequencies, where the acoustic spectrum is governed by the peak-and-valley structure, and an increase of 5 dB in high frequency broadband noise. However, at high speed forward flight, the mean flow distortion does not exist, thus the resulting noise will not change relative to the noise calculated using an inflow of homogeneous isotropic turbulence (Amiet, 1986b).

3.2.2 Numerical Techniques Associated with Karman Spectrum

In order to implement the Karman spectrum in the method of George and Kim, several modifications had to be made to the analysis. Following the same procedure as George and Kim's original analysis (1976), the far field sound can be found to be

$$<S_1(\mathbf{x},f)> = 0.7859 \frac{B f^2 \rho Q^2 b^2 c^2 w^2 \Lambda^4 \sin^2\phi}{c_0^3 r^2 \ (1-M^2)} \sum_{n=-\infty}^{n=+\infty} J_n^2(M \frac{f}{\Omega} \cos\phi)$$

$$\cdot \frac{1}{U + \omega_0 b} \int_0^\infty dk_2 \frac{k_t^2 \ (J_0^2(\psi k_t) + J_1^2(\psi k_t))}{\left(1 + \frac{2\pi^2 c}{1-M^2} k_t\right)\left(1 + 1.7929\Lambda^2 k_t^2\right)^{7/3}} \qquad (3.14)$$

where

$$\psi = \frac{M_0^2 \pi c}{1-M_0^2}$$

$$k_t^2 = (\omega_0/U)^2 + k_2^2$$

$$\omega_0 = |f-n\Omega|$$

To evaluate equation (3.14), one has to handle an infinite summation of an integral function. As shown by George and Kim (1976), the infinite summation can indeed be trimmed to a finite number of terms. Thus our major task is to find an efficient way to evaluate the integral in equation (3.14).

Rewrite the integral in equation (3.14) as

$$\int_0^\infty dx \frac{\theta^2 \ (J_0^2(\psi\theta) + J_1^2(\psi\theta))}{\left(1 + \frac{2\pi^2 c}{1-M_0^2}\theta\right)\left(1 + 1.7929\Lambda^2\theta^2\right)^{7/3}}$$

where

$x \equiv k_2$

$P \equiv \dfrac{f - n\Omega}{U}$

$\theta^2 \equiv x^2 + P^2$

The above equation can be approximated by:

$$\int_0^A \Pi \, dx + \frac{(1 - M_0^2)^2}{380.392 \, M_0^2 c^2 A^{14/3}} \int_A^\infty \frac{dx}{(x^2 + P^2)^{7/3}}$$

where A is a constant above which the asymptotic expressions are accurate to within a given limit, and Π represents the original integrand.

Since the finite integral from 0 to A can be handle easily, we will focus our attention on the second integral (from A to infinity). This integral can be done by first finding the integration from 0 to infinitity and then subtracting the integral of the same integrand from 0 to A. The integration from 0 to infinity can be found analytically, which is

$$\int_0^\infty \frac{dx}{(x^2 + P^2)^{7/3}} = \frac{15 \, \pi \, \Gamma(2/3)}{(2P)^{11/3} \Gamma(1/3) \, \Gamma(1/3)} \approx 0.7 \, P^{-11/3}$$

Thus the original integral can be found by evaluating the following equation:

$$\int_0^A \Pi \, dx + \frac{(1 - M_0^2)^2}{380.392 \, M_0^2 c^2 A^{14/3}} \left(0.7P^{-11/3} - \int_0^A \frac{dx}{(x^2 + P^2)^{7/3}} \right) \qquad (3.15)$$

3.2.3 Effects of Length Scale and Spectrum on Noise

The difference between the two turbulent spectral equations is quite apparent as shown in Figure 3.6. Although the Doppler shifts make it more complicated, one can roughly identify a given frequency radiation with the inverse time required for a blade to pass through a turbulence component of length 1/k, where k is the wavenumber. Thus, for frequencies on the order of 10 kHz, at a tip speed of 100 m/sec, one is interested in turbulence component wavenumbers of order 100 m^{-1}. For a full scale helicopter, the typical turbulent integral scale is of order 100 m, then the peak of the spectrum is at wavenumber k of order 0.01 m^{-1}. This implies that the high frequencies come from wave numbers 10^4 higher than the inverse integral scale. Refering to Figure 3.6, we see that the difference between the two atmospheric turbulence models can be of order of 10 dB at these wavenumbers.

From another perspective, Figure 3.7 shows comparisons between von Karman and Dryden inflow turbulence noise calculations for a full scale UH-1 helicopter main rotor for both 0.1 m and 67.0 m integral scales. It is apparent that for small integral scales and low frequencies the inflow turbulence noise results for different turbulent models are in close agreement, but the difference becomes marked at high frequencies.

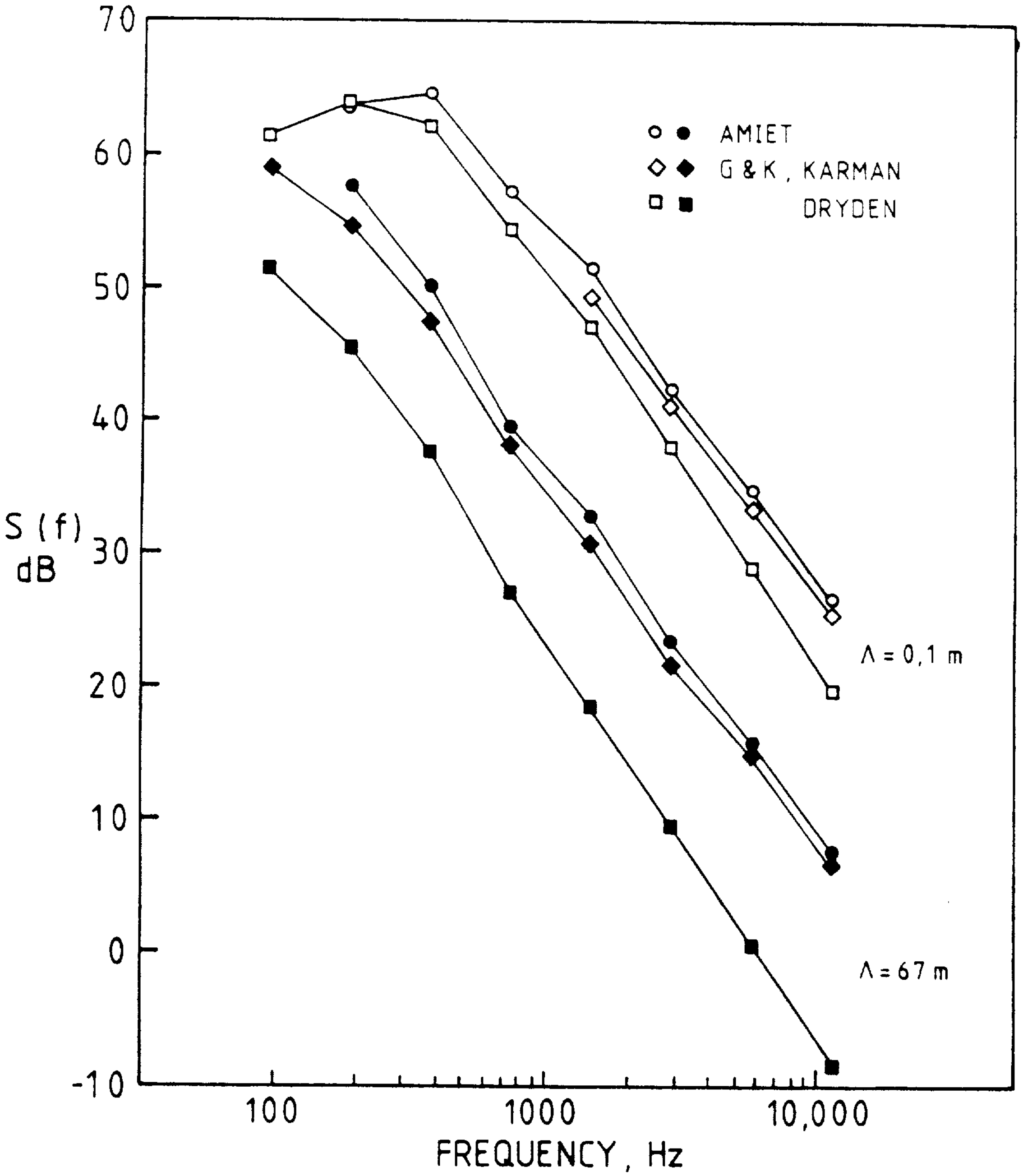

Figure 3.7: Effect of Turbulent Length Scale on Rotor Inflow Turbulence Noise Calculations, UH-1 Main Rotor, $\phi = -90^{o}$, w = 1 m/sec.

3.3 BOUNDARY LAYER/TRAILING EDGE NOISE

Previous analyses of the boundary layer/trailing edge noise assumed zero blade angle of attack (Kim and George, 1980; Schlinker and Amiet, 1980). In practice, to produce desired loadings, rotor blades are seldom operated in such condition. Rather, they are operated at various non-zero angles of attack. In this section, we will extend the analysis to account for the important effect of angle of attack on rotor trailing edge noise.

We start from the result of Kim and George (1980), which is given in equation (3.9). Examining this equation, we can see that a change in angle of attack will affect the noise radiation through the changes on S_{pp}, the surface pressure spectrum. With the normalization factor suggested by previous investigators, S_{pp} can be written in the following form

$$S_{pp} = Q^2 \frac{\delta^*}{U} S_0(\tilde{\omega}) \tag{3.16}$$

In order to accurately predict the trailing edge noise, clearly we have to find better approximations for both δ^*, the displacement thickness, and the normalized pressure spectrum $S_0(\tilde{\omega})$.

3.3.1 Displacement Thickness

The displacement thickness (δ^*) on rotor blades can be influenced by a number of parameters such as Reynolds number, Mach number, blade angle of attack, etc. Previous studies used flat plate boundary layer theory to calculate δ^* and used the result as an input to the analysis. As pointed out by Schlinker and Amiet (1980), the plate boundary layer theory cannot predict the correct displacement thickness for a rotor blade, except approximately for the zero lift case. Theoretically, displacement thickness is affected by Reynolds number, Mach number, angle of attack, etc. With increasing Reynolds number, δ^* decreases slowly with $Re^{-1/5}$; with increasing Mach number, the compressibility effect tends to increase δ^*.

Brooks and Marcolini (1984a) made a number of measurements of the displacement thickness on two-dimensional airfoils of various size. Their results suggest that after appropriate normalization, the displacement thickness can be expressed in functional form as

$$\delta^* = \delta_0^*(Re,M)\ F(\alpha) \tag{3.17}$$

where δ_0^* is the displacement thickness on an airfoil with zero angle of attack, and $F(\alpha)$ is the correction factor for changes on angle of attack.

The displacement thickness at zero angle of attack, after normalization by the airfoil chord, can be expressed as a function of Reynolds number, Re, and Mach number, M. In the present study, we use the experimental correlation given by Bies (1966):

$$\delta = 0.37\ c \left[1 + \left(\frac{Re}{6.9\times10^7} \right)^2 \right]^{0.1} Re^{-0.2}$$

$$\delta_0^* = \delta \frac{(1.3 + 0.43M^2)}{(10.4 + 0.5M^2(1 + 2\times10^{-8}Re)^{1/3})} \tag{3.18}$$

To find $F(\alpha)$, we use the experimental results of Brooks and Marcolini (1984a). A curve fitting technique led to the following empirical expression for $F(\alpha)$:

$$F(\alpha) = 1 + 0.028\alpha, \qquad \text{for } \alpha < 0^{\circ}, \text{ and}$$

$$F(\alpha) = 1 + 0.028\alpha + 0.016942\alpha^{2.56}, \qquad \text{for } \alpha > 0^{\circ}$$

For an airfoil with positive angle of attack, the first equation gives the correction factor of the displacement thickness at the lower surface and the second equation gives the correction factor at the upper surface. The above correlations are generally valid for α within -20° and 15°, and for Re within 8×10^{4} and 5×10^{6}, and for $M < 0.25$, where the boundary layer is turbulent and attached. This curve is shown in Figure 3.8.

3.3.2 **Surface Pressure Spectrum**

Next we examine S_{pp}, the spectral density of the fluctuating surface pressures. As can be seen in equation (3.17), the term that is still left undetermined is $S_0(\tilde{\omega})$. An empirical expression for $S_0(\tilde{\omega})$ can be obtained from experiments. In the present study, two sets of experiments were used, by Yu and Joshi (1979), and by Brooks and Hodgson (1980). Their data agree fairly well with each other, and curve fitting with the basic high frequency form of the spectrum leads to the following expression (Chou and George, 1983):

$$S_0(\tilde{\omega}) = \frac{1.732\times10^{-3}\tilde{\omega}}{(1 - 5.489\tilde{\omega} + 36.74\tilde{\omega}^2 + 0.1505\tilde{\omega}^5)} \qquad (3.19)$$

for $0.01 \leq \tilde{\omega} \leq 0.06$, $(\tilde{\omega} = 2\pi f\delta^{*}/U)$, and

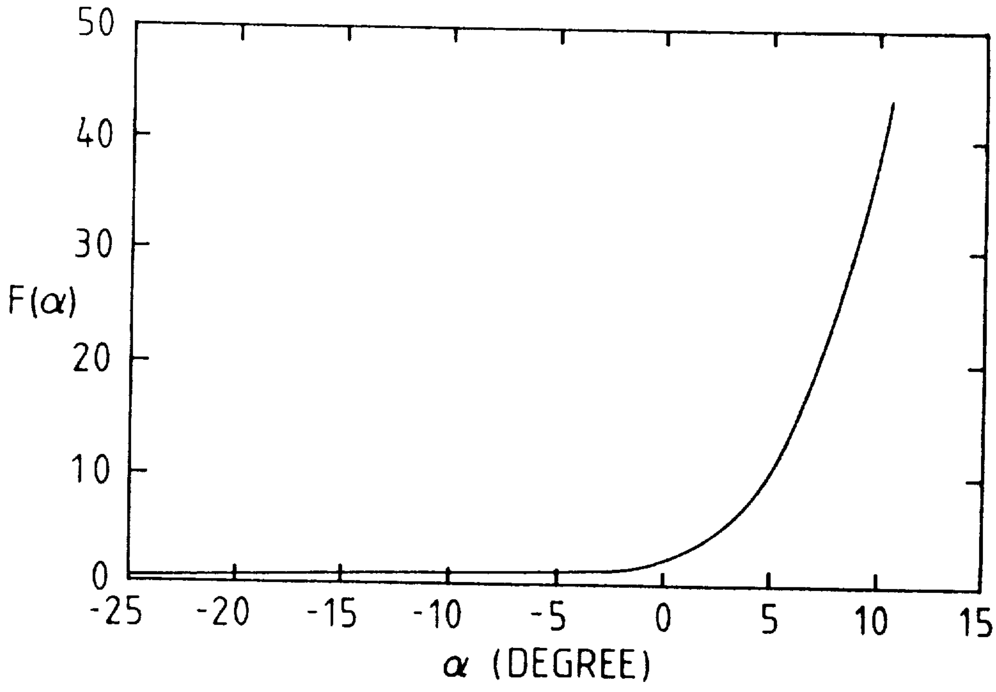

Figure 3.8: Plot of F(α) vs. α.

$$S_0(\tilde{\omega}) = \frac{1.4216\times10^{-3}\tilde{\omega}}{(0.3621 + 4.1837\tilde{\omega} + 22.818\tilde{\omega}^2 + 0.0013\tilde{\omega}^3 + 0.0028\tilde{\omega}^5)} \quad (3.20)$$

for $0.06 \leq \tilde{\omega} \leq 20$.

Figure 3.9 shows the plot of $S_0(\tilde{\omega})$ vs. $\tilde{\omega}$ along with the range of experimental data and the flat plate result.

3.3.3 Effects of Blade Angle of Attack on Broadband Noise

Figure 3.10 shows the effect of angle of attack on rotor trailing edge noise demonstrated by calculations for a UH-1 helicopter main rotor. The results lead to the conclusion that the primary effect of angle of attack is in the low to mid frequency range, where the noise

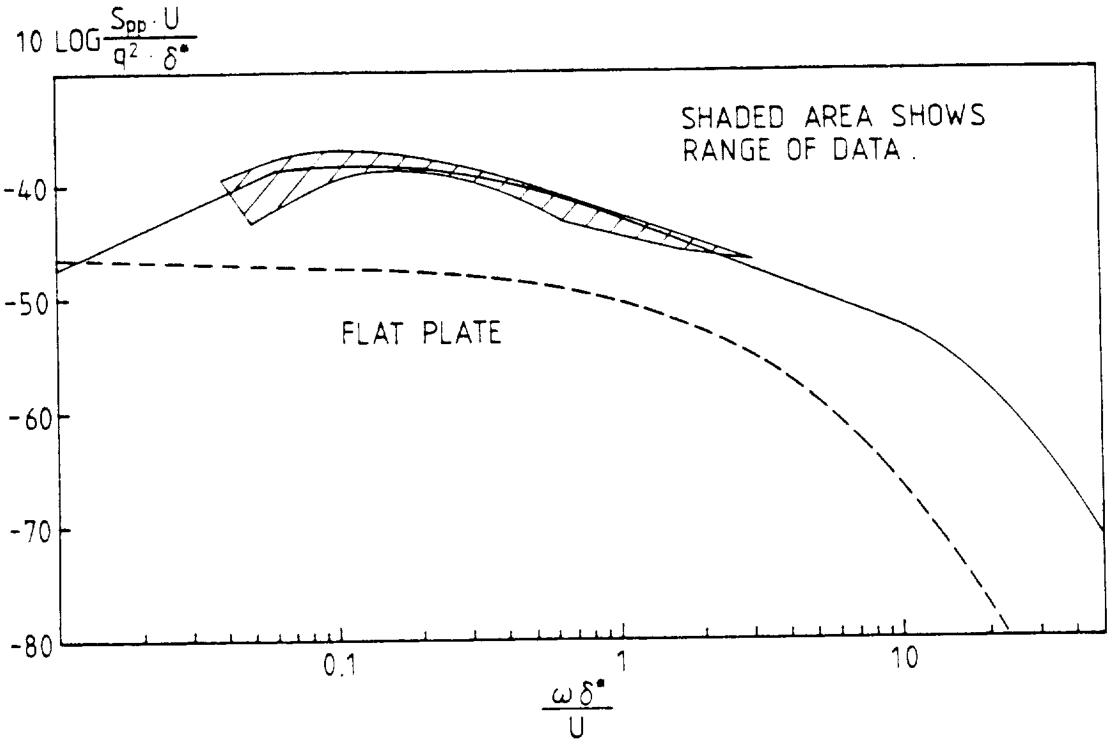

Figure 3.9: Plots of $S_0(\tilde{\omega})$ vs. $\tilde{\omega}$ with Equations (3.19) and (3.20).

level increases with angle of attack. However, in high frequency range, this change of noise level due to change of angle of attack is not very significant. The comparison of predictions using present analysis to that using flat plate data only (e.g. Kim and George, 1980) shows the important effect of the angle of attack on rotor trailing edge noise.

Trailing edge noise is only one source of rotor broadband noise. Other mechanisms such as inflow turbulence and tip vortex separation also contribute significantly to the noise radiation. Trailing edge noise can be important for low inflow turbulence cases or when considering a large sized rotor (George and Chou, 1983a, 1984a). Thus to evaluate the present analysis by comparing with existing experiments, one must also include other possible sources.

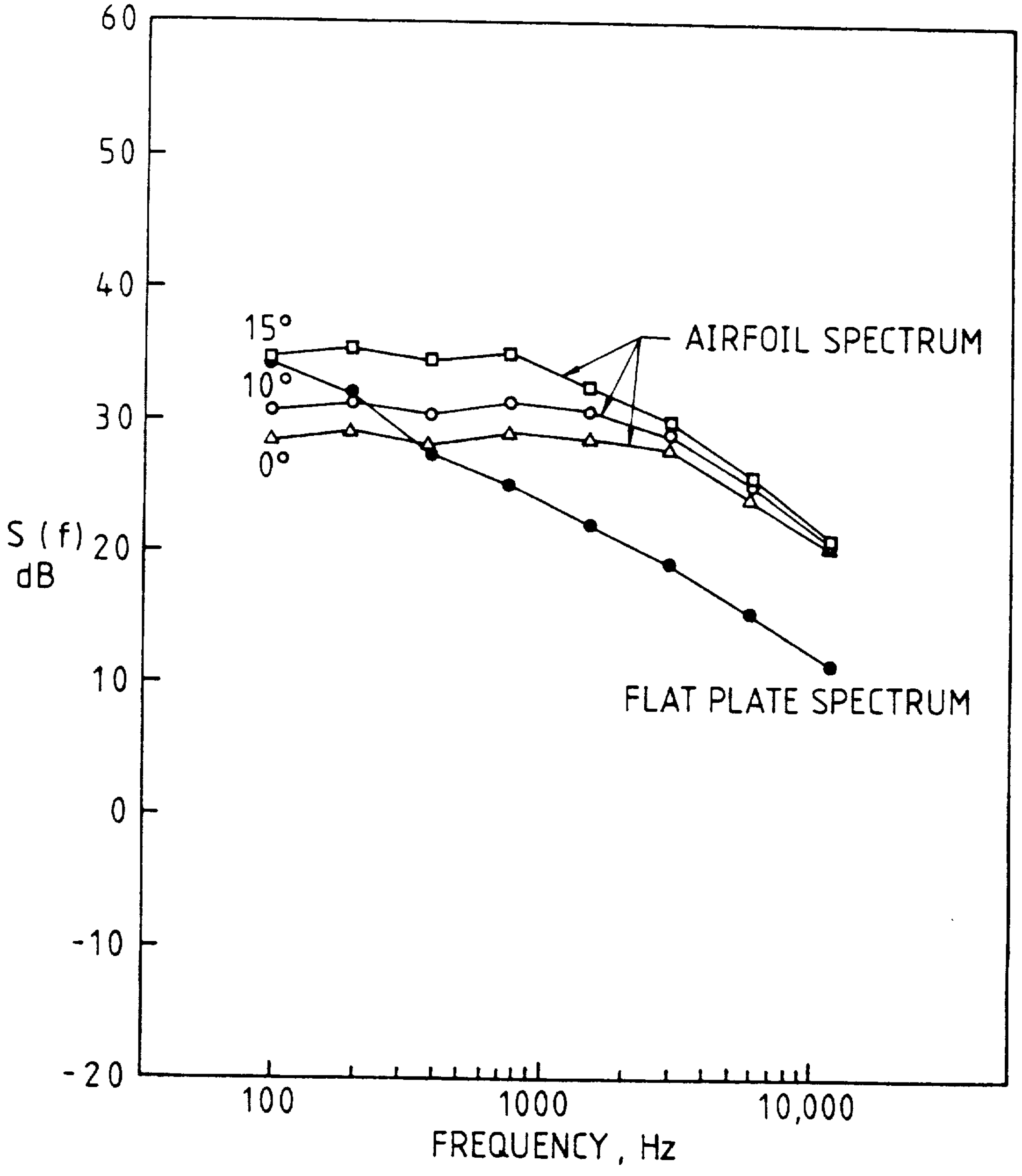

Figure 3.10: Effect of Angle of Attack on Rotor Trailing Edge Noise, UH-1 Main Rotor, ϕ = -27°.

3.4 TIP VORTEX FORMATION NOISE

The original analysis of turbulence/trailing edge interaction in the tip vortex separation area used a simplified cross-flow analogy to estimate the turbulence level and the surface pressure spectrum in the tip separation region (George et al., 1980). In the present study, this analysis is extended, with the pressure spectrum being replaced by that associated with the leading edge vortices on delta wings (George and Chou, 1984a).

3.4.1 Surface Pressure Spectrum from Delta Wings

Again we start with the result of George et al. (1980), i.e. equation (3.11). As mentioned previously, the accuracy of the prediction depends upon the accuracy of the model used for describing the surface pressure fluctuation and upon parameters such as the extent of the tip separation region.

The original analysis used surface pressures measured from the separation region behind a 2-dimensional fence. The model used in the present study is based on the pressure spectra measured under the similar edge separation vortices on delta wings. As sketched in Figure 3.2, the delta wing flow geometry is very similar to helicopter rotor tip flow, including both the primary and secondary separations from the edge and the axial outer flow. The separation geometry is also influenced by rounded or sharp edges as in the delta wing tip case. Our goal is to construct a suitable correlation for the pressure spectra in the delta wing case and relate this correlation to the rotor tip flow case of interest.

Richard and Fahy (1965) have analyzed the turbulent flow beneath the leading edge vortices of several delta wings of different planforms and various angles of attack. They presented spectra from a number of investigators, non-dimensionalized in several ways, however, none of which were satisfactory for our case.

In order to find a normalization suitable for application to our tip vortex separation case, we first studied the delta wing flow geometry and pressure data measured in the comprehensive experiments of Peckham (1961). Based on flow visualization results, the locations of peak negative pressures, and on pressure distributions, the value of the transverse separation scale L was found to be related to the local chord length. The edge shape is definitely important as noted also by Barlett and Vidal (1955).

Next the maximum negative pressure coefficients under the vortices relative to those on the nearby surface were used with the Bernoulli's equation to estimate the maximum velocity ratio V_m/U. Assuming that the velocity in the vicinity of the vortex is approximately the same as that on nearby surface, one obtains:

$$V_m/U = (1-c_{p_{min}})^{1/2}$$

Then we used the estimated values of V_m and L to normalize the spectra given by Richard and Fahy (1965). The results, as shown in Figure 3.11, give a fairly good correlation.

With the usual curve fitting techniques, these spectra can be approximated by

$$\log_{10}(S_1(\tilde{\omega})) = -3.475 - 1.654(\sigma + 0.82)^2 \qquad (3.21a)$$

for $\sigma \leq -0.82$ ($\sigma = \log_{10}\tilde{\omega}$), and

$$\log_{10}(S_1(\tilde{\omega})) = -3.475 - 0.984(\sigma + 0.82)^2 \tag{3.21b}$$

for $\sigma > -0.82$. But $S_1(\tilde{\omega}) = 0$ for $\tilde{\omega} < 0$. The fitted curve is plotted against data as shown in Figure 3.11.

3.4.2 Other Parameters

In order to define the appropriate spectrum for a rotor tip case, we need the estimates of L and V_m for rotor tip flows at different angles of attack. The flow visualization, pressure measurements, and velocity measurements of Gray et al. (1980) and of Chigier and Corsiglia (1971) were used to estimate values of L/c and V_m/U. Figures 3.12 and 3.13 show the plots of L/c and V_m/U versus α respectively. V_m/U can be expressed as

$$V_m/U = 1 + 0.0359\ \alpha \tag{3.22}$$

where α is the tip angle of attack in degrees.

The spanwise extent of the separation bubble remains to be determined. George and Chou (1984a) suggested the following correlations

$$L/c = 0.023 + 0.0089\ \alpha \tag{3.23a}$$

for square tip blades, or

$$L/c = 0.0074\ (\alpha - 2), \quad \text{for } \alpha > 2^\circ \tag{3.23b}$$

for blades with rounded tips.

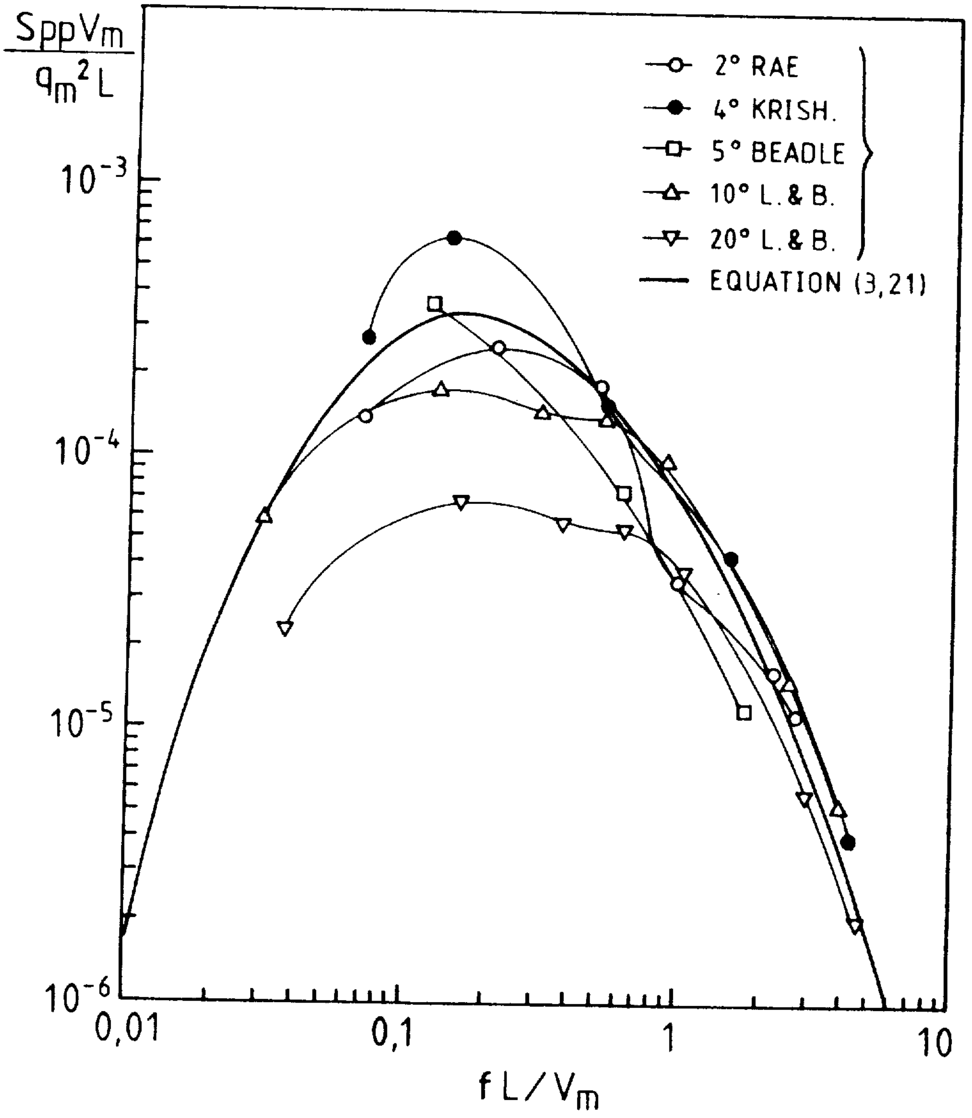

Figure 3.11: Normalized Spectra from Richard and Fahy (1965) and the Fitted Curve (3.21).

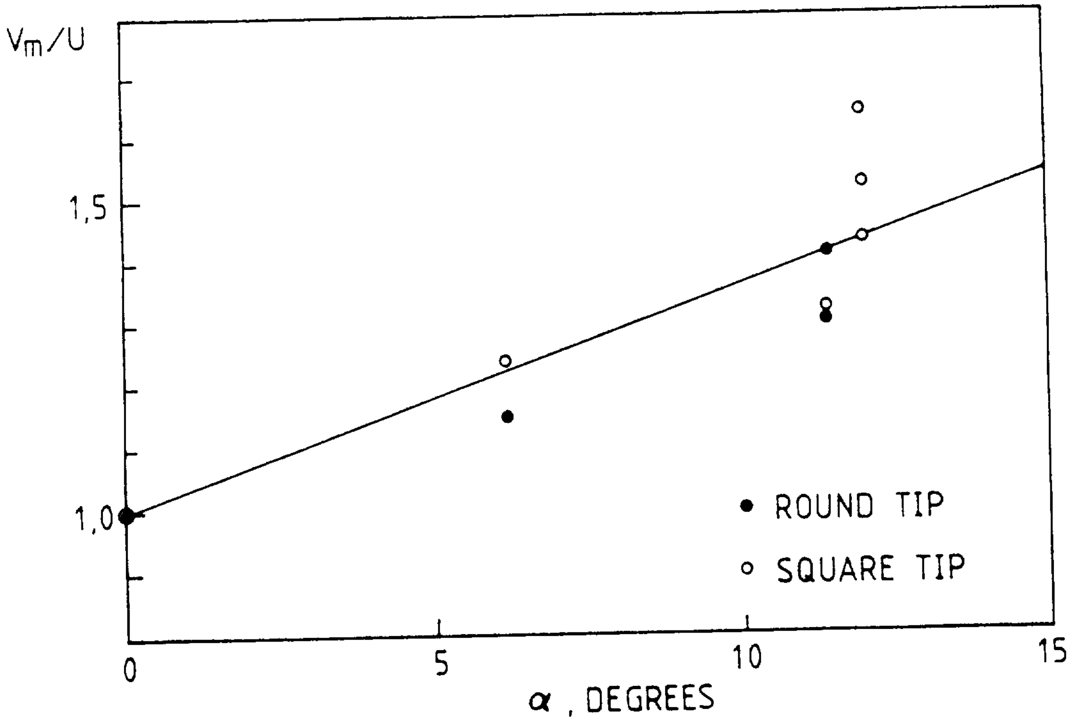

Figure 3.12: Maximum Circumferential Velocity Ratio vs. Angle of Attack.

Brooks and Marcolini (1984b) have performed a series of experiments on the tip vortex formation noise from airfoils with rounded tips. They found that the basic scaling of the tip vortex formation noise appears to be correct. The correlation for V_m as given in equation (3.22) is found to be consistent with the experiments (within 5 to 10 percent). However, they also found that if one chooses 4 to 5 percent turbulent intensity contours as a guide to determine the separation length scale L, the correlation given in equation (3.23b) does not seem to be appropriate. They suggested that equation (3.23b) should be replaced with

$$L/c = 0.008\ \alpha \tag{3.24}$$

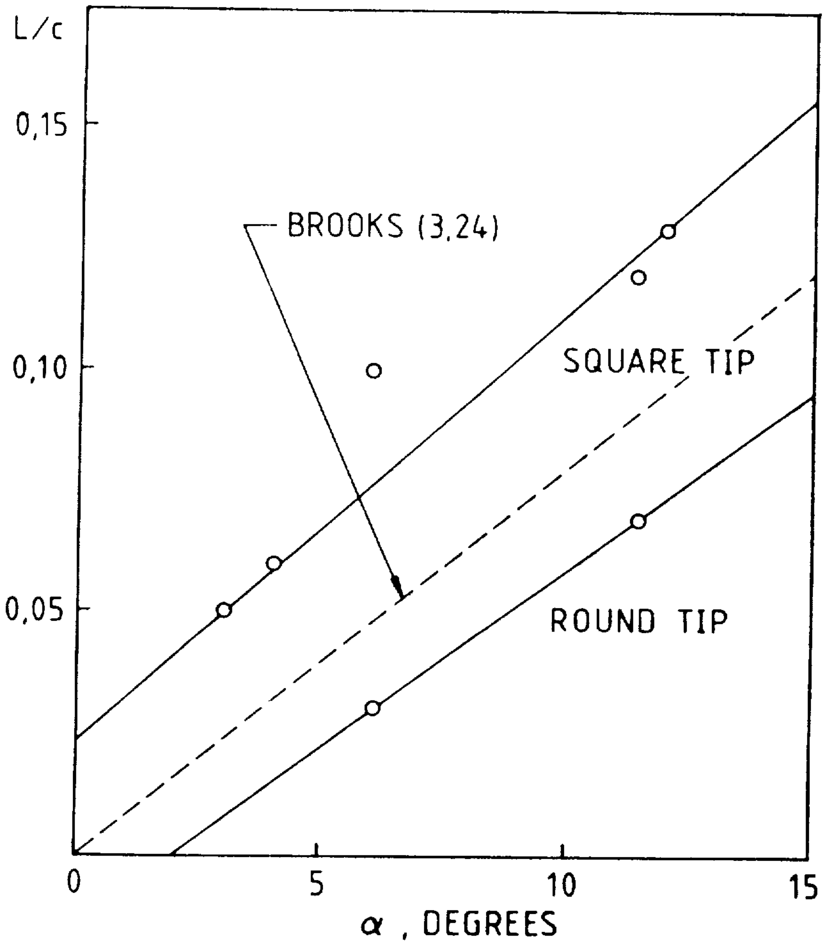

Figure 3.13: Lateral Extent of the Separation Bubble on Rotor Tips vs. Angle of Attack.

3.4.3 Effects of Tip Shape and Angle of Attack on Noise

It is clear that tip vortex formation noise is extremely sensitive to the change of angle of attack and the shape of the rotor tip. **Figure** 3.14 shows the results of some calculations for a UH-1 helicopter main rotor. Calculated spectra using (3.23) for L are shown for pitch angles of 10^o and 15^o for both square and rounded tip rotor. Also shown in the figure are the corresponding boundary layer/trailing edge noise calculations. Clearly, tip vortex formation

C-2

noise is favored by high angles of attack, square tips, and wide tip chords (low aspect ratio, untapered blades).

3.5 TRAILING EDGE THICKNESS NOISE

Turbulent vortex shedding from blunt trailing edges is a source of rotor high frequency broadband noise (Schlinker and Brooks, 1982). Brooks and Hodgson (1980) were the first to demonstrate the importance of this self-generated noise mechanism. In their experiment with an isolated airfoil, they found that the radiated noise increased significantly for airfoils with thickened trailing edges.

The first attempt to study this noise mechanism theoretically for rotors was done by Chou and George (1985). They studied the parametric dependence of this noise mechanism and developed a method to predict rotor broadband noise associated with turbulent vortex shedding from blunt trailing edges. Further work is needed to definitively establish the turbulent vortex-shedding properties of wings and rotor tips.

3.5.1 Surface Pressure Spectrum

Blunt trailing edge noise radiation is a result of higher surface pressure fluctuations near the airfoil's trailing edge due to turbulent vortex shedding. To predict this noise mechanism, our first task is to scale the fluctuating surface pressures. Using dimensional analysis or physical reasoning, the following relationships for the parametric dependence for S_{pp} and f were found

$$S_{pp} \sim Q^2 t^3 / U$$

$$f \sim U / t$$

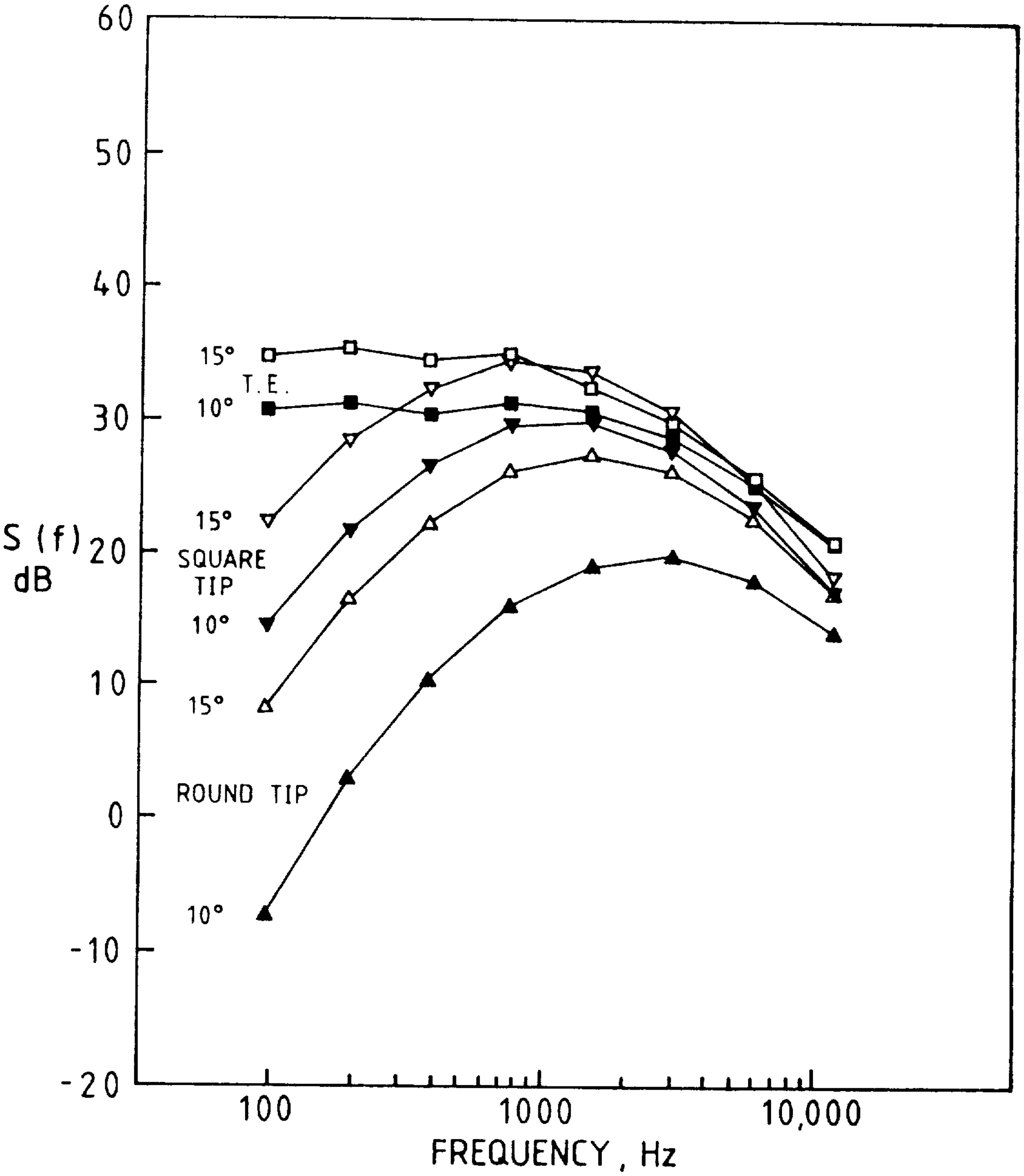

Figure 3.14: Effect of Angle of Attack on Tip Vortex Formation Noise, $\phi = -27^o$, UH-1 Main Rotor.

where S_{pp} is the power spectral density of surface pressure fluctuation, f is the frequency in Hz, t is the trailing edge thickness and U is the free stream velocity. By using the above relationships, the surface pressure spectrum S_{pp} is assumed to have the following form

$$S_{pp}(f) = q^2 t^3 S_2(\tilde{\omega}) / U \tag{3.25}$$

where $\tilde{\omega} = 2\pi ft/U$. The normalized spectrum $S_2(\tilde{\omega})$ can be found empirically from experimental data. Due to the lack of measurements for surface pressure fluctuation near blunt trailing edges, such data were obtained by inverting the acoustic data measured by Brooks and Hodgson (1980) using their stationary airfoil analysis. Using the above scaling relation, the data representing a wide range of free stream velocities and trailing edge thickness are collapsed reasonably well to a single curve. By using curve fitting techniques, the empirical expression for the normalized spectrum S_2 is found as follows

$$\begin{aligned}\log_{10} S_2(\tilde{\omega}) = 17.394 - 106.57\sigma - 158.12\sigma^2 + 99.27\sigma^3 \\ -33.249\sigma^4 + 16.721\sigma^5\end{aligned} \tag{3.26a}$$

for $0.2 < \sigma < 2$. ($\sigma = \log_{10}(\tilde{\omega})$), otherwise

$$S_2(\tilde{\omega}) = 0 \tag{3.26b}$$

Figure 3.15 shows the fitted curve along with the experimental data.

To predict the additional broadband noise radiation from a rotor due to its blunt trailing edges, several assumptions have to be made. First, the source is modelled as rotating radiating dipoles; this

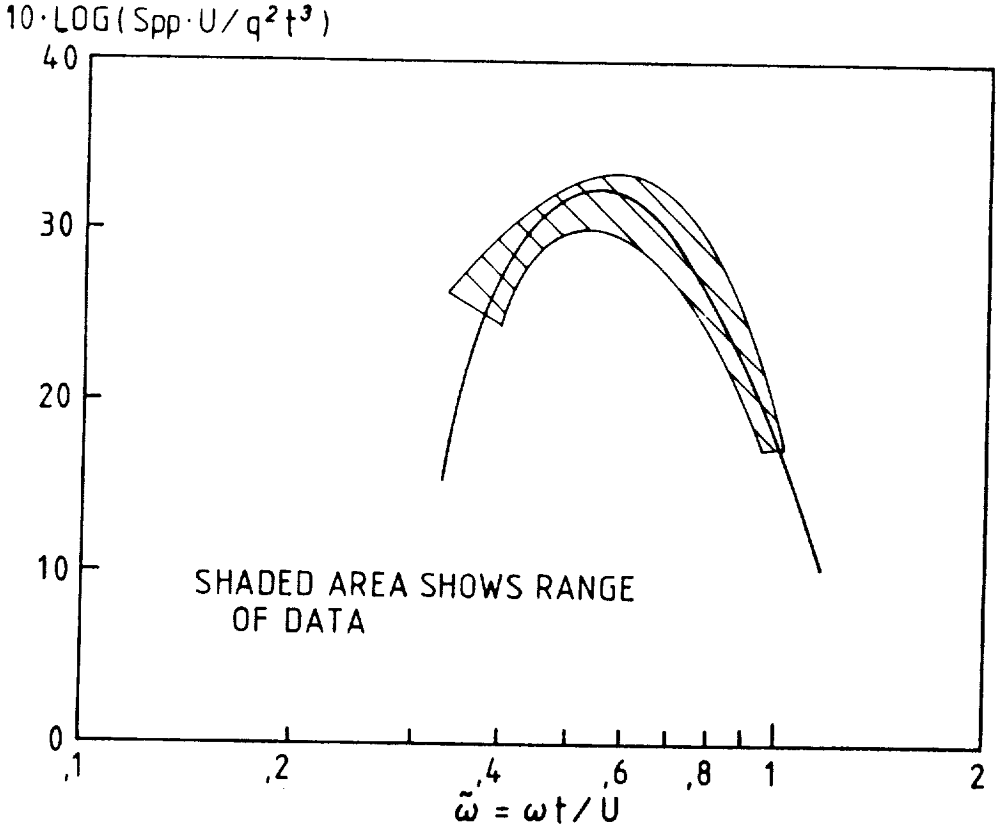

Figure 3.15: Normalized Surface Pressure Spectrum $S_2(\tilde{\omega})$ and the Experimental data of Brooks and Hodgson (1980).

assumption can be justified from the acoustic data measured by Brooks and Hodgson (1980), in which a strong dipole radiation pattern was observed. Then the noise can be predicted with an analysis similar to that of Kim and George for boundary layer/trailing edge noise (1980), with surface pressure spectrum replaced with (3.26). The result of this analysis is given in equation (3.9).

3.5.2 Effect of Trailing Edge Thickness on Broadband Noise

Figure 3.16 shows the effect of trailing edge thickness on rotor broadband noise. Calculations were made based on the low speed fan as used in Lowson's experiments (1972). It is clear that trailing edge thickness is a very important parameter for the rotor noise problem. Generally speaking, the noise spectra due to turbulent vortex shedding from blunt trailing edges are peaks occurring at various frequency ranges. The peak frequency depends on the trailing edge thickness; a small trailing edge thickness will generate a high frequency peak and a thick trailing edge will result in a peak of lower frequencies. The level of the spectrum peak also depends on the thickness of trailing edge; peak level increases roughly according to the third power of trailing edge thickness.

In conclusion, turbulent vortex-shedding noise from blunt trailing edges is a very important broadband noise source for rotors. A slightly blunted rotor trailing edge can contribute significantly to the overall noise spectrum. The present analysis provides reasonable predictions for such mechanisms. However, a more accurate prediction could be achieved with a better empirical expression for $S_2(\tilde{\omega})$, the normalized spectrum. Clearly, more measurements of surface pressure fluctuations near blunt trailing edges are needed.

3.6 RESULTS AND DISCUSSIONS

In the present work, we reviewed and made significant extensions to rotor broadband noise analyses to allow more accurate prediction of rotor noise spectra. Our analyses, although evaluated by computer

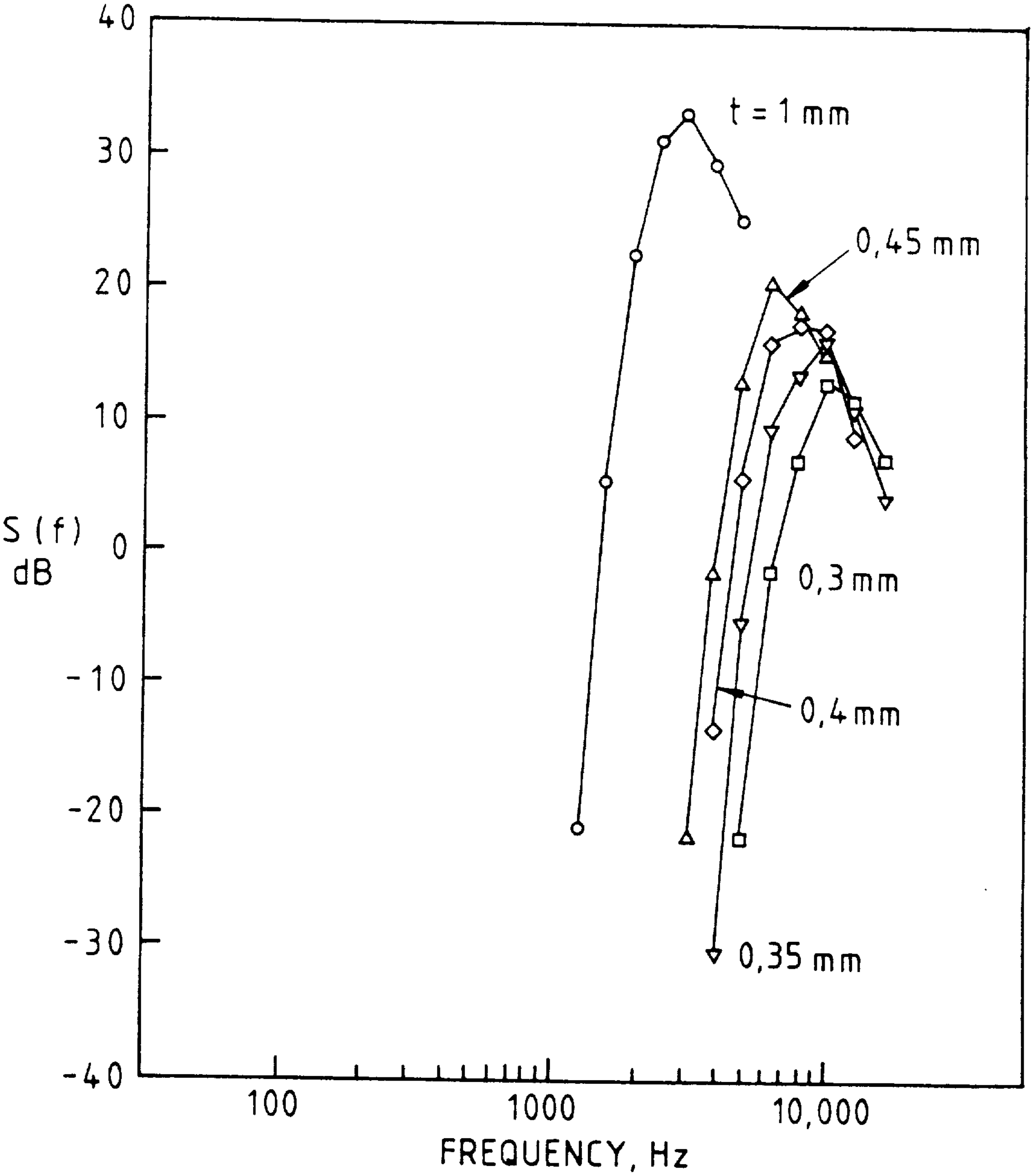

Figure 3.16: Effect of Trailing Edge Thickness on Rotor Broadband Noise.

programs, are primarily analytical and thus helpful in understanding the nature of the noise generation. The sources considered are load or surface pressure fluctuations due to inflow turbulence, due to turbulent boundary layers passing the blades' trailing edges, due to tip vortex formation, and due to turbulent vortex shedding from blunt trailing edges.

Comparisons to more numerically based approaches show that our analyses are accurate but restricted to advance ratios less than approximately 0.4 (which include all cases of practical interest). The present study neglects in-plane noise mechanisms and is thus restricted to angles which are not very close to the rotor plane.

The results of the present study indicate that inflow turbulence noise depends strongly upon ambient conditions and dominates at low frequencies. Trailing edge noise and tip vortex noise are important at higher frequencies if inflow turbulence is weak. Boundary layer trailing edge noise is important, especially for large sized rotors. This noise increases slowly with angle of attack but not as rapidly as tip vortex noise, which can be important at high angles of attack for wide chord, square tips rotors. Turbulent vortex shedding noise from blunt trailing edges can be very important in mid- to high-frequencies depending upon the type of rotor and its trailing edge thickness.

3.6.1 Comparisons of Analysis to Experiments

An extensive search was made of existing experiments and calculations based on the various prediction methods were made for comparison purposes. This study shows that present analyses are adequate to predict the spectra from a wide variety of experiments on fans, full scale and model scale helicopter rotors, wind turbines to within about 5 to 10 dB. Better knowledge of the inflow turbulence improves the accuracy of the predictions.

In the comparisons, the data estimated as input to the analyses and the correlations are given in the figure captions. Other input parameters were taken from the experimental papers. Inflow velocities were estimated using simple momentum theory with thrusts determined by simple blade element theory. As mentioned above, the inflow turbulence values were often estimated. In cases where separate calculations are shown for separate mechanisms, the results should be summed in order to compare to the experiments. However, in order not to clutter the figures, this was not done in most cases.

First we compare the present analyses to the experimental data for full scale helicopter rotors. Generally there are two types of full-scale helicopter rotor tests available: the whirl tower test and the flight test. The whirl tower test has several advantages over the flight test. Since only one rotor is involved, there is no problem with aerodynamic interactions with other rotors such as main rotor/tail rotor interactions. Also, other polluting noises such as noises generated by drive motor and gear box, etc. are comparatively easy to control. Therefore, these tests are considered cleaner than the flight tests. However, the flight tests do give more information on the overall helicopter noise problem.

First we compare the present analyses to a whirl tower test by Leverton (1973). He tested a full scale S-55 rotor on a test rig in an inverted position in order to eliminate the effect of recirculation which occurs when a rotor wake is directed toward the ground. The spectra measured were taken from a tethered balloon at various angles to the test rotor plane. His tests varied both load and RPM. The primary missing information in Leverton's results is any data on the inflow turbulence. Neither the turbulent intensity nor the scale were measured. As the inflow was drawn from near the ground, the turbulent integral scale could be quite reasonably estimated from the fairly well established empirical relationship that

$$\Lambda = 0.9\ h$$

where Λ is the turbulent integral scale and h is the height above the ground (Etkin, 1961). Similarly, values for turbulent intensity for various weather conditions can also be estimated from the extensive data and correlations in Lumley and Panofsky's monograph (1964).

The first set of data we choose were taken at an angle of -75° from the rotor plane where all of the analyses would be expected to be within the range of their assumptions. Figure 3.17 shows the comparison of a range of predictions. It is also clear that at the lower frequencies, say below 1000 Hz, the boundary layer trailing edge noise and the tip vortex noise mechanisms are not important. However, at frequencies above 1000 Hz they become quite important, with boundary layer trailing edge noise being the more important one in this case. Fink's boundary layer noise correlation is seen to be a reasonable approximation to the more exact boundary layer trailing edge noise calculations. Most of the noise below 1000 Hz is shown to

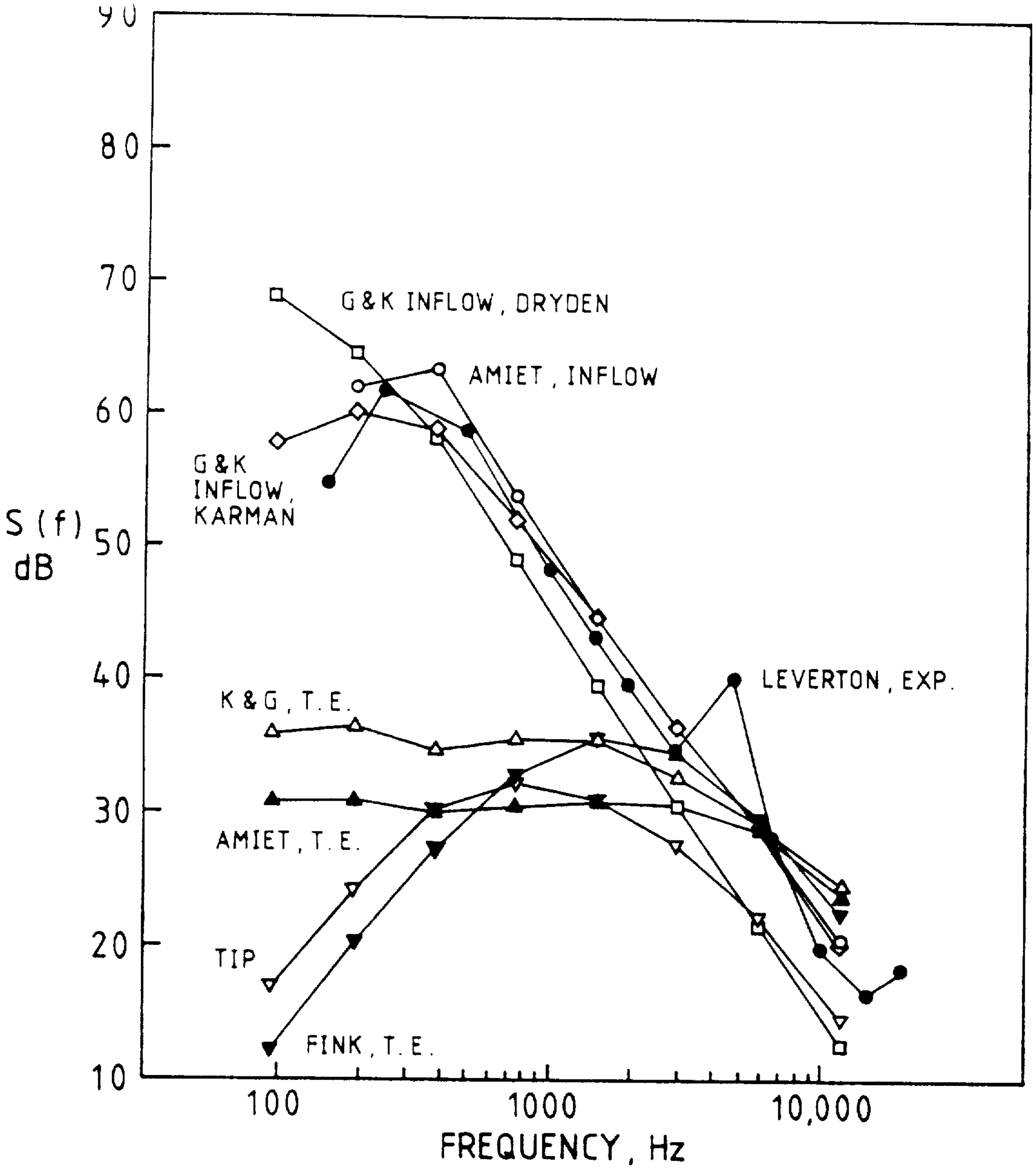

Figure 3.17: Comparison of the Range of Predictions for a Full Scale Helicopter Rotor with the Experimental data of Leverton (1973), $\phi = -75^{o}$, $\Lambda = 0.57$ m, $w = 1$ m/sec.

be inflow turbulence noise based on the estimated turbulent properties. Both the analyses of George and Kim (1976) and of Amiet (1976) agree within 5 dB with each other and with Leverton's data.

In Figure 3.18, a comparison is shown among calculations based on the three mechanisms of George and co-workers, the two of Amiet, and some data of Leverton at an angle of -11.5° from the rotor plane. As all of these analyses ignore in-plane force components and as George and co-workers use a blade dipole directivity, the agreement would not be expected to be quite as good. It is not clear, however, how many of the differences are due to which of these effects. The inflow turbulence no
however seem to be in better agreement with the experiments in this case.

Next we examine the analyses against the experiments of full scale wind turbines. Figure 3.19 shows the comparison to full scale MOD-2 wind turbine data presented by Hubbard et al. (1981). The background noise was measured and shown to be well below the measured spectra. But again no information on turbulent intensity or integral length scale was given. Thus the calculations are based on estimated turbulence properties, aided slightly by the fact that at least the wind speed is known. There is little question that the predictions using the Karman spectrum are in better agreement with the experiments than those using the Dryden spectrum. The results shown used calculated trailing edge thickness, which is based on standard NACA 23XXX series airfoil sections as in the MOD-2 blade application. The results compare favorably to the acoustic data obtained from the

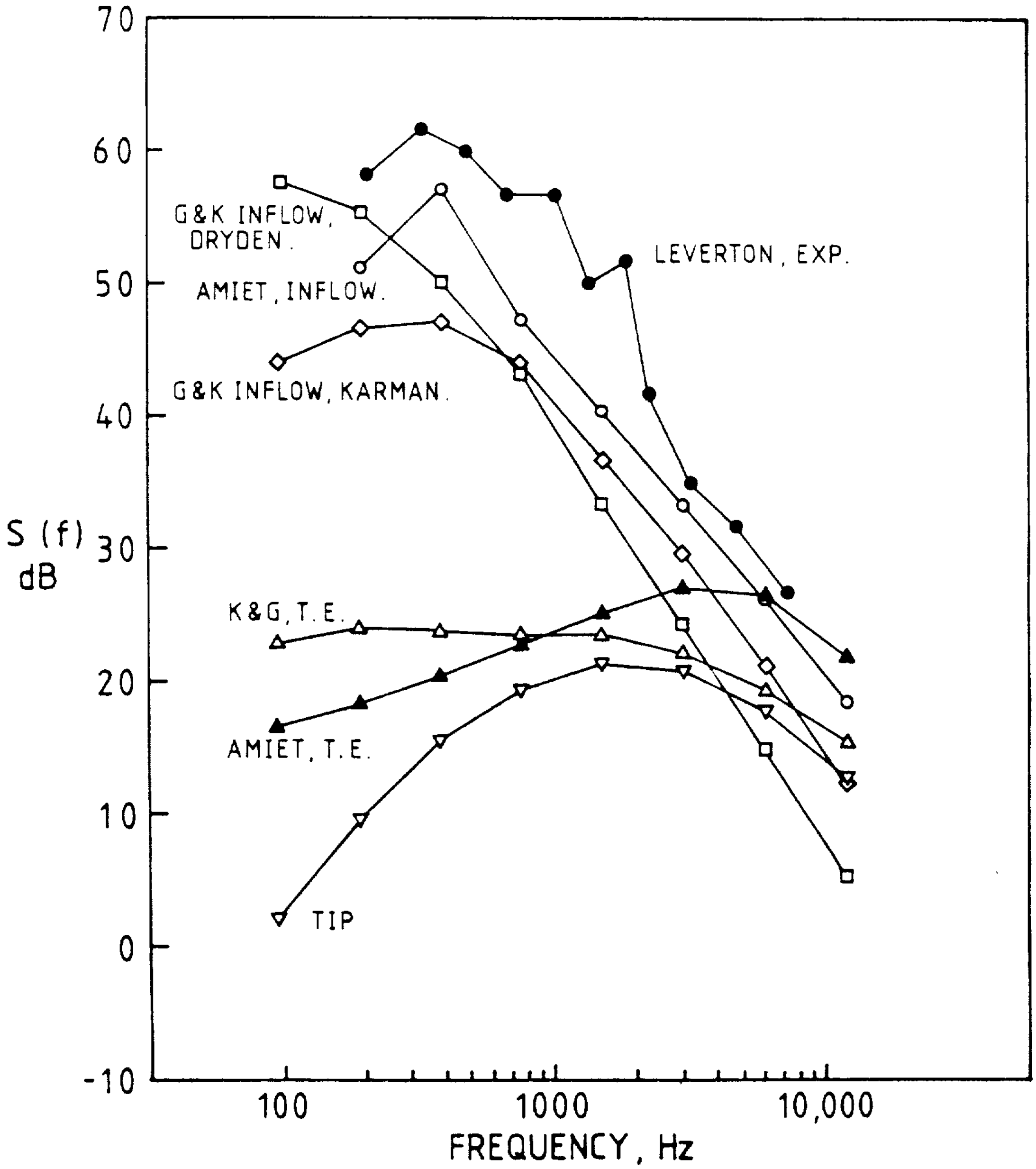

Figure 3.18: Comparison of Predictions with the Experimental Data of Leverton (1973), $\phi = -11.5^\circ$, Other Parameters are Same as in Figure 3.17.

experiment. It is clear that the primary noise sources above a few hundred Hertz are boundary layer/trailing edge noise and trailing edge thickness noise.

The noise from small low speed axial flow fans is also considered. The indoor experiments of Lowson et al. (1972) are chosen for our comparison. Tests were run in an anechoic room for both a ducted and an unducted fan, both before and after recirculation built up in the room. The non-recirculation cases are chosen for our comparisons since test conditions are better defined. RPM, tip angle, and tip shape were varied as well. The turbulence was measured by a hot wire anenometer with limited frequency response in this experiment. We estimated the turbulent integral scale as 0.1 meter. Figure 3.20 shows the comparison of the present analyses with Lowson's experimental data. Again all possible broadband noise sources are included. The results show excellent agreement with the experiment.

The model scale helicopter rotor tests are also considered. A set of high quality tests has been carried out by Paterson and Amiet in the UTRC anechoic wind tunnel facility (1979). In these tests, both vertical ascent and forward flight were simulated and different grids were used upstream to generate controlled inflow turbulence. Measurements were made of both the turbulent intensity and integral scale so that, in these cases, none of the parameters needed to be estimated. Figures 3.21 through 3.23 show comparisons of calculations to data presented by Paterson and Amiet. In the no grid case (low inflow turbulence), it is clear that both tip vortex and boundary layer noise are important at the higher frequencies. In all the

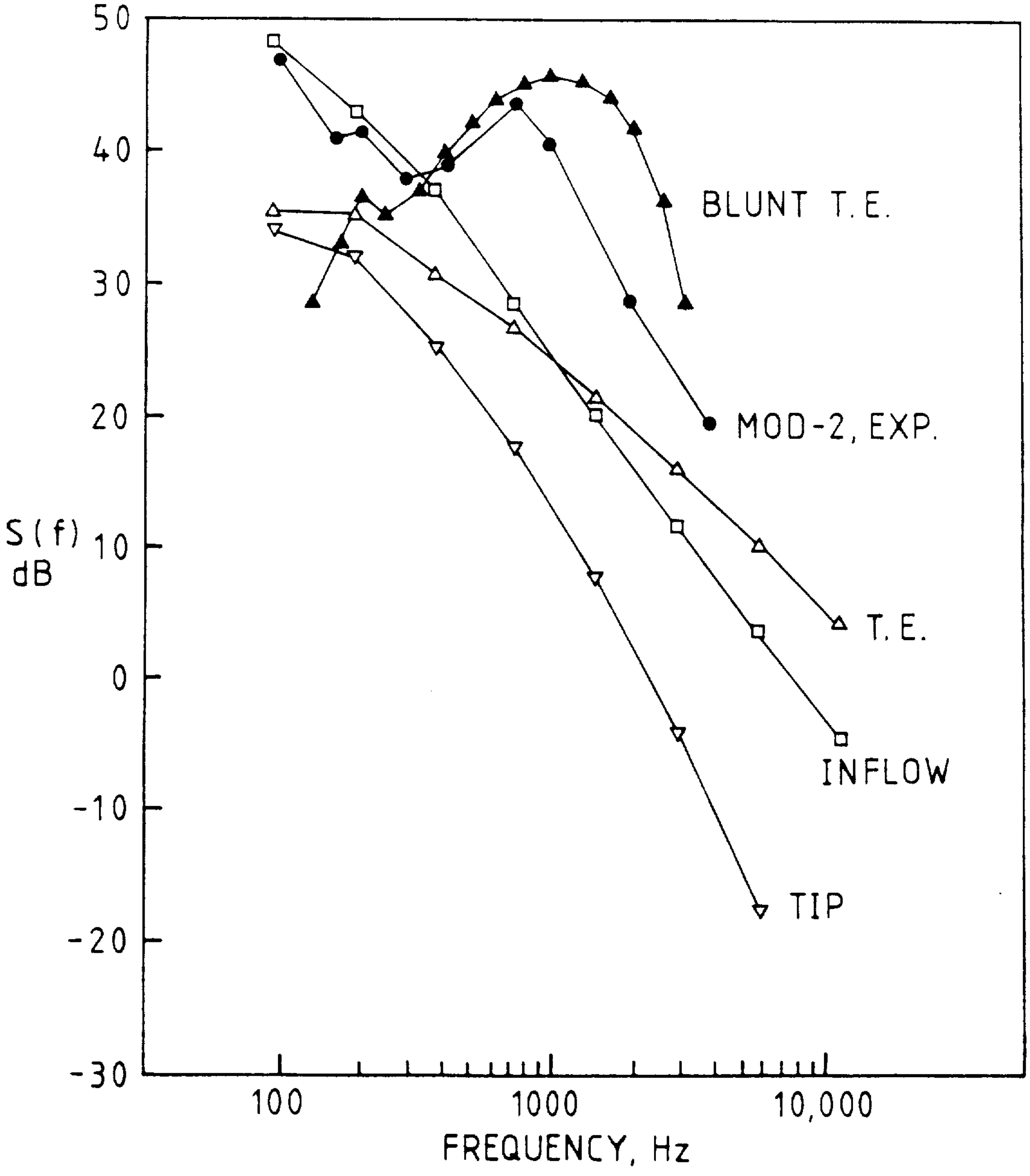

Figure 3.19: Comparison of Predictions with the MOD-2 Wind Turbine Data of Hubbard et al. (1981), $\Lambda = 55$ m, $w = 1$ m/sec, Ground Distance = 69 m.

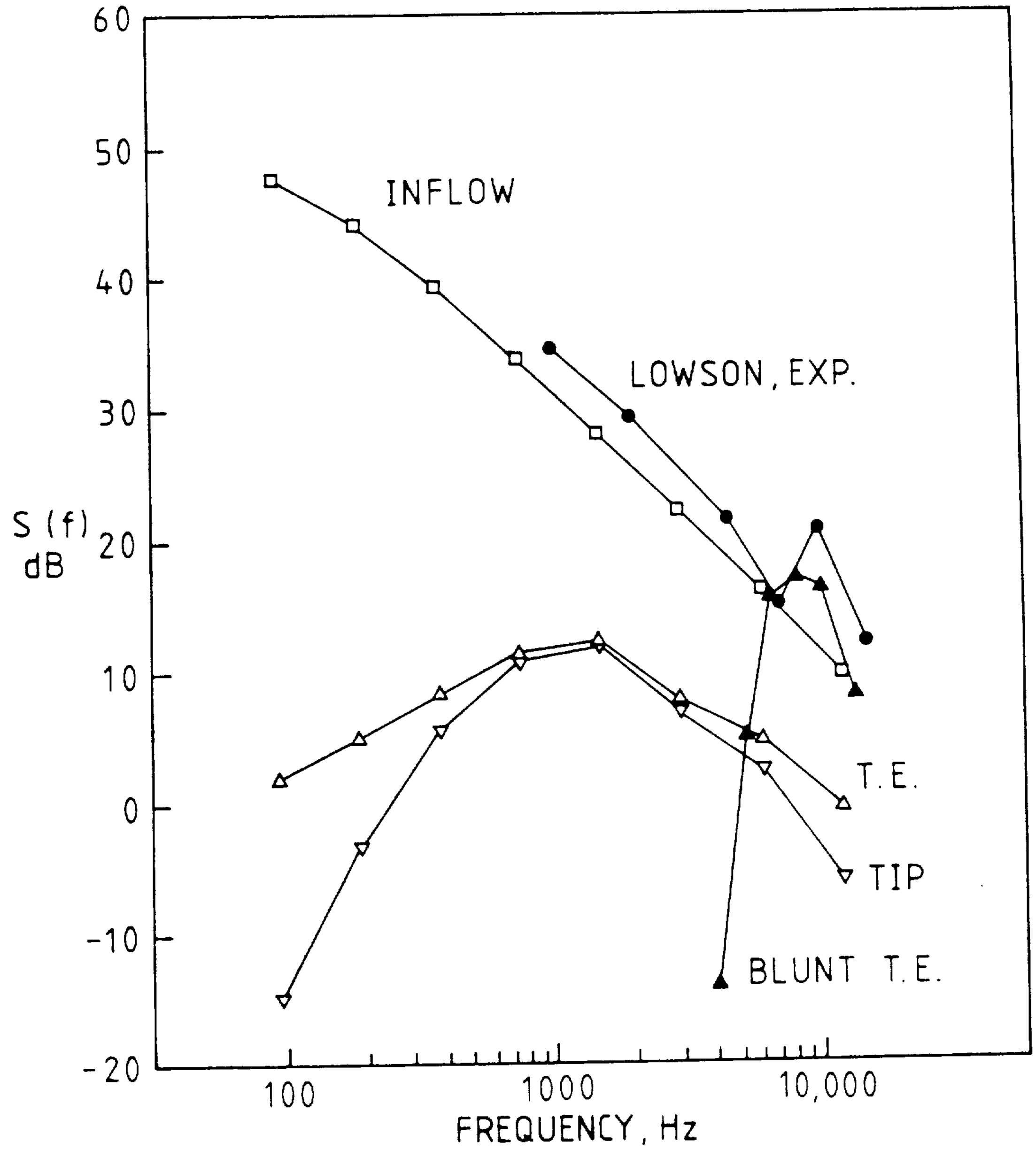

Figure 3.20: Comparison of Predictions for Low Speed Fan Noise, Experiment of Lowson (1972), 1000 RPM, Tip Pitch = 15°.

cases, the calculations and experiments agree to within about 5 dB. Unlike the full scale rotor cases, inflow turbulence noise calculations using the Dryden spectrum agree better with the experiments than those using the Karman spectrum. In Paterson and Amiet's original report, they had also shown good agreement with Amiet's inflow turbulence noise analysis whenever the primary noise source was inflow turbulence.

3.6.2 Comparisons of Analysis to Each Other

In this section the results calculated by the methods of Amiet and of George and co-workers are compared to show the effects of different assumptions in the analyses. The computational approach of Amiet allows treatment of forward flight (non-zero advance ratios) and more accurate basic blade noise directivity. The George and Kim approach has been implemented for both the Von Karman model and the Dryden model of the inflow turbulence spectrum. We will examine each of these effects by comparing the results of the calculations made by different methods.

Figure 3.24 shows the effect of forward flight on inflow turbulence noise as calculated by Amiet's analysis and compared to hover calculations based on George and Kim's analysis. It is notable that the advance ratio effect is not very important for any case of interest to helicopters (i.e. advance ratio below 0.4).

Similarly, Figure 3.25 compares changing advance ratio for boundary layer/trailing edge noise. Here, the basic inputs vary since the calculation using the Kim and George approach uses an airfoil

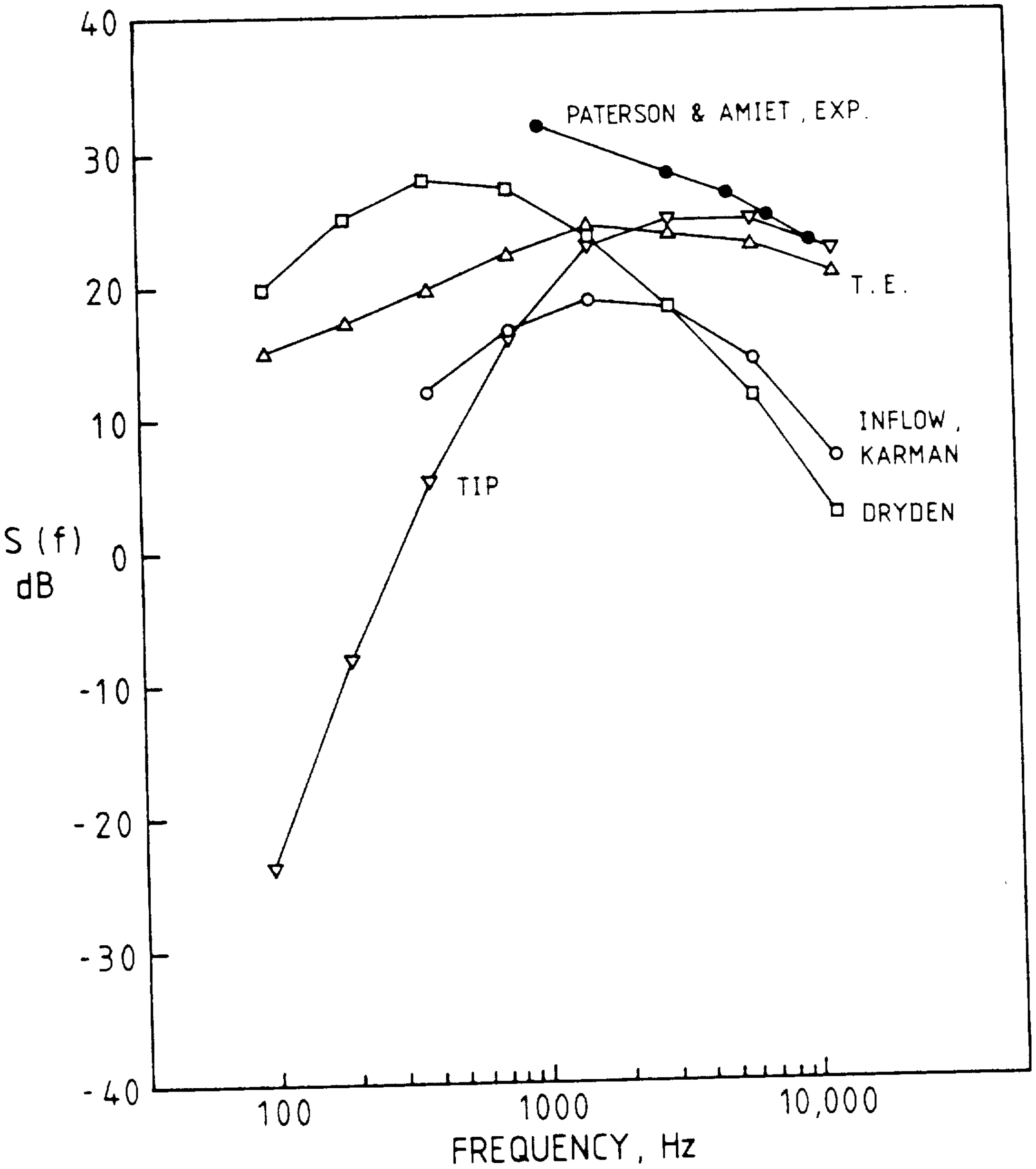

Figure 3.21: Comparison of Predictions for Model Helicopter Rotor, Experiment of Paterson and Amiet (1979), Test VA-C-1.

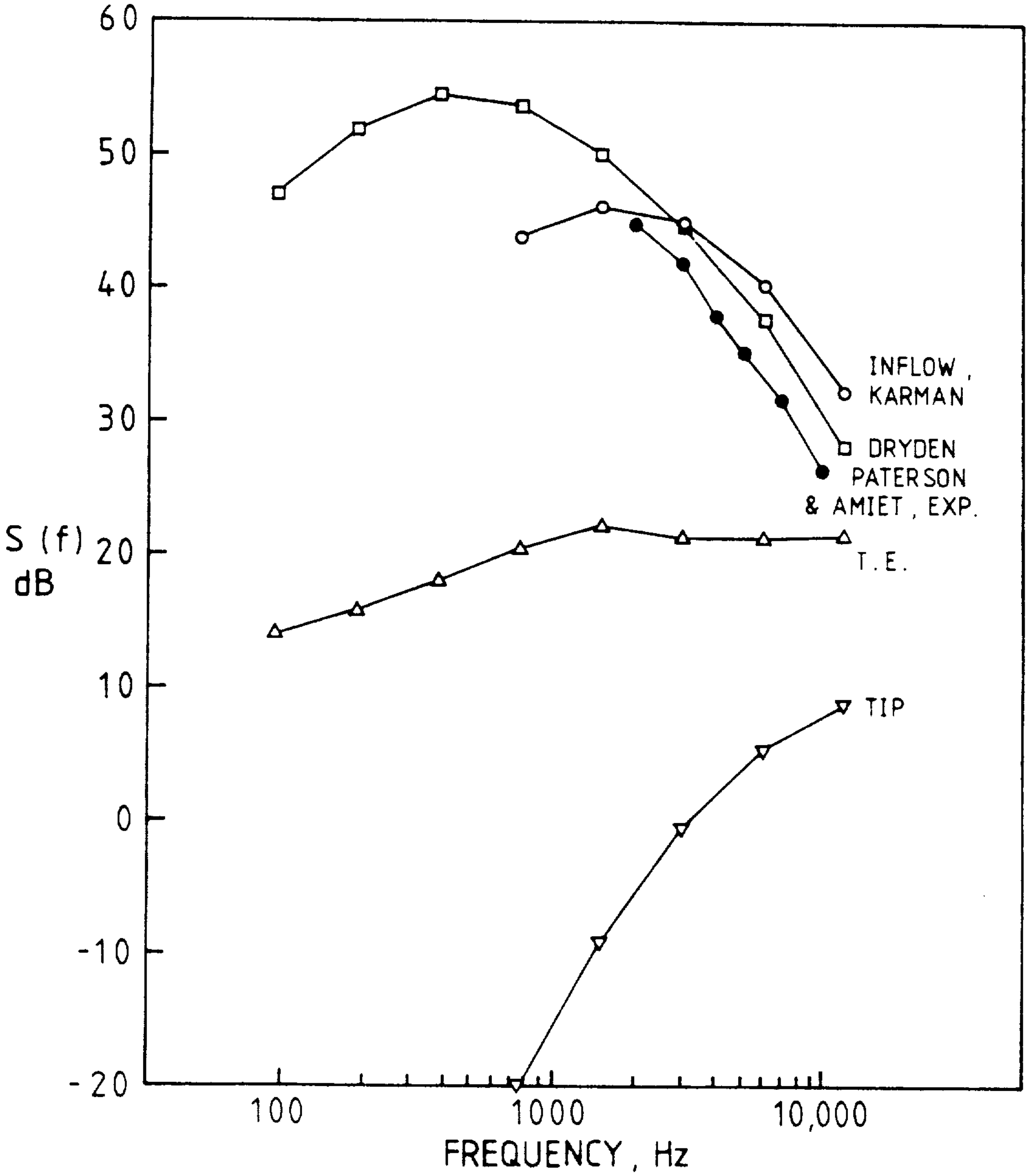

Figure 3.22: Comparison of Predictions for Model Helicopter Rotor, Experiment of Paterson and Amiet (1979), Test VA-M-4.

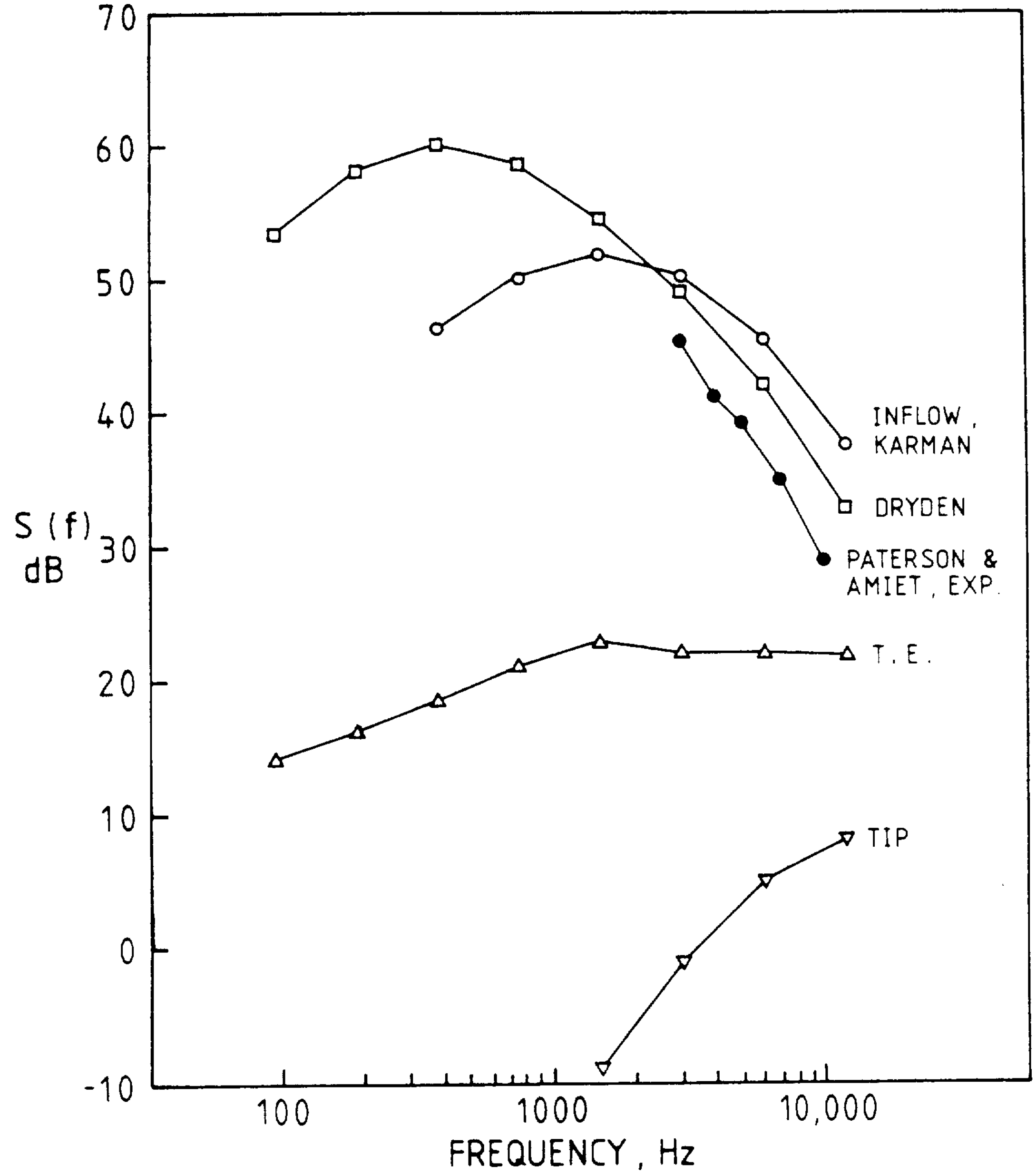

Figure 3.23: Comparison of Predictions for Model Helicopter Rotor, Experiment of Paterson and Amiet (1979), Test VA-L-3.

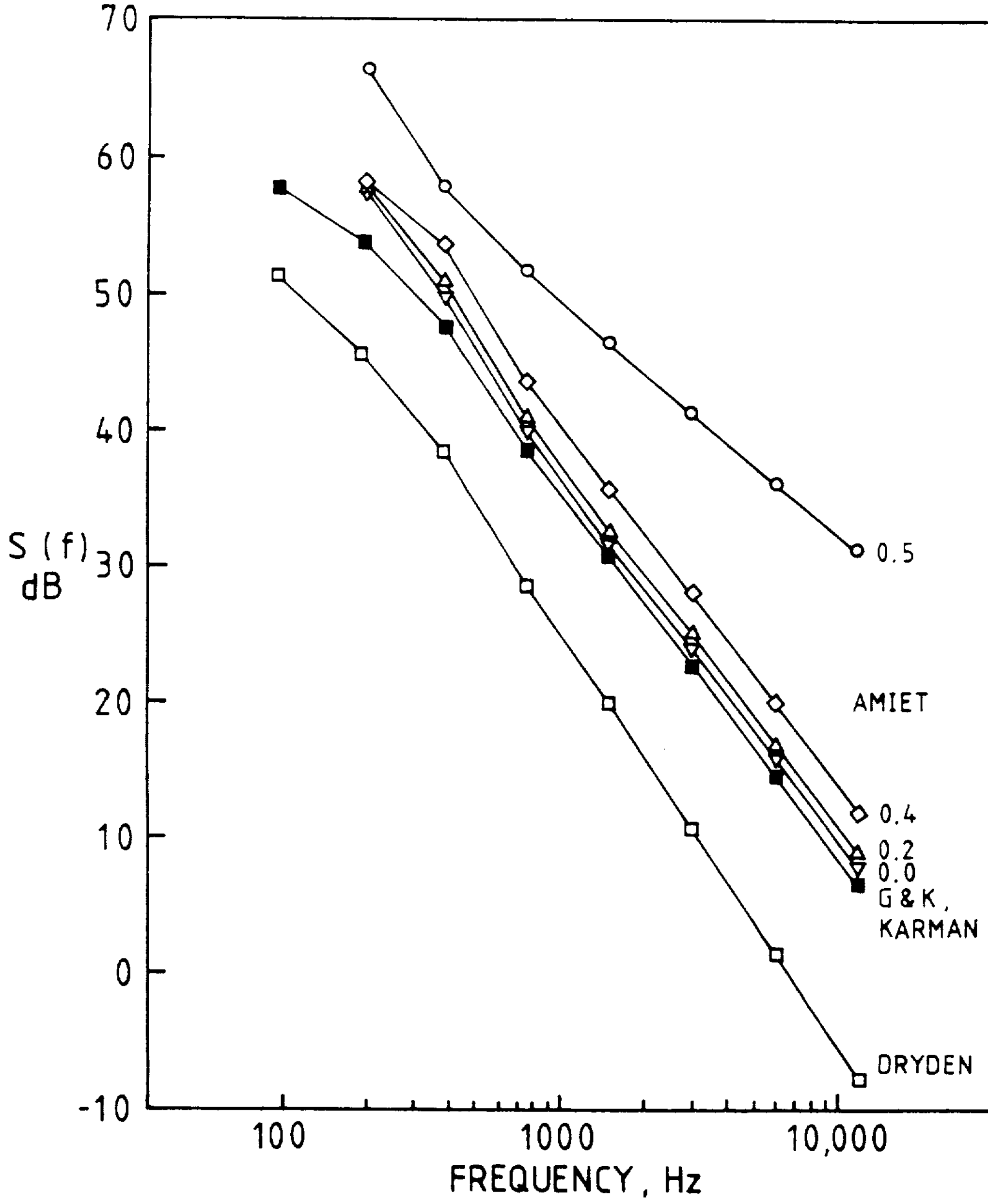

Figure 3.24: Effect of Advance Ratio on Rotor Inflow Turbulence Noise Calculation, UH-1 Main Rotor, $\phi = -60^o$, $\Lambda = 67$ m, w = 1 m/sec.

boundary layer thickness correlation rather than the flat plate results incorporated in their publications and in those of Amiet. In this boundary layer trailing edge noise case, the results again show that the effects of advance ratio are not important for values less than 0.4.

As discussed in a previous section, Amiet's computational model incorporates an accurate basic blade noise radiation directivity for the pressure normal to the blade mean chord line. The methods of George and co-workers approximate the basic directivity by a dipole normal to the rotor plane, which would be expected to lead to underestimates for angles near the rotor plane. Both Amiet's and George and co-workers' analyses ignore in-plane forces/noise mechanisms. Figures 3.26 through 3.28 compare the directivities for both inflow turbulence and trailing edge noises.

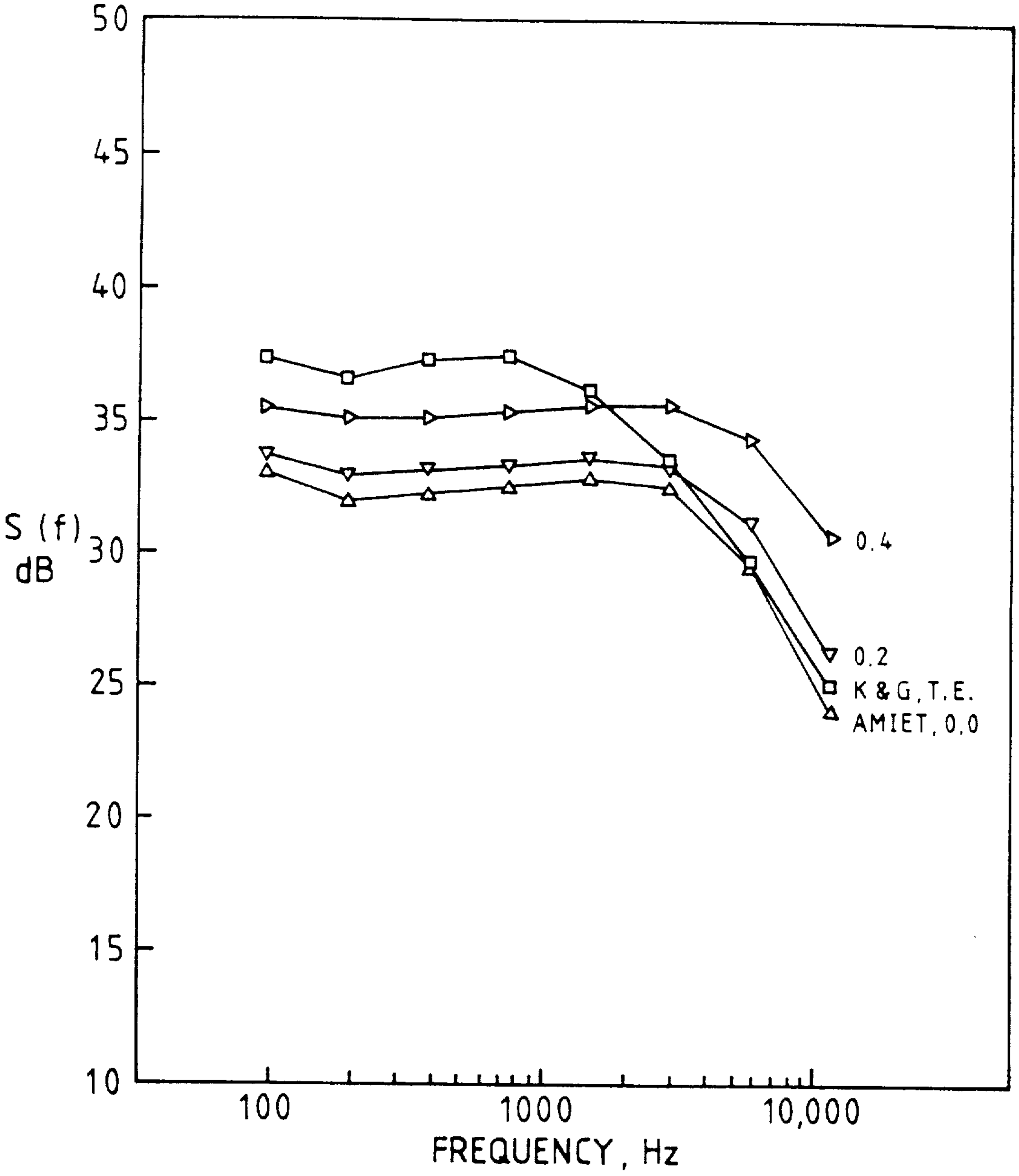

Figure 3.25: Effect of Advance Ratio on Rotor Trailing Edge Noise Calculation, UH-1 Main Rotor, $\phi = -90^{\circ}$.

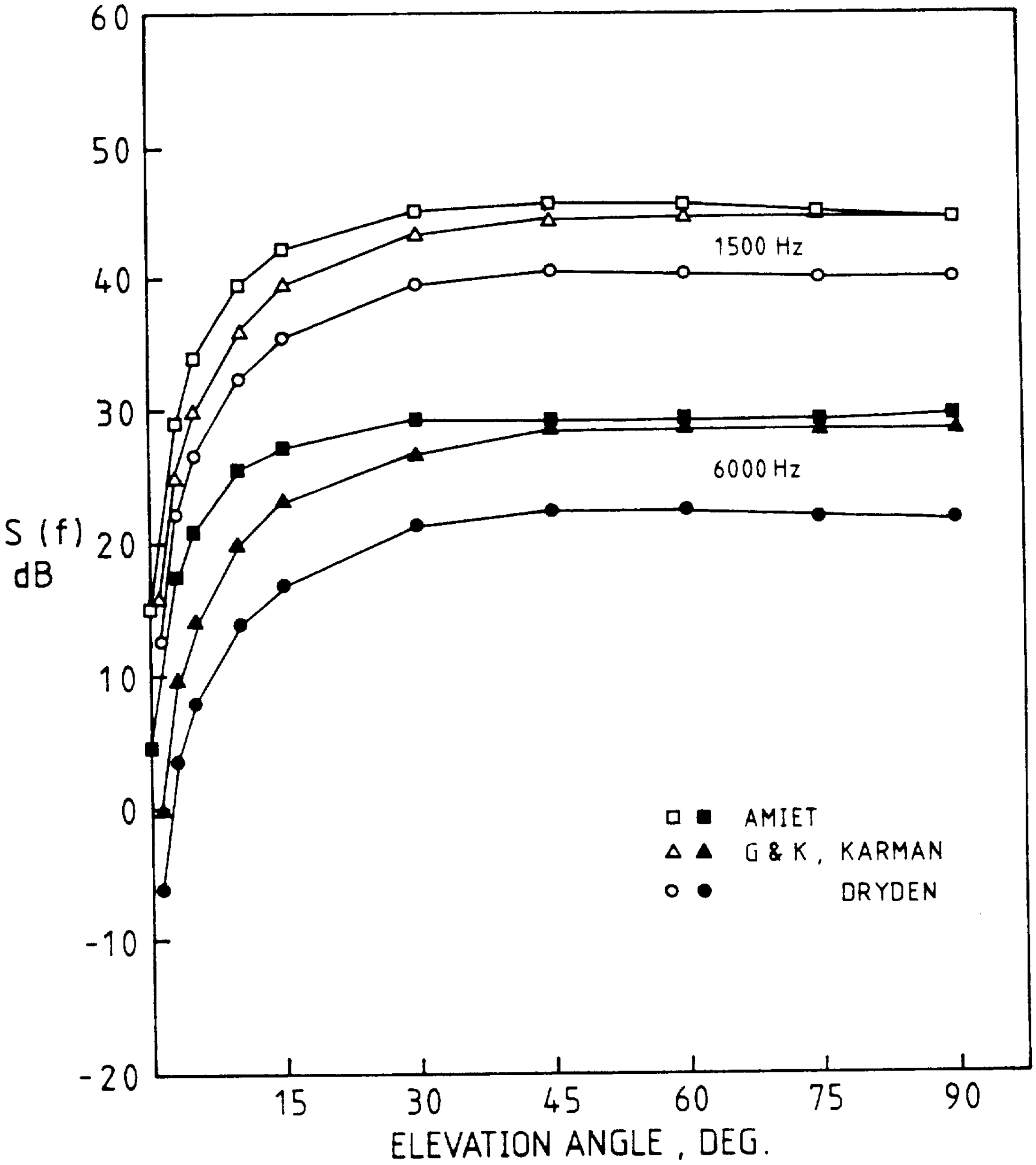

Figure 3.26: Directivity of Rotor Inflow Turbulence Noise 1500 Hz and 6000 Hz, S-55 Full Scale Rotor, $\Lambda = 0.57$ m, w = 1 m/sec.

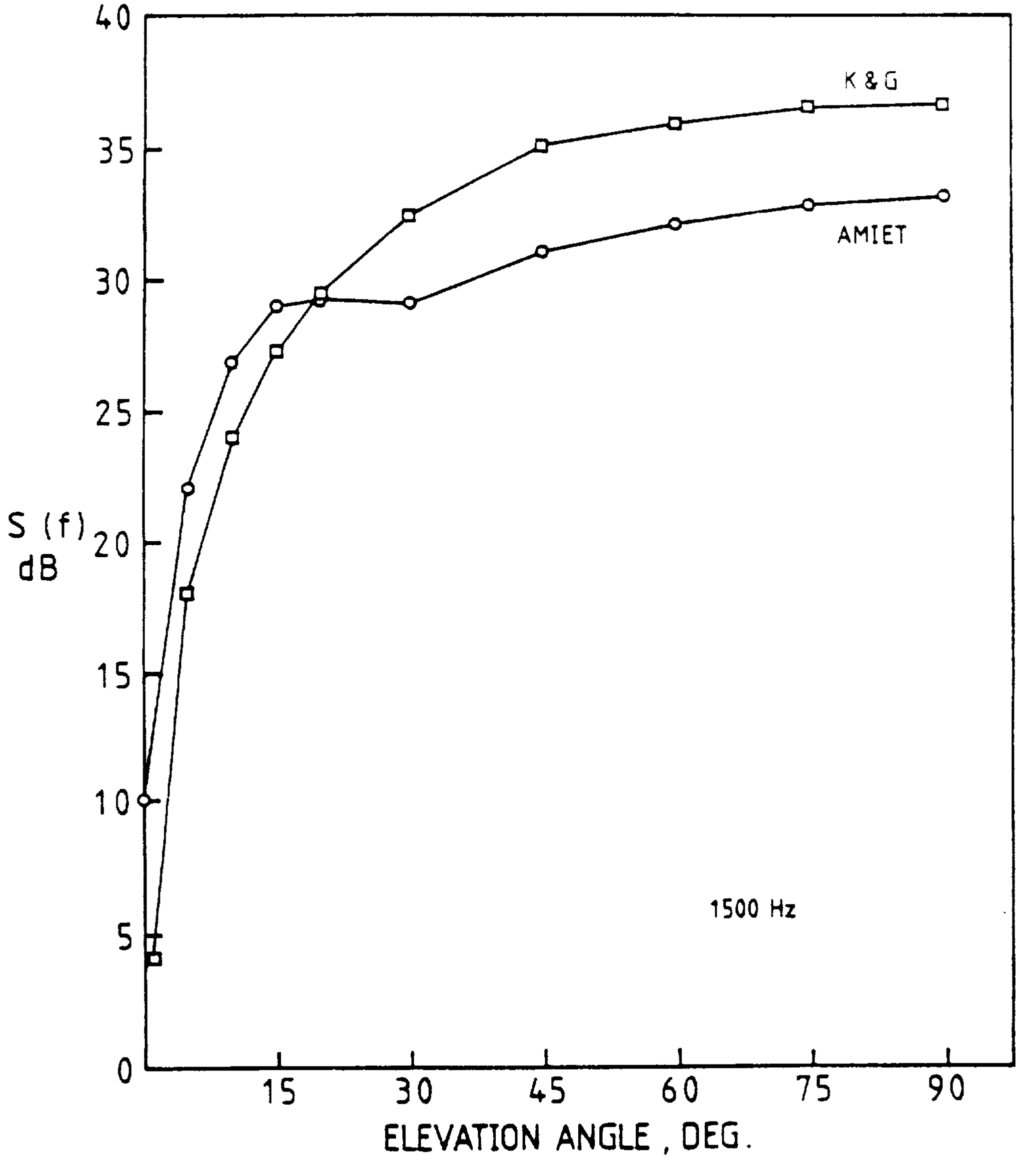

Figure 3.27: Directivity of Rotor Trailing Edge Noise, 1500 Hz, S-55 Full Scale Rotor.

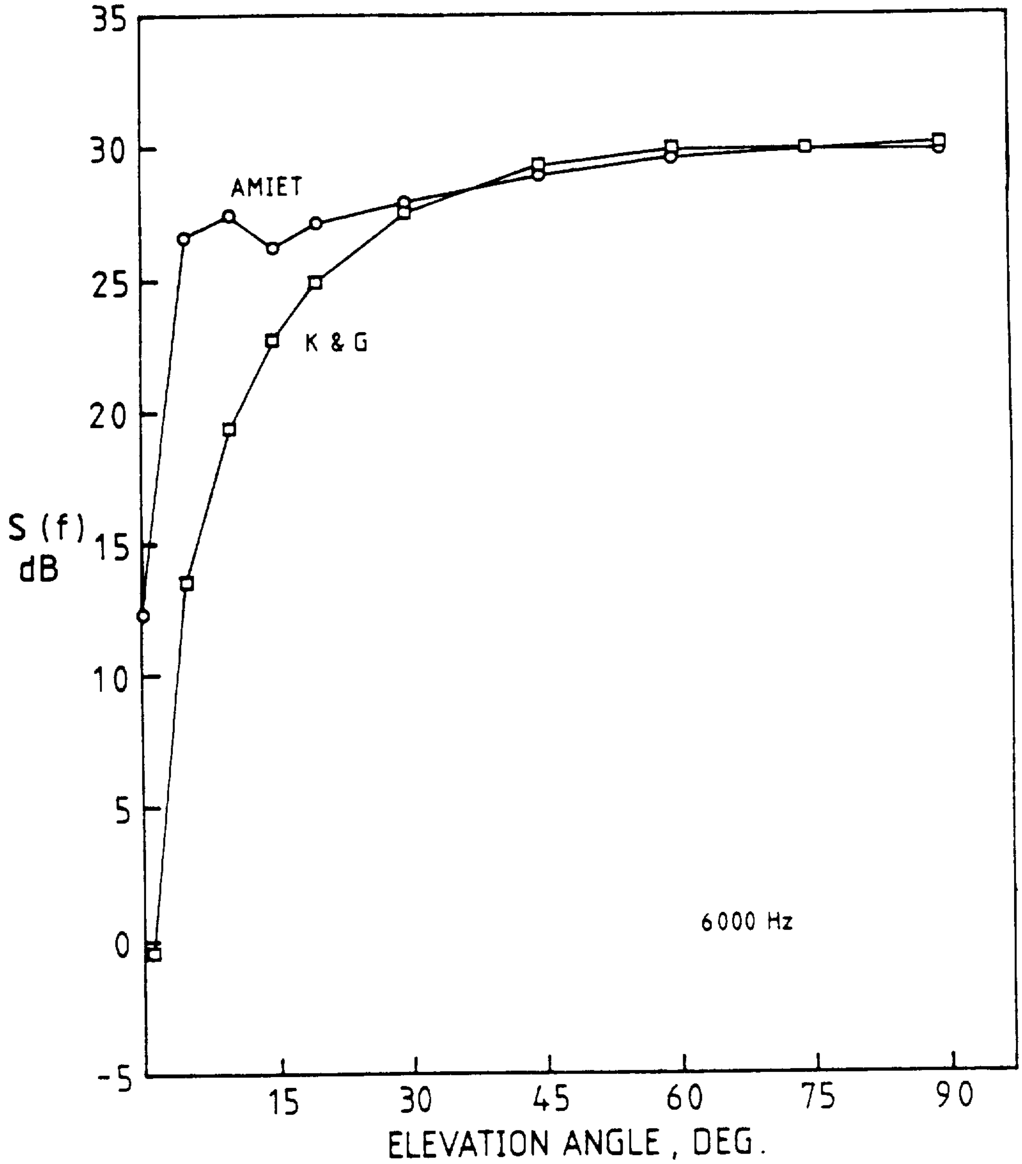

Figure 3.28: Directivity of Rotor Trailing Edge Noise, 6000 Hz, S-55 Full Scale Rotor.

Chapter IV

HELICOPTER TAIL ROTOR NOISE

In this chapter, various helicopter tail rotor harmonic and broadband noise mechanisms are studied and new source models are proposed. Of particular importance are those sources due to interactions with the wakes of the main rotor, the main rotor hub, the fuselage, and the engine exhaust are examined. The flow field around the tail rotor and the noise it generates are modeled using available aerodynamic and acoustic analysis along with some necessary estimates of turbulence properties. Representative calculations show that main rotor wake is the strongest contributor to both tail rotor harmonic and broadband noise. The fuselage separation wake, the engine exhaust, the main rotor hub, and the hub-shaft wakes are important to the tail rotor broadband noise only. The main rotor tip vortices are not important to tail rotor broadband noise. However, they have a major effect on the tail rotor harmonic noise; details of the tail rotor blade-main rotor tip vortices interaction will be discussed later in chapter V. The goal of the study discussed in this chapter is to determine the relative importance of various tail rotor harmonic and broadband noise mechanisms.

4.1 REVIEW OF PREVIOUS TAIL ROTOR NOISE RESEARCH

As mentioned in the Introduction, the importance of tail rotor noise was well appreciated by the year 1970 (Lynn, 1970). The complexity of the flow field around tail rotor has also been studied for some time because of its impact on tail rotor sizing, blade stall, fin interference, and directional control of helicopters. Some of the flows which have been identified are:

1) interaction of the tail rotor with the mean downwash flow field of the main rotor;
2) interaction with the rolled-up "ground vortices";
3) interactions with the main rotor blades' individual tip vortices;
4) interactions with the main rotor disk's "wingtip vortices" (from the overall horseshoe vortex due to the mean lift of the main rotor disk);
5) interactions with the wakes of stabilizer, fin, and tail boom;
6) operation of tail rotor in the "vortex ring" state.

One important finding of these studies was that it is desirable for the tail rotor to rotate "bottom forward" to minimize interactions with ground and wingtip vortices. Later, it was realized through other experiments that this direction of rotation is also desirable for noise reduction (Leverton, 1977, 1980). This is because the noise due to high speed interactions of the tail rotor blades with the main rotor tip vortices seem to be beamed in the blade motion direction. Leverton (1980) reported noise reductions of approximately 15 dBA in approach and 5 dBA overhead for an optimized tail rotor design.

While the transonic, near parallel and streamwise interaction characteristic of main rotors has been treated by several investigators (George and Chang, 1983c, 1984b; George and Lyrintzis, 1986; Srinivasan and McCroskey, 1984; McCroskey, Yu, and Smetana, 1984), the high speed, near normal incidence blade-vortex interaction characteristic of tail rotors has not been studied to date. The low speed, near normal incidence case has been studied by Schlinker and Amiet (1983), Amiet (1986), and by Ahmadi (1984a, 1984b).

The importance of wake ingestion on rotor-generated noise was shown in the study of Levine (1976). He reported increases of 5 to 10 dB in both narrowband and broadband noise when a Sikorsky S-58T operated with the main rotor wake being blown into the tail rotor.

Another experimental study of tail rotor-main rotor wake interaction noise involved wind tunnel tests of a model scale UH-1 with tail rotor position and direction of rotation as test parameters (Balcerak, 1976; Pegg and Shidler, 1978). Balcerak (1976) made a parametric study which varied tail rotor location, fin blockage area, tail rotor rotation direction, rotor speed, thrust, and the tail rotor operating mode (i.e. pusher/tractor). Later, Pegg and Shidler (1978) tested the same model, extending the work and emphasizing identification of the aeroacoustic mechanisms producing the noise. They found an approximately 12 dB increase in broadband noise when the main rotor flow was drawn through the tail rotor and significant increases in harmonics under various conditions. Combination tones due to the main rotor shed vortices and turbulent wake were apparent in the non-zero advance ratio cases.

Some of the representative results of Balcerak (1976) are given in Figures 4.1 through 4.4. Figures 4.1 and 4.2 give the noise spectra for isolated main and tail rotors. Figure 4.3 shows the measured noise spectrum in a hover condition when both rotors are operated. Notice that it is essentially the sum of the spectra shown in Figures 4.1 and 4.2. Figure 4.4 shows the noise spectrum measured for a forward flight condition (advance ratio based on main rotor tip speed is 0.28) when both rotors are operated; significant increases in both harmonic and broadband noise are apparent. These studies also showed, as did Leverton's (1977, 1980), that interaction noise is more severe when the advancing rotor blades interact with the main rotor wake. Further discussions of these and Leverton's experiments were given by White (1978).

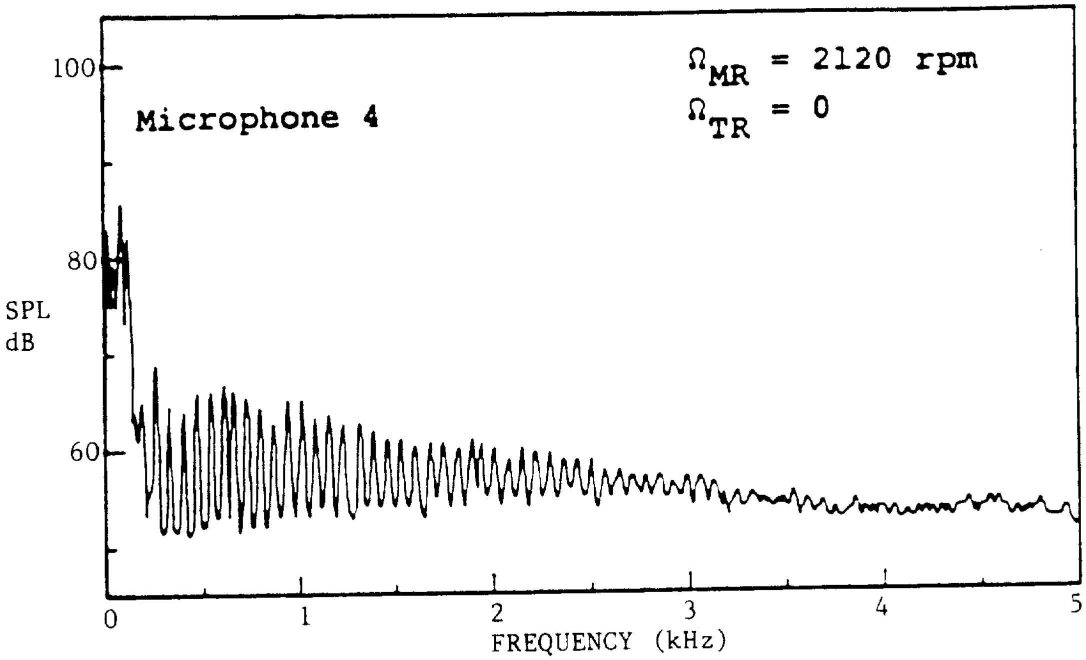

Figure 4.1: Noise Spectrum, Main Rotor Only, from Balcerak (1976).

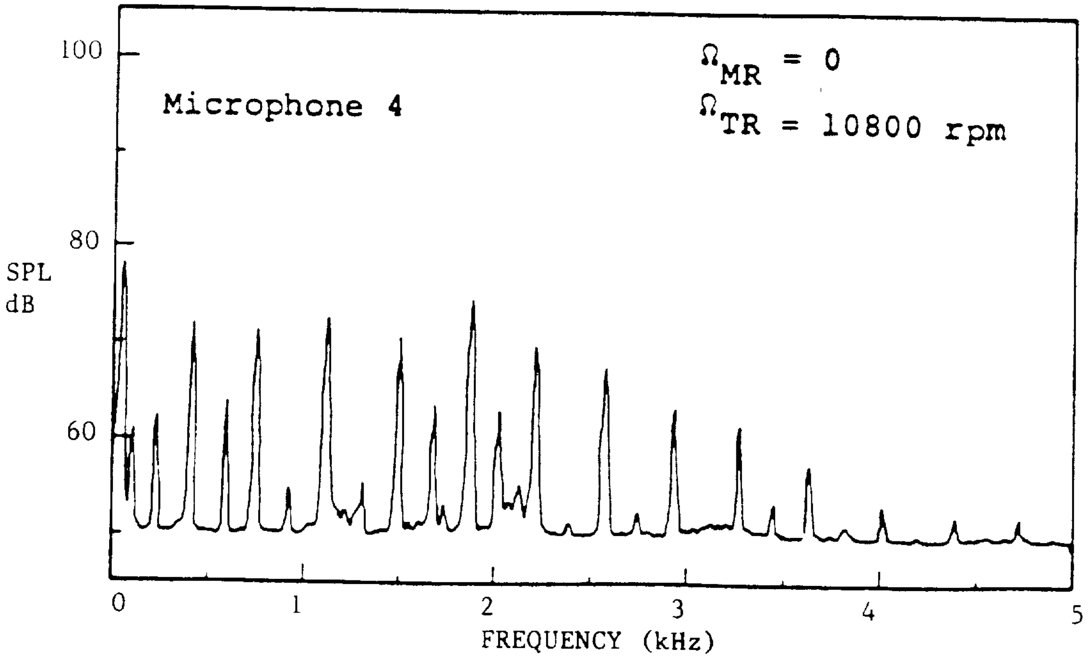

Figure 4.2: Noise Spectrum, Tail Rotor Only, from Balcerak (1976).

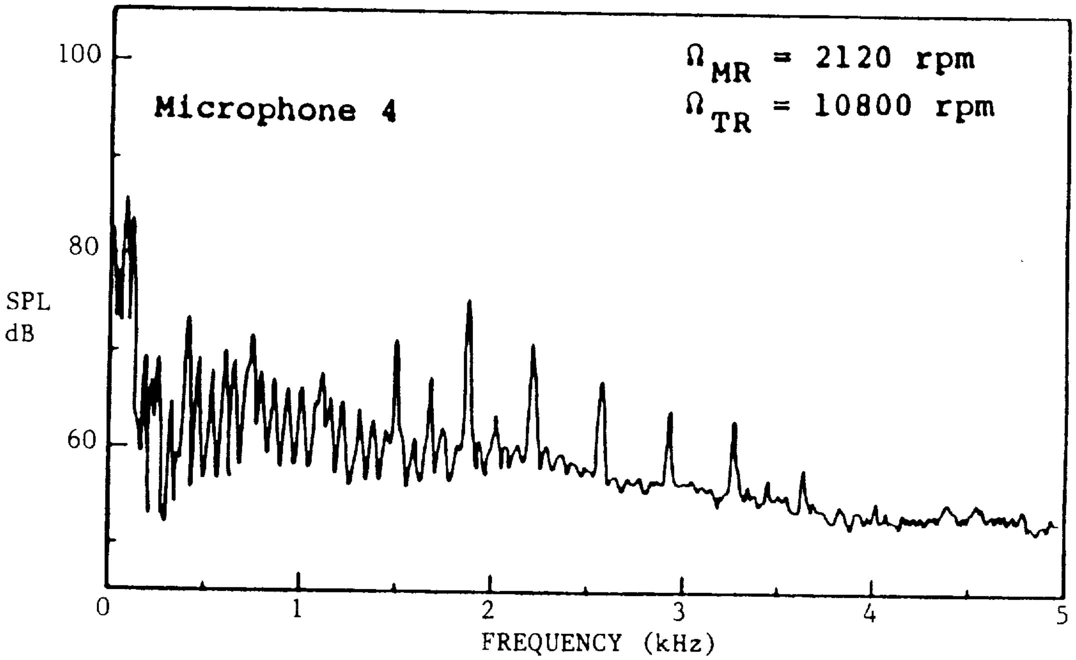

Figure 4.3: Noise Spectrum, Both Rotors, Hover, from Balcerak (1976).

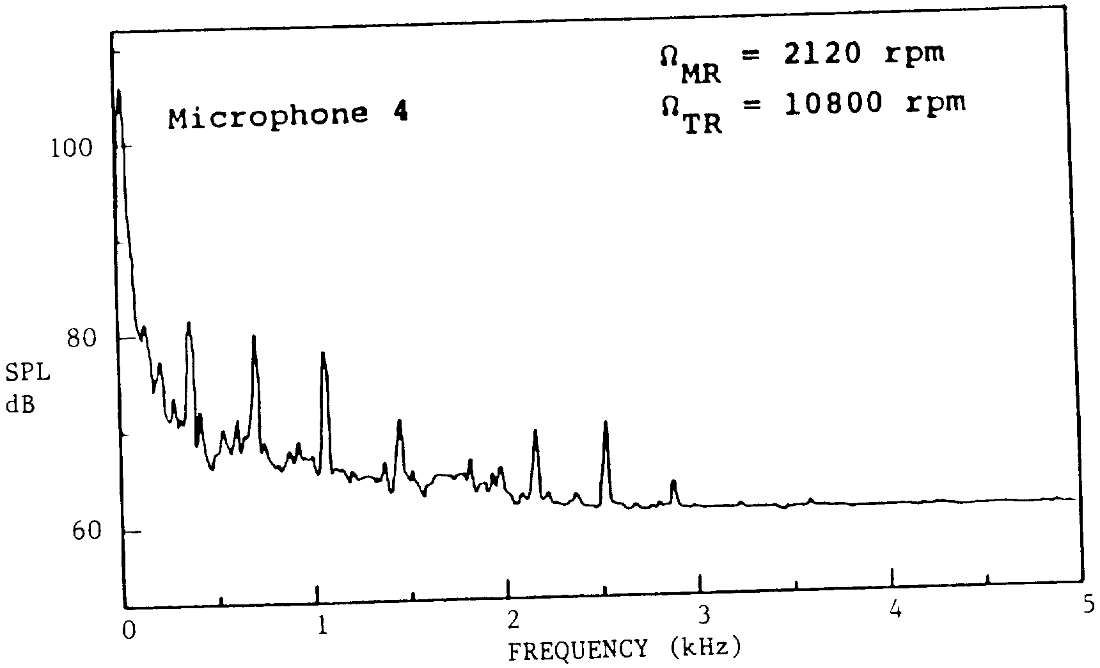

Figure 4.4: Noise Spectrum, Both Rotors, $\mu = 0.28$, from Balcerak (1976).

Tail rotor noise reduction techniques have been studied by Levine (1976) using the methodology available at that time. He modeled the wake using a simple average rigid wake model of Heyson (1961). This model assumes the wake to be a skewed cylinder of radially varying vorticity of the same diameter as the main rotor. Using the velocities from Heyson's model, Levine computed the low-order airload harmonics on the tail rotor blades. Then, the noise due to the azimuthally-varying blade loading is calculated using the analysis of Lowson and Ollerhead (1969). This approach obviously leaves out most of the complexities of a real problem.

4.2 PRESENT RESEARCH

In the present study, sample calculations are made for a UH-1 type helicopter in order to compare the noise spectra from the various mechanisms. In each case the helicopter is assumed to fly in a condition such that maximum interaction occurs. For example, when calculating fuselage wake effects, the full wake width is assumed to impinge on the tail rotor.

4.2.1 Isolated Tail Rotor Noise

In the present study, isolated tail rotor broadband noise is calculated using the analyses we discussed in chapter III. The results are compared to those from the main rotor to determine the relative importance of isolated tail rotor broadband noise. Mechanisms considered are inflow turbulence noise (due to the interaction with ambient turbulence), boundary layer/trailing edge noise, tip vortex formation noise, and trailing edge thickness noise (due to turbulent vortex shedding).

4.2.2 Harmonic Noise Due to Non-uniform Inflow

In order to predict the tail rotor harmonic noise due to the interactions with various non-turbulent mean wakes, three steps are necessary:

1) Predict the inflow velocities at the tail rotor disk (which include the wakes of main rotor, main rotor hub/shaft, fuselage, and engine exhaust);

2) Calculate tail rotor blade airload harmonics using the known incident velocity;

3) Calculate the harmonic noise from the known loading harmonics.

The comprehensive rotorcraft prediction code (CAMRAD) of Johnson (1980, 1981) is used for the prediction of main rotor mean wake. This code calculates the main rotor blade section loadings based on non-uniform induced inflow and on the forward-flight free-wake model of Scully (1975). The induced velocities at the tail rotor disk can then be found. Figure 4.5 shows the sketches of the boundaries of the main rotor wake at various air speeds.

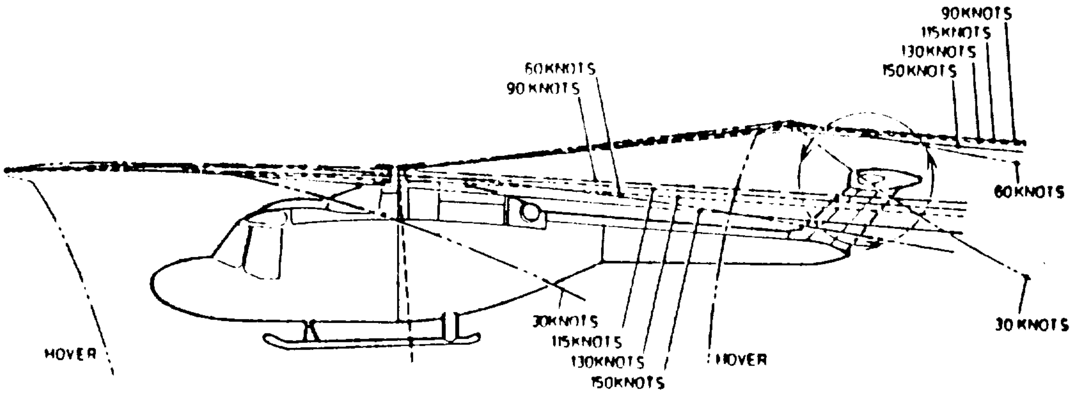

Figure 4.5: Sketches of the Main Rotor Wake and Engine Exhaust Flow, from Leverton (1977).

For tail rotors with rotational speeds which are different from that of the main rotors, the CAMRAD code does not allow the detailed loading calculation on individual tail rotor blades. Instead the code uses the velocity at the tail rotor hub to find the tail rotor blades' loading. Thus, the noise calculated from these loadings may be inaccurate if the interactions with the smaller scale velocity perturbations in the main rotor wake are dominant.

The engine exhaust mean flow is approximated by the far field results of turbulent jets (Schlichting, 1979):

$$u_x = \frac{3K}{8\pi\epsilon_0 x(1+\eta^2/4)^2}$$

$$u_r = \frac{(3K)^{1/2}(\eta-\eta^3/4)}{4\pi^{1/2}x(1+\eta^2/4)^2} \tag{4.1}$$

where

K = $(1.59b_{1/2}U_{jet})^2$

$b_{1/2}$ = radius of the engine exhaust jet ($\simeq 0.848x$)

η = $((3K)^{1/2}/(4\pi^{1/2}\ \epsilon_0))\ (y/x)$

ϵ_0 = $0.0256b^{1/2}U_{jet}$

x = streamwise coordinate

y = radial coordinate

For the fuselage wake, we estimated the velocity field at the tail rotor using a velocity distribution:

$$\frac{U}{U_0} = 1 - C\ e^{-(y^2/\beta^2)} \tag{4.2}$$

The values of C and β are estimated from the measurements on a BK-117 helicopter (Huber and Polz, 1982) and scaled to UH-1D. The fuselage separation wake can also be similarly modelled by scaling the results of Polz and Quentin (1981).

For the main rotor hub, the characteristics of axisymmetric far wakes are:

$$\frac{U}{U_0} = 1 - \left[\frac{C_d A}{b^2 x^2} \right]^{1/3} e^{-(y^2/b^2)} \tag{4.3}$$

where

C_d = drag coefficient

$b = (0.18 C_d A x)^{1/3}$

A = frontal area of the rotor hub

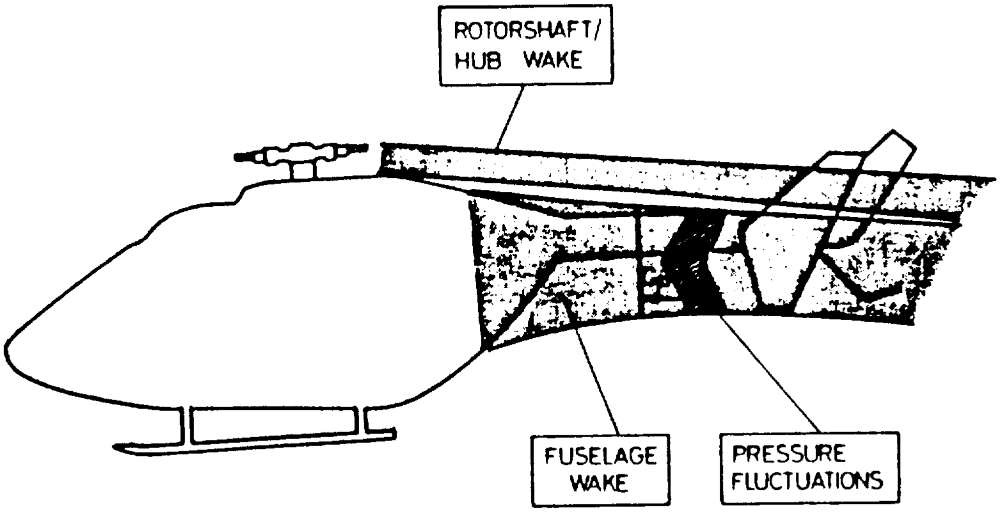

Figure 4.6: Sketches of the Wakes from Fuselage and Main Rotor Hub, from Polz and Quentin (1981).

The loadings on the tail rotor are calculated with Johnson's CAMRAD code (Johnson, 1980, 1981) or with the quasi-steady, blade-element theory for rotors (Dommasch et al., 1967). These loadings are then decomposed to find the harmonics using a Fast Fourier Transform algorithm (Bergland and Dolan, 1979). The harmonic noise is then calculated using the analysis of Lowson and Ollerhead (1969). This approach should be accurate enough for the present comparisons, but it would be better to use the non-compact methods of Farassat for more accurate results (Farassat, 1975, 1983).

4.2.3 Broadband Noise Due to Various Turbulent Wake Effects

The primary broadband noise mechanism is the inflow turbulence noise. Both Dryden and Karman spectrum are used in the present study to define the turbulent inflow. We need to estimate the turbulent intensities and the turbulent integral scales for the cases considered.

The turbulence due to the overall main rotor wake was estimated in two ways:

1) based on shear layer results for the edge of the wake, we estimate the intensity and the turbulent length scale as (Townsend, 1976)

$$\Lambda = 0.5 \text{ (main rotor radius), and} \tag{4.4}$$

$$w = 0.15\, U_{downwash}; \text{ or}$$

2) based on the blade drag, we estimate

$$\Lambda = 0.4 \text{ (main rotor chord), and} \tag{4.5}$$

$$w = 0.5 \text{ (main rotor blade speed).}$$

These estimates are quite approximate, but there is currently no information available to support more accurate estimates. Some work has begun on turbulence in wind turbine wakes (Bossanyi, 1983) but it has not developed to the stage of being applicable to the rotor near wake region.

In order to estimate the turbulence in the core of the main rotor tip vortices, several experimental studies are considered (Schlinker and Amiet, 1983; Biggers and Orloff, 1975; Tangler, 1978; and Owen, 1970). From their results, it is estimated that

Λ = vortex core diameter $\simeq$ 0.15 (main rotor chord), and

$w = 0.13\ U_{c,max}$

where $U_{c,max}$ is the maximum circumferential velocity of the main rotor tip vortex.

The turbulence properties of the engine exhaust jet and hub wakes were estimated based on the properties of similar flows (Schlichting, 1979; Tennekes and Lumley, 1972). For the 2-D hub shaft wake, we estimate

Λ $\simeq$ hub shaft diameter, and

$w = 0.35\ U$

where U is the forward flight speed of the helicopter. For the engine exhaust jet, we estimate

Λ $\simeq$ diameter of the exhaust jet, and

$w = 0.25\ U_{jet}$

where U_{jet} is the engine exhaust centerline velocity.

For the fuselage near wake, it is estimated that

$\Lambda \simeq 0.66\ D_{sep}$, and

$w = 0.16\ U$

where D_{sep} is the diameter of the fuselage wake.

The properties of the axially symmetric far wake are used to model the wakes of main rotor hub or the fuselage, we estimate

$\Lambda \simeq D$, and

$w = 0.2\ U$

For an unseparated fuselage boundary layer we estimate

$\Lambda \simeq \delta_{BL}$, and

$w = 0.13\ U$

where δ_{BL} is the boundary layer thickness on the fuselage.

For each turbulent flow it is also necessary to estimate the fraction of the tail rotor disk immersed in the turbulence. For the present exploratory calculations, we assumed the maximum values possible for each case, i.e., the helicopter is trimmed so that the maximum amount of the flow in question (e.g., wake or jet) are incident on the tail rotor.

For the engine exhaust jet, the effective tail rotor area is estimated to be 1/2 of the entire tail rotor disk; for the fuselage wake, 2/5; for the unseparated fuselage boundary layer, 1/8; and for the main rotor wake, the entire tail rotor disk is effective. For the tip vortices the intersection area was time-averaged over the passage of the vortices through the disk; for "unburst" vortices the effective area is about 6 x 10^{-4} of the tail rotor disk, and for "burst" vortices the effective area is about 10^{-2} of the tail rotor disk.

It should be noticed that these turbulent properties are not conservative estimates thus the results represent maximum noise that may be generated by the tail rotor.

4.3 RESULTS AND DISCUSSIONS

In the present study, calculations were made for parameters representative of a UH-1 helicopter. In order to calculate the interactions with the main rotor wake, conditions of level flight at approximately 100 mph are assumed.

The first cases calculated were the basic broadband noise sources of the isolated main rotor and tail rotor, the results are shown in Figure 4.7. The sources include atmospheric inflow turbulence, boundary layer-trailing edge interaction, tip vortex turbulence-trailing edge interaction, and trailing edge thickness noise. The last mechanism is calculated for both 1.27 mm (0.05 inches for typical UH-1 tail rotor blades) and for 2.54 mm trailing edge thickness. The results are given in terms of one Hertz bandwidth spectra for an observer at a distance of 62.5 meters to the rotor hub and at an angle of 63^o from the tail rotor plane (-27^o from the main rotor plane). It is clear that the isolated tail rotor generates far less broadband noise than the main rotor, except perhaps when the tail rotor blades' trailing edge are blunted.

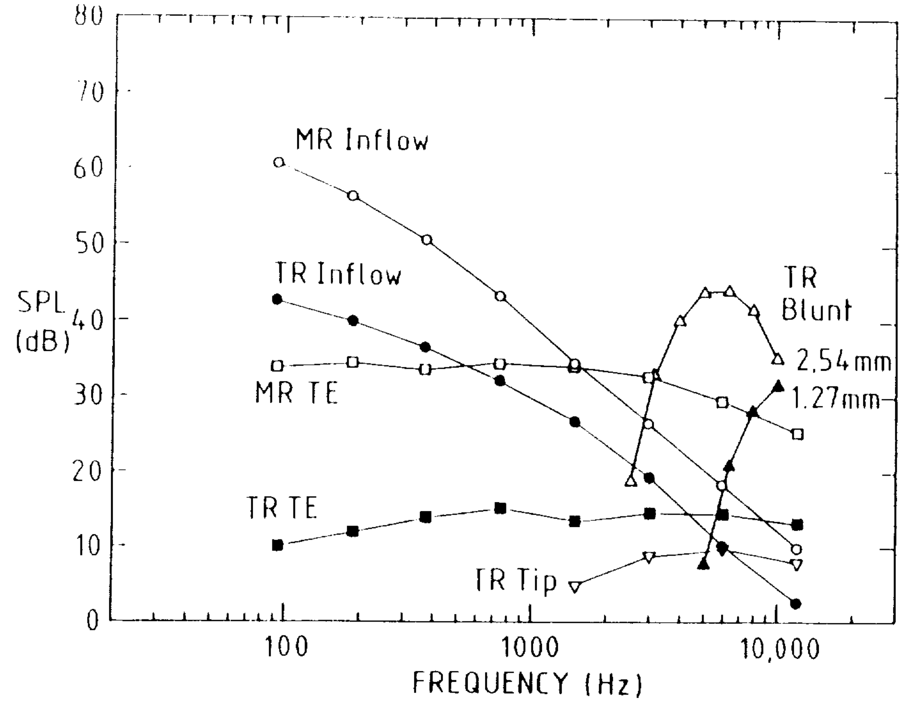

Figure 4.7: **Main Rotor and Tail Rotor Broadband Noise (Inflow Turbulence Noise Due to Ambient Turbulence).**

Figure 4.8 presents the calculated tail rotor noise due to the interactions with the main rotor wake, which is calculated using Johnson's CAMRAD code. Clearly the lower harmonics are very important. The tail rotor broadband noise due to the main rotor wake turbulence is also very important; it can be on the order of 15 dB greater than the main rotor broadband noise in some frequency ranges, depending upon the actual turbulence scales.

Figure 4.9 presents calculations for the tail rotor broadband noise due to interactions with the turbulence in the vortex cores of the main rotor wake. Clearly the noise is much less than that due to the main rotor turbulent wake. This is because the effective area in this case is much less than other tail rotor broadband noise mechanisms.

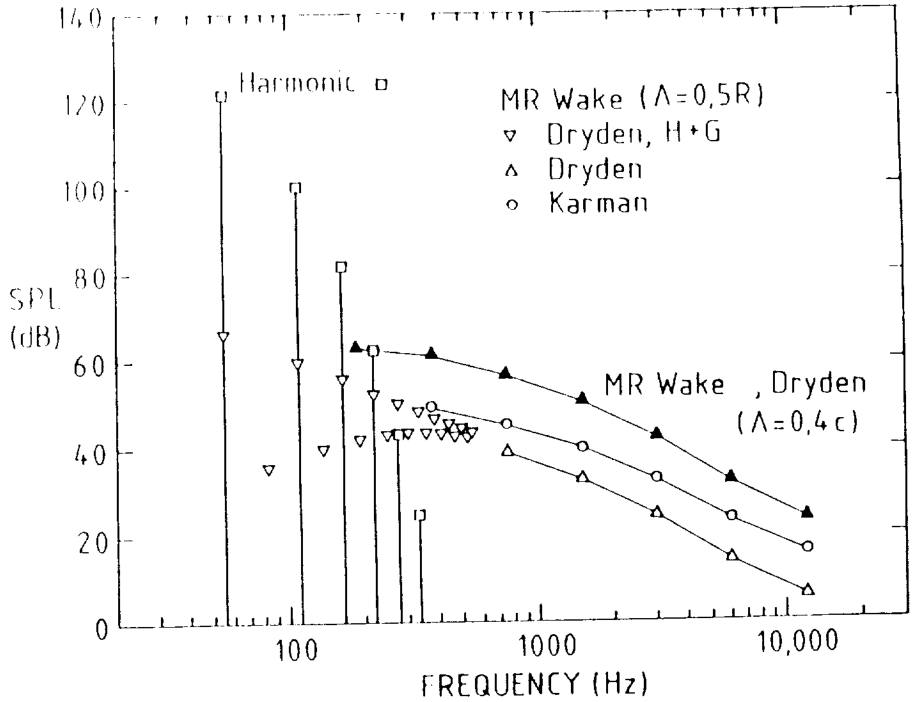

Figure 4.8: **Tail Rotor Harmonic and Broadband Noise Due to Interactions with the Main Rotor Wake.**

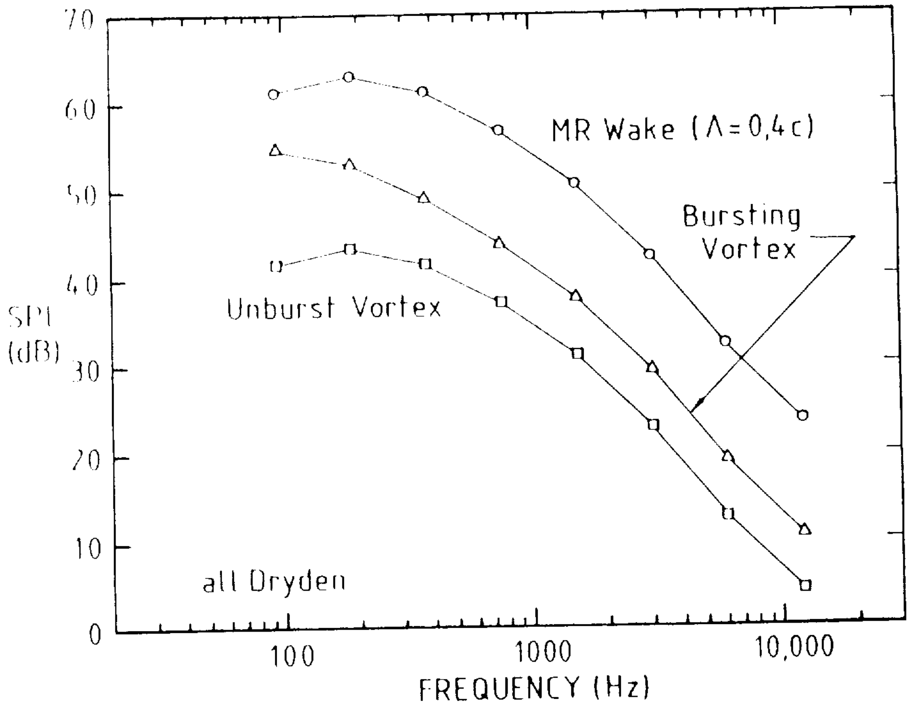

Figure 4.9: Tail Rotor Harmonic/Broadband Noise Due to Interactions with Main Rotor Tip Vortices.

Figure 4.10 shows the tail rotor noise due to interactions with the fuselage wake. The separated flow harmonic noise is well below that calculated for the tail rotor - main rotor wake interaction shown in Figure 4.8. The broadband noise is quite important since the turbulent intensity is high and the effective area is large. The calculations using the analysis of Homicz and George (1974) show the peak and valley structure of the broadband noise at low frequencies. The attached fuselage boundary layer wake effects are also shown. Here the effect of turbulent length scale is evident; an attached boundary layer generates smaller scale turbulence in its wake compared to the fuselage separated flow case. Thus, the noise spectra differ primarily in the low frequency region where the larger scales of the separated turbulence contribute more strongly.

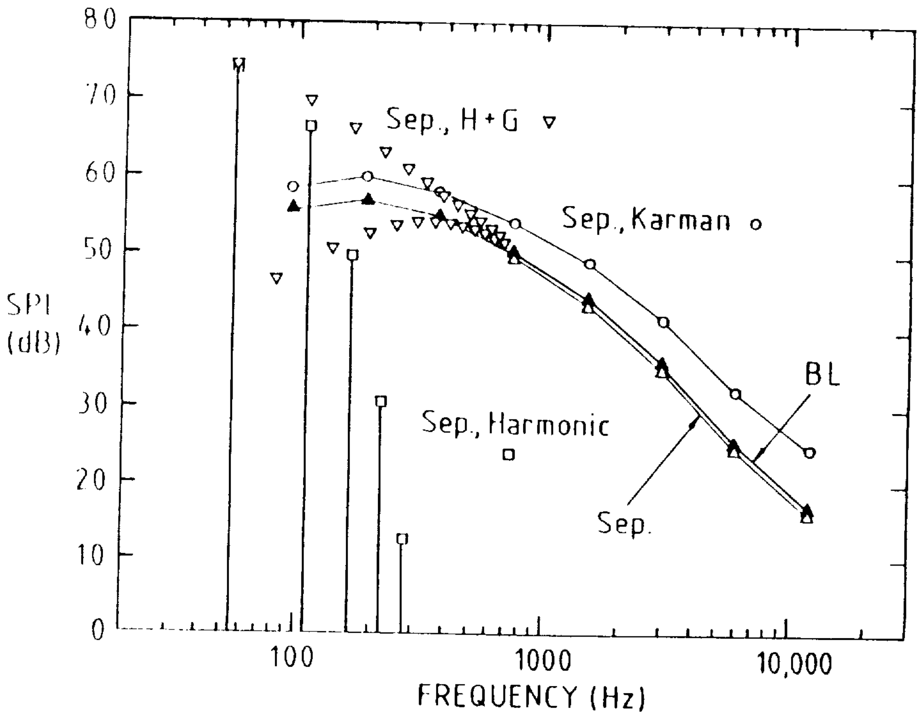

Figure 4.10: Tail Rotor Harmonic/Broadband Noise Due to Interactions with the Fuselage Wake.

The engine exhaust flow interaction effects are shown in Figure 4.11. Both the harmonic and broadband noise are important. The effect of turbulent spectral shape (i.e. Dryden vs. Karman) is evident. Figure 4.12 shows calculations for different relative positions of the tail rotor and the assumed engine exhaust. The harmonics are higher for the case where the advancing blade is interacting with the maximum velocity increment.

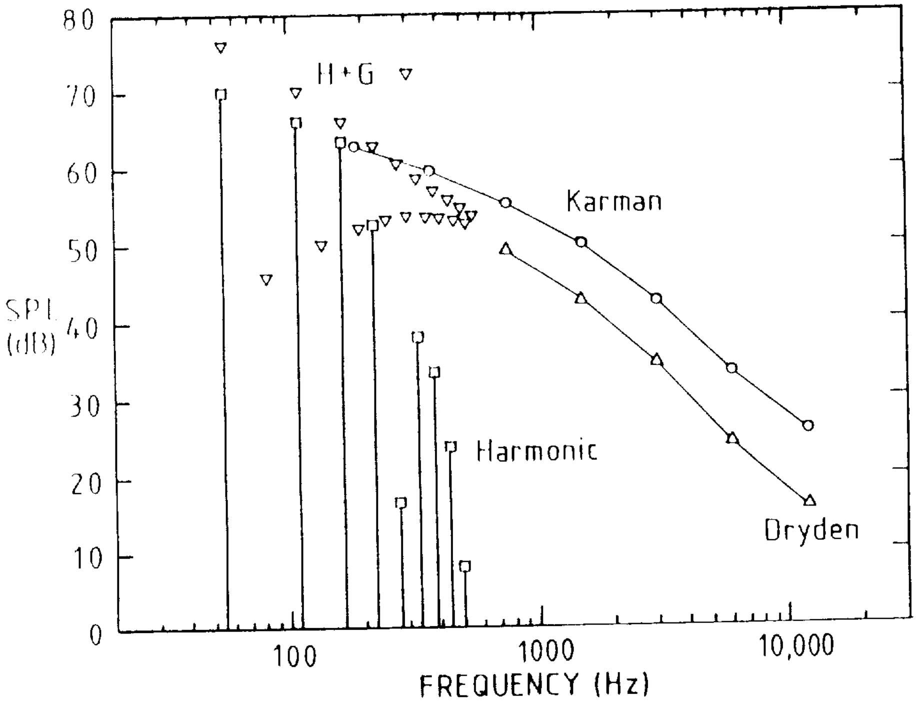

Figure 4.11: Tail Rotor Harmonic/Broadband Noise Due to Interactions with the Engine Exhaust Flow.

The main rotor hub/shaft flow interaction effects are shown in Figure 4.13, the wakes of the main rotor hub and shaft are both shown to be important.

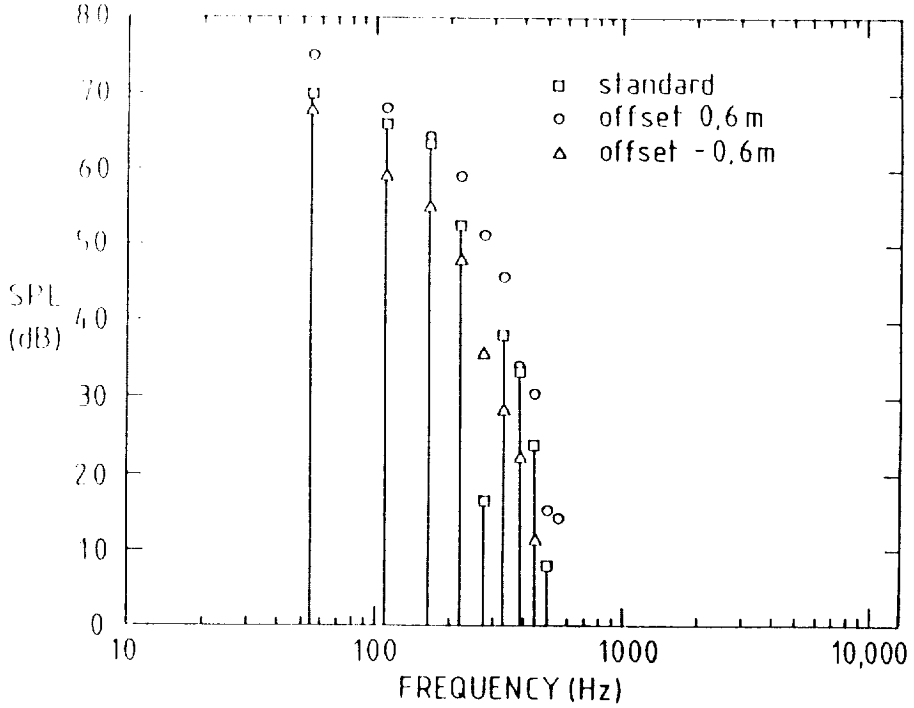

Figure 4.12: **Effects of the Engine Exhaust Flow Position on Tail Rotor Harmonic Noise.**

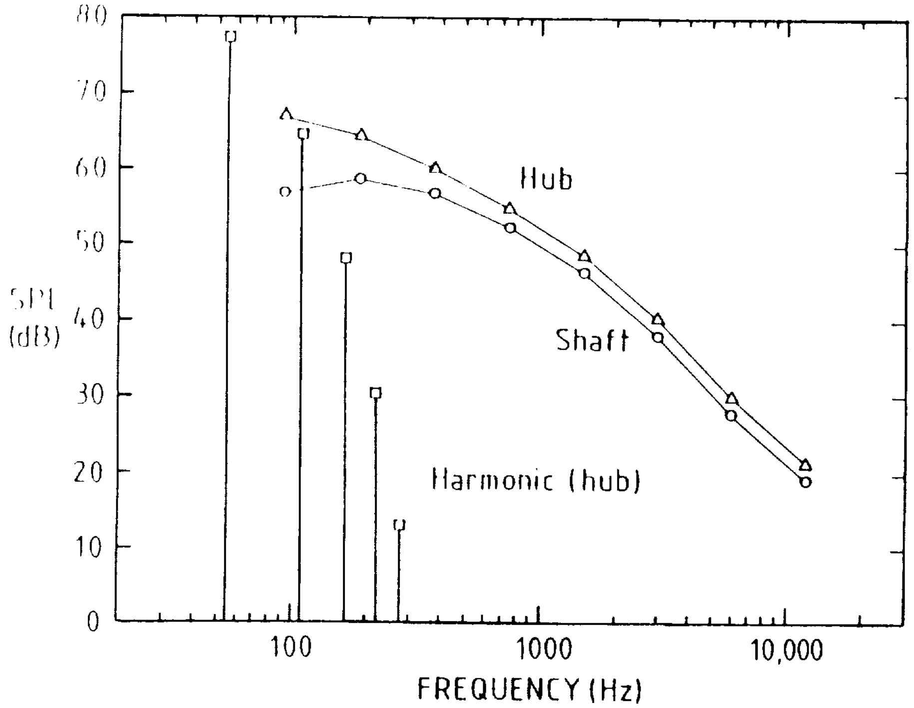

Figure 4.13: **Tail Rotor Harmonic/Broadband Noise Due to Interactions with the Main Rotor Hub/Shaft Wake.**

Chapter V

TAIL ROTOR BLADE-VORTEX INTERACTION

In the preceding chapter, we pointed out that under most operating conditions, tail rotors contribute significantly to overall helicopter noise in both harmonic and broadband forms. In this chapter, we study the tail rotor harmonic noise due to interactions between tail rotor blades and the main rotor tip vortices. It is found that this noise source accounts for previously not understood harmonic component of the noise spectrum.

Figure 5.1 sketches the geometries of the tail rotor blade-vortex interaction and the main rotor blade-vortex interaction. These interactions are similar in a sense since, in both cases, the rotor blades are interacting with the vortices shed from the main rotor. However, they are different because of the relative orientations. The tail rotor blade-vortex interactions generally occur with vortices with near-normal orientations to the tail rotor plane.

In the present study, the acoustics of the tail rotor blade-vortex interaction is treated by the analysis of Amiet (Schlinker and Amiet, 1983, 1986a). The acoustic analysis requires information on vortex properties and individual vortex geometry as its inputs. In the present study, these inputs are calculated using the CAMRAD main rotor free wake geometry analysis (Johnson, 1980; Scully, 1975).

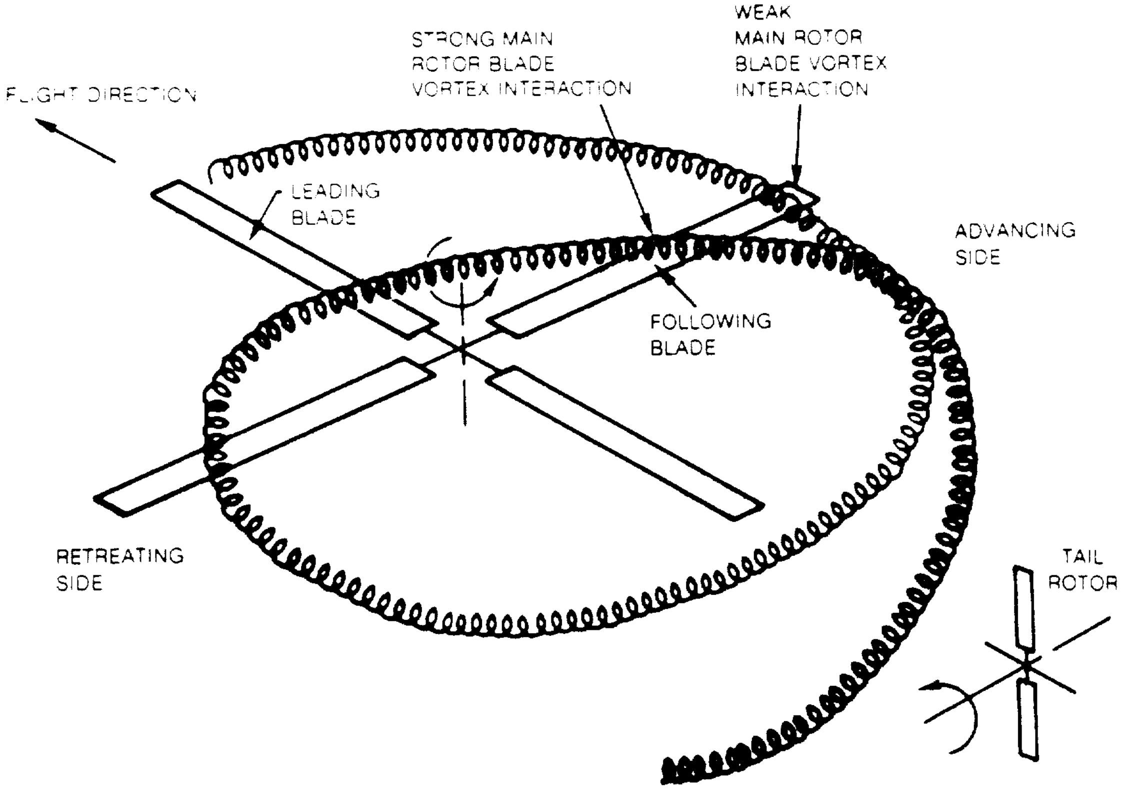

a) Illustration of Main Rotor and Tail Rotor Blade-Vortex Interactions.

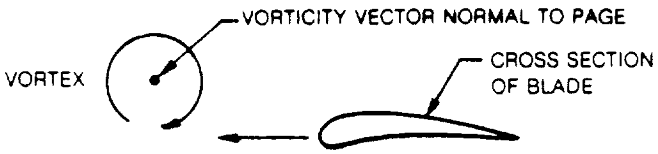

b) Illustration of Main Rotor Blade-Vortex Interaction with Vortex Parallel to Leading Edge.

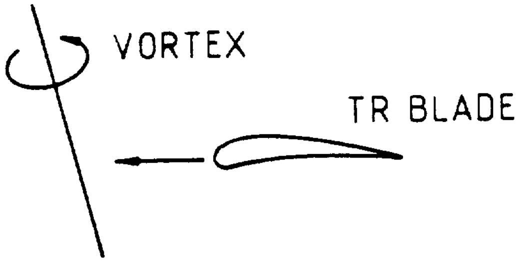

c) Illustration of Tail Rotor Blade-Vortex Interaction.

Figure 5.1: Geometry of the Helicopter Tail Rotor Blade-Vortex Interactions, from Schlinker and Amiet (1983).

The acoustic pressure histories are calculated for selected cases for representative helicopters; the results are compared to the tail rotor loading and high speed thickness noise calculated by Farassat's linear acoustic analysis (Farassat, 1983), and are found to be very important. This noise mechanism will be seen to depend strongly upon the helicopter operating conditions and the location of the tail rotor relative to the main rotor.

5.1 ACOUSTICS OF NEAR-NORMAL BLADE-VORTEX INTERACTION

In the present study, the tail rotor blade-vortex interaction is modelled as a 2-dimensional blade-vortex interaction problem (an airfoil of infinite span chopping through a moving vortex with near normal orientation). The analysis was originally developed by Amiet (Schlinker and Amiet, 1983; Amiet, 1986a), who assumed that the noise is generated by an unsteady loading fluctuation (i.e. dipole) on a tail rotor blade when it chops through a near normally incident vortex. The unsteady loadings can be calculated using thin-airfoil theory, and the far-field noise can then be calculated using Lowson's moving dipole theory (section 2.4).

5.1.1 Unsteady Loadings and Far Field Sound

Since the incident vortices can be viewed as an unsteady upwash gust field, we start by treating the general problem of an airfoil interacting with an arbitrary gust field. Assume that the flow field is linear, which means that the incident unsteady upwash remains fixed relative to the mean flow at infinity. After being Fourier decomposed, the z component of the unsteady upwash field in the x-y plane can be written in terms of sinusoidal gusts of the form

$$w_g(x,y) = \tilde{\tilde{w}}(k_x,k_y)\ e^{-i(k_x(x-Ut)+k_y y)} \qquad (5.1)$$

Consider a flat plate of infinite span lying in the x-y plane, with leading edge at y = -b (b is half chord of the airfoil). The pressure jump across the plate due to the incidence of sinusoidal gusts defined by (5.1) can be written as

$$\Delta p(x_1,y_1,k_x,k_y) = 2\pi\rho_0 U\ \tilde{\tilde{w}}(k_x,k_y)\ g(x_1,k_x,k_y)\ e^{-i(k_y y_1-k_x Ut)} \qquad (5.2)$$

where $g(x_1,k_x,k_y)$ is the airfoil gust response function which will be given in the next section.

Using the result of Lowson for a moving dipole (equation 2.29), the far field pressure p induced by a point dipole $F\ e^{i\omega t}$ at coordinates $(x_1,y_1,0)$ can be written as

$$p(x,y,z,t) = \frac{iF\omega z}{4\pi c_0\sigma^2}\ e^{i(\omega t+\mu(Mx-\sigma))}\ e^{-i\mu(Mx_1-(xx_1+\beta^2 yy_1)/\sigma)} \qquad (5.3)$$

where

$\mu = k_x M/\beta^2$
$\beta^2 = 1-M^2$
$\sigma^2 = x^2+\beta^2(y^2+z^2)$

The dipole (force) is assumed to be aligned with the positive z direction, and the source dimension is assumed to be small compared to the source-observer distance.

The far field pressure due to the unsteady gust component w_g can then be found simply by replacing the force in (5.3) with Δp from (5.2), noting that

$$\omega = k_x U \tag{5.4}$$

After integrating over the entire airfoil surface, we have

$$\tilde{\tilde{p}}(k_x,k_y) = \frac{i\pi\rho_0 U^2 b k_x z}{c_0 \sigma^2} \delta(k_y - \mu\beta^2 y/\sigma)\ \tilde{\tilde{w}}(k_x,k_y)\ L(k_x,k_y,M) \cdot e^{i(k_x Ut + \mu(Mx-\sigma))} \tag{5.5}$$

where

$$L(k_x,k_y,M) = \frac{1}{b} \int_{-b}^{+b} g(x_1,k_x,k_y,M)\ e^{-i\mu(M-x/\sigma)x_1}\ dx_1 \tag{5.6}$$

L is actually the lift per unit span on the airfoil. The exponential phase factor in (5.6) accounts for the retarded time effects for the sound propagating from source to observer.

To find the far field pressure-time response, we have to integrate (5.5) over all k_x and k_y gust components. The result is given by Amiet (Schlinker and Amiet, 1983) as

$$p(x,y,z,t) = -\frac{\pi b z \rho_0 U^2}{c_0 \sigma^2} \int_{-\infty}^{+\infty} -ik_x\ \tilde{\tilde{w}}(k_x,K_y)\ L(k_x,K_y,M) \cdot e^{i(k_x Ut + \mu(Mx-\sigma))}\ dk_x \tag{5.7}$$

where

$K_y = \mu\beta^2 y/\sigma$

The factor of $\exp(i\mu(Mx-\sigma))$ represents the time Δt for the sound wave to propagate from the airfoil leading edge to the far field observer ($\Delta t = (\sigma - Mx)/\beta^2 c_0$).

5.1.2 Airfoil Gust Response

Amiet has shown that the trace velocity (V_r) of the gust for the present case is always supersonic (Schlinker and Amiet, 1983). Thus the surface pressure gust response function $g(\mu,k_x,k_y,M)$ for a skewed gust can be written in terms of that for a parallel gust in compressible flow (a 2-dimensional flow field) using Graham's similarity rule (Graham, 1970). The relation is

$$g(\mu,k_x,k_y,M) = \frac{b}{\beta}\, g(\mu,k_{x\infty},0,M_\infty)\, e^{i(\mu k_y^2/k_x)} \tag{5.8}$$

where

$k_{x\infty} = k_x\beta_\infty^2/\beta^2$

$\beta_\infty^2 = 1 - M_\infty^2$

$M_\infty = M(1-\nu^{-2})^{1/2}$

$\nu = Mk_x/\beta k_y$

$\mu_\infty = M_\infty k_x/\beta^2$

According to Amiet (Schlinker and Amiet, 1983), the response function is divided into two ranges in which two different approximate solutions are used. For $\mu_\infty \le 0.4$, the response function can be found using a low frequency approximation. The final result for g is given by Amiet as

$$g(x,k_x,k_y,M) = \frac{1}{\pi\beta}\left(\frac{b-x}{b+x}\right)^{1/2} S(k_x^*)\ e^{i(\mu Mx+K_x^*f(M_\infty))} \tag{5.9}$$

where

$k_x^* = k_x b/\beta^2$

$f(M) = (1-\beta)\ln(M)+\beta\ln(1+\beta)-\ln(2)$

S is the Sears function (Sears, 1940) used in the incompressible theory, it can be written as

$$S(k) = \frac{2}{\pi k(J_0(k)-Y_1(k)-i(J_1(k)+Y_0(k)))} \tag{5.10}$$

Y_0 and Y_1 are the Bessel functions of the second kind, subscripts denote their orders. With equation (5.6), L can be found to be

$$L(k_x,k_y,M) = \frac{1}{\beta}\,S(k_x^*)\ e^{i(k_x^*f(M_\infty))}\ (J_0(\mu bx/\sigma)-iJ_1(\mu bx/\sigma)) \tag{5.11}$$

where J_0 and J_1 are Bessel functions of the first kind, and the subscripts denote their orders.

For the high frequency case where $\mu_\infty > 0.4$, The first two terms of g are (Amiet, 1976)

$$g_1(x,k_x,k_y,M) = \frac{1}{\pi(\pi k_x(1+M_\infty)(b+x))^{1/2}} e^{-i(k_x^*(M_\infty(b+x)-M^2x-b)/b-\pi/4)}$$

$$\begin{aligned} g_2(x,k_x,k_y,M) = & \frac{1}{\pi(2\pi k_x b(1+M_\infty))^{1/2}} e^{-i(k_x(M_\infty^*(b+x)-M^2x-b)/b-\pi/4)} \\ & \cdot ((1+i)E^*(2K_x^*M_\infty(b-x))-1) \end{aligned} \tag{5.12}$$

And L can be found to be

$$L_1(k_x,k_y,M) = \frac{2^{1/2}}{\pi\ (k_x b(1+M_\infty)\Theta_1)^{1/2}} E^*(2\Theta_1)\ e^{i\Theta_2}$$

$$\begin{aligned} L_2(k_x,k_y,M) \approx & \frac{e^{i\Theta_2}}{\pi\Theta_1(2\pi k_x b(1+M_\infty)^{1/2}} \left\{ i(1-e^{-i2\Theta_1}) + (i-1) \left[E^*(4k_x^*M_\infty) \right.\right. \\ & \left.\left. - \frac{2^{1/2}\ e^{-i2\Theta_1}}{(1+(M/M_\infty)(x/\sigma))^{1/2}} E^*(2\mu b(\frac{M}{M_\infty} + \frac{x}{r})) \right] \right\} \end{aligned} \tag{5.13}$$

where

$$\Theta_1 = \mu b(M_\infty/M - x/\sigma)$$

$$\Theta_2 = k_x b + \mu b(M-x/\sigma) - \pi/4$$

E^* is a combination of Fresnel integrals defined by

$$E^*(x) = \frac{1}{(2\pi)^{1/2}} \int_0^x \frac{e^{-i\xi}}{\xi^{1/2}} d\xi$$

5.1.3 Vortex Velocity Field

Figure 5.2 sketches the geometry of a near-normal blade-vortex interaction. The tangential velocity component in the z direction for a vortex tilted by θ_v from the z axis whose $\phi_v = 0$ can be written as

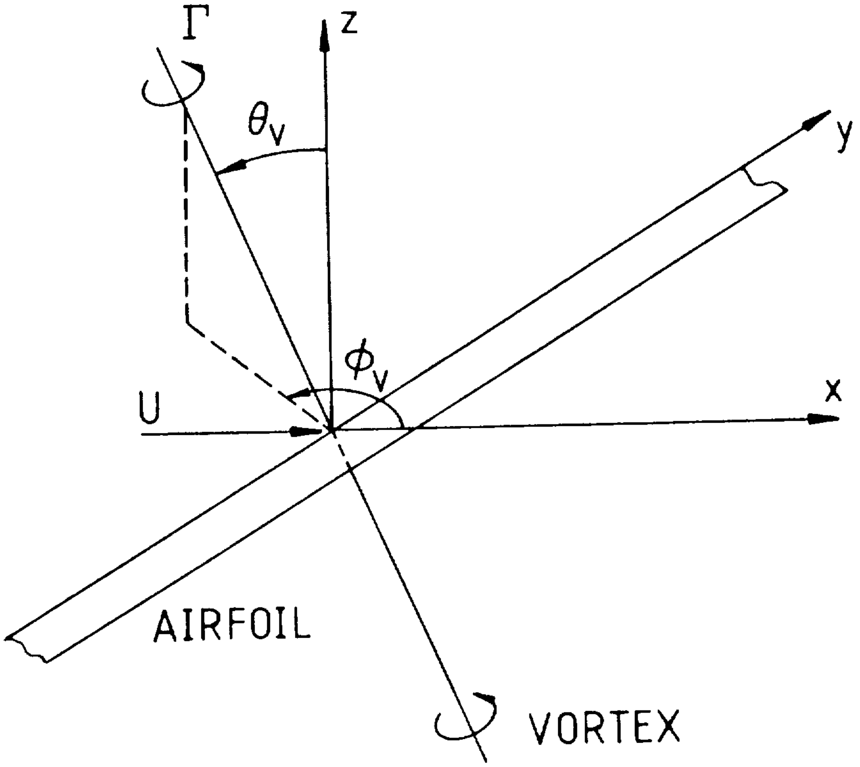

Figure 5.2: Sketch of 2-Dimensional Near-Normal Blade-Vortex Interaction.

$$w = \frac{y}{R} \sin\theta_v \, v_\theta(R) \tag{5.14}$$

It should be noted that R is the normal distance to the center of the vortex, i.e.

$$R^2 = (x\cos\theta_v - z\sin\theta_v)^2 + y^2 \tag{5.15}$$

The upwash velocity field due to the vortex can also be expressed in terms of the sinusoidal gusts $\bar{\bar{w}}(k_x, K_y)$. This can be done by taking a double Fourier transform of equation (5.14) with respect to x and y:

$$\tilde{w}(k_x,k_y) = \frac{\sin\theta_v}{(2\pi)^2} \iint_{-\infty}^{+\infty} \frac{y}{R}\, v_\theta(R)\, e^{-i(k_x x+k_y y)}\, dxdy \tag{5.16}$$

Several vortex models may be used to define the tangential velocity field $v_\theta(R)$. The vortex model Amiet used in his analysis is given by

$$v_\theta = (1 + \frac{1}{2\alpha}) \frac{r_0}{r} v_0 \,(1 - e^{-\alpha(r/r_0)^2}) \tag{5.17}$$

where $\alpha = 1.25643$, $r_0 v_0 = \Gamma/2\pi$, and Γ is the strength of the vortex. Substituting (5.17) into (5.16) and performing the integrals, we can get

$$\tilde{w}(k_x,k_y) = \frac{ik_y(1+1/2\alpha)\tan\theta_v}{2\pi(k_y^2+k_x^2/\cos^2\theta_v)}\, r_0 v_0\, e^{-(k_y^2+k_x^2/\cos^2\theta_v)r^2/4\alpha} \tag{5.18}$$

In order to be consistent with the aerodynamic analysis (i.e. CAMRAD), we used a vortex model different from the original Amiet analysis. In the present analysis, the tangential velocity v_θ is defined by the widely used turbulent vortex model

$$v_\theta = \frac{\Gamma}{2\pi r} \frac{r^2}{r^2+r_c^2} \tag{5.19}$$

where r_c is the vortex core radius (r_c is taken to be 0.0025 of the main rotor tip radius in the present study). In Figure 5.3, this vortex model is compared to the one used by Amiet.

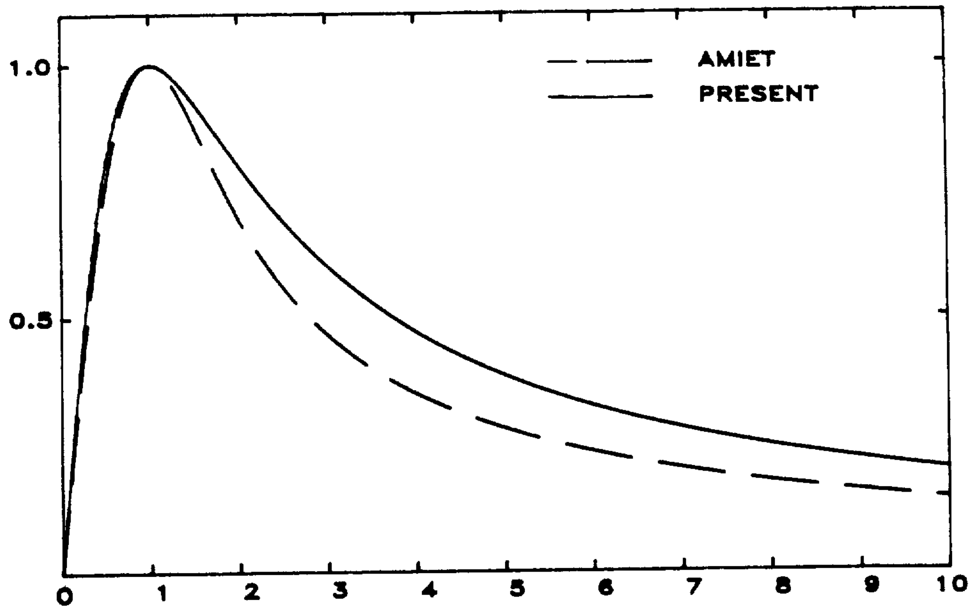

Figure 5.3: Comparison of the Tangential Velocity for Different Vortex Models, v_θ is normalized by $\Gamma/4\pi r_c$ and r is normalized by r_c.

At large radial distances, the vortex model used in the present study decays more slowly than the model used by Amiet. Since a different vortex model is used, $\tilde{w}$, the Fourier decomposed vortex velocity field ($\tilde{w}$ considers only the velocity component that is normal to the tail rotor disk), is replaced by

$$\tilde{w}(k_x,k_y) = \frac{ik_y\Gamma r_c\tan\theta_v}{4\pi^2(k_y^2+k_x^2/\cos^2\theta_v)^{1/2}} K_1(r_c(k_y^2+k_x^2/\cos^2\theta_v)^{1/2}) \qquad (5.20)$$

where K_1 is the modified Bessel function of the second kind, and θ_v is defined in Figure 5.2.

The acoustic pressure-time history for a given blade-vortex interaction, calculated by the present vortex model, is compared to that obtained using Amiet's original analysis. The comparison is shown in Figure 5.4. The results for the two different vortex models show close similarities and only minor differences.

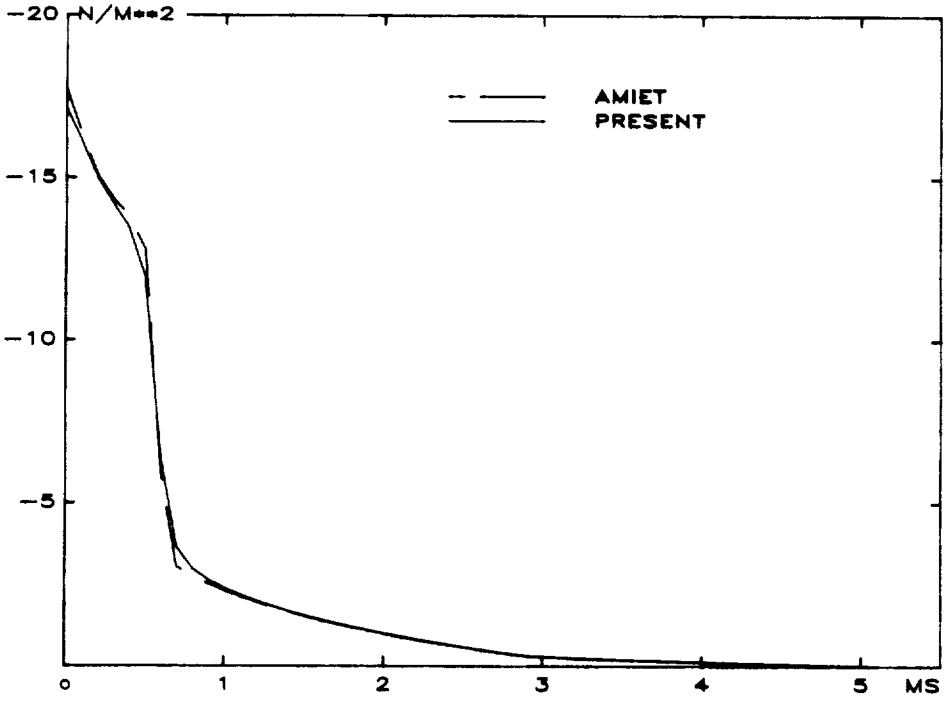

Figure 5.4: Comparison of the Noise Generated from Blade-Vortex Interactions with Different Vortex Models.

In general, ϕ_V is not zero. Let ξ, η, ζ represent the coordinate system which rotate the original system by ϕ_V about the z axis. Then x, y, z are related to ξ, η, ζ by

$$\begin{aligned} x &= \xi \cos\phi_v - \eta \sin\phi_v \\ y &= \xi \sin\phi_v + \eta \cos\phi_v \\ z &= \zeta \end{aligned} \tag{5.21}$$

Amiet (Schlinker and Amiet, 1983) has shown that in order to accommodate various vortex orientations, k_x and k_y should be replaced by k_ξ and k_η, where k_ξ and k_η are given by

$$\begin{aligned} k_\xi &= k_x \cos\phi_v + k_y \sin\phi_v \\ k_\eta &= -k_x \sin\phi_v + k_y \cos\phi_v \end{aligned} \tag{5.22}$$

It should also be noted that $\bar{\bar{w}}$ only accounts for the effect of the tangential velocity of the vortices; the axial flow in the main rotor tip vortices is neglected in the present analysis, although it can be very important as noted in the conclusion.

5.2 HELICOPTER MAIN ROTOR TIP VORTEX-TAIL ROTOR INTERACTION

As noted previously, the acoustic analysis requires inputs from an aerodynamic analysis; particularly the information on how the vortices are moving on the tail rotor disk, what the properties of the vortices are, and what the relative geometry of the vortices and the tail rotor blades is. In this section, we will discuss in detail how these aerodynamic inputs are obtained.

5.2.1 Main Rotor Tip Vortex Free Wake Geometry

Since the main rotor tip vortex system is generally highly distorted under most helicopter operations, classical rigid wake analysis can not predict accurate trajectories of the main rotor tip vortices (Scully, 1975). The calculation of the free wake geometry of main rotor tip vortices is, therefore, very important to the present study since the trajectories of vortices directly affect the characteristics of the blade-vortex interaction and thus, the noise generated.

In the present study, we use the comprehensive analysis of rotorcraft aerodynamics and dynamics code (CAMRAD) by Johnson (1980) to obtain information on the properties of the main rotor tip vortices and their individual geometries. The free wake geometry analysis of CAMRAD is based on a rotor, free wake geometry model of Scully (1975).

In the present application, the free wake geometry analysis is driven by calculated main rotor airloads assuming non-uniform inflow at the main rotor disk. It is also assumed that the presence of a tail rotor has no effect on the upstream main rotor loading and its tip vortex system. Also no fuselage wake or ground effect is considered when calculating the free wake geometry.

5.2.2 Definition of Tail Rotor Blade-Vortex Interactions

The tail rotor blade-vortex interaction can be calculated provided that the following information is given: the normal incident velocity of the ingested vortex relative to the tail rotor blade (U), the strength of the ingested vortex element (Γ), the skew angle between the ingested vortex element and the tail rotor axis (θ_V), and the ingested vortex orientation (ϕ_V). Refer to Figure 5.2 for the definitions of U, θ_V, and ϕ_V. It should be noticed that these parameters are generally not constant as a vortex sweeps through the tail rotor disk.

Since the tail rotor RPM is generally not an integer multiplier of the main rotor RPM, the locations of the blade-vortex interactions are different for each main rotor revolution. In the present study, both #1 blades of the main and the tail rotors are set such that both blades will start from $\psi = 0^o$ initially. (Figure 5.5 shows the definitions of azimuthal angles ψ for both main and tail rotors.) The information defining a series of blade-vortex interactions can then be determined numerically by interpolating the results of the main rotor free wake geometry analysis.

5.3 RESULTS AND DISCUSSIONS

In this section, we will present several examples calculated for UH-1D helicopters to demonstrate the general procedures developed in the present study.

5.3.1 Results on Free Wake Geometry Analysis

Our simulation begins with the calculation of the main rotor, free wake geometry. Results for two speeds are presented; they correspond to a UH-1D in level flight at 100 and 60 Knots. The free wake geometry results for the 100 Knot case are presented in Figure 5.6. From the results shown, the interactions between tail rotor blades and main rotor tip vortices are evident.

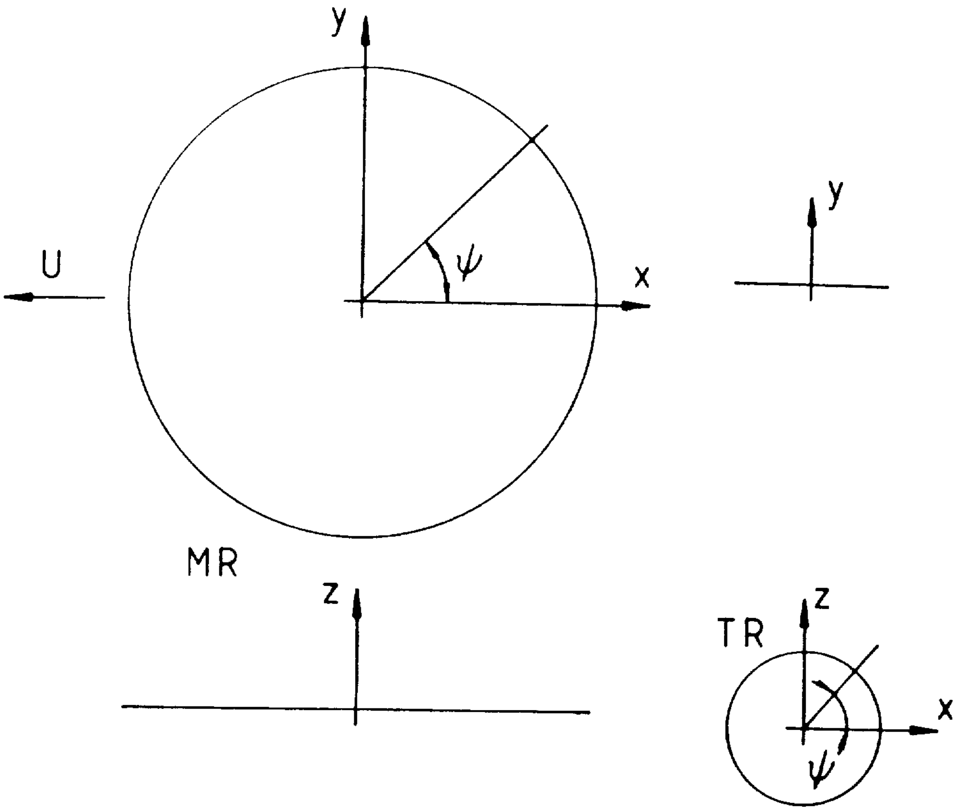

Figure 5.5: Definitions of Main Rotor and Tail Rotor Coordinates and Azimuthal Angles.

After the main rotor tip vortex free wake geometry is found, we can plot its trajectory/trajectories on the tail rotor disk. Figure 5.7 shows the possible patterns of the vortex trajectories on the tail rotor disk. Figures 5.8 and 5.9 present the actual main rotor tip vortex trajectories on the tail rotor disk for our UH-1D examples (100 and 60 Knot cases). The points shown are interpolated from the free wake geometry analysis, and each point represents the location of the main rotor tip vortex at an interval of 15° rotation (main rotor azimuthal angle).

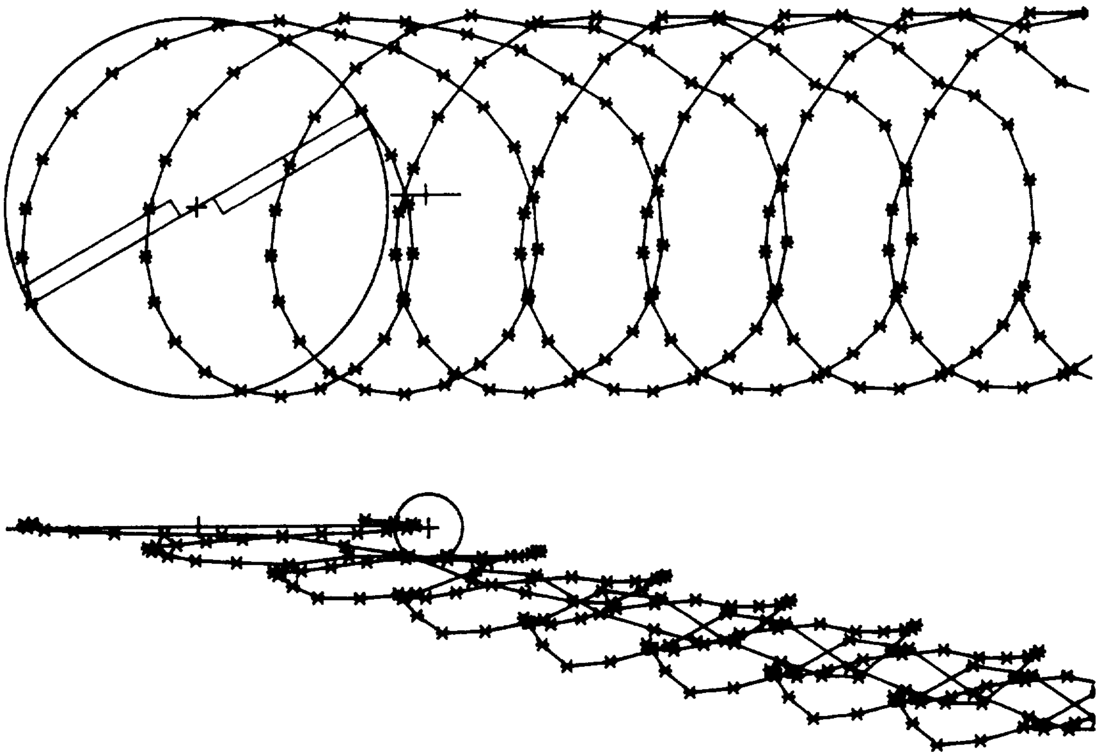

Figure 5.6: UH-1D Free Wake Geometry Analysis Results, 100 Knot Level Flight, Main Rotor $\psi = 30^{o}$.

Notice that the tip vortices involved in the interactions with the tail rotor are shed from main rotor blades at approximately 0^{o} of azimuthal position. Also they are relatively "young" (vortex age are generally less than 180^{o} for both cases considered), which implies that the ingested vortices are not fully rolled-up. (Johnson (1980) has suggested that a vortex is not fully rolled-up unless the vortex age is larger than 180^{o} or so.) Since a vortex is not fully rolled-up, the strength of the ingested vortex should be less than the maximum bound circulation on the main rotor blade; we followed the assumption made by Scully (1975), and set the strength of the tip vortex strength to 0.8 of the maximum bound circulation on the main

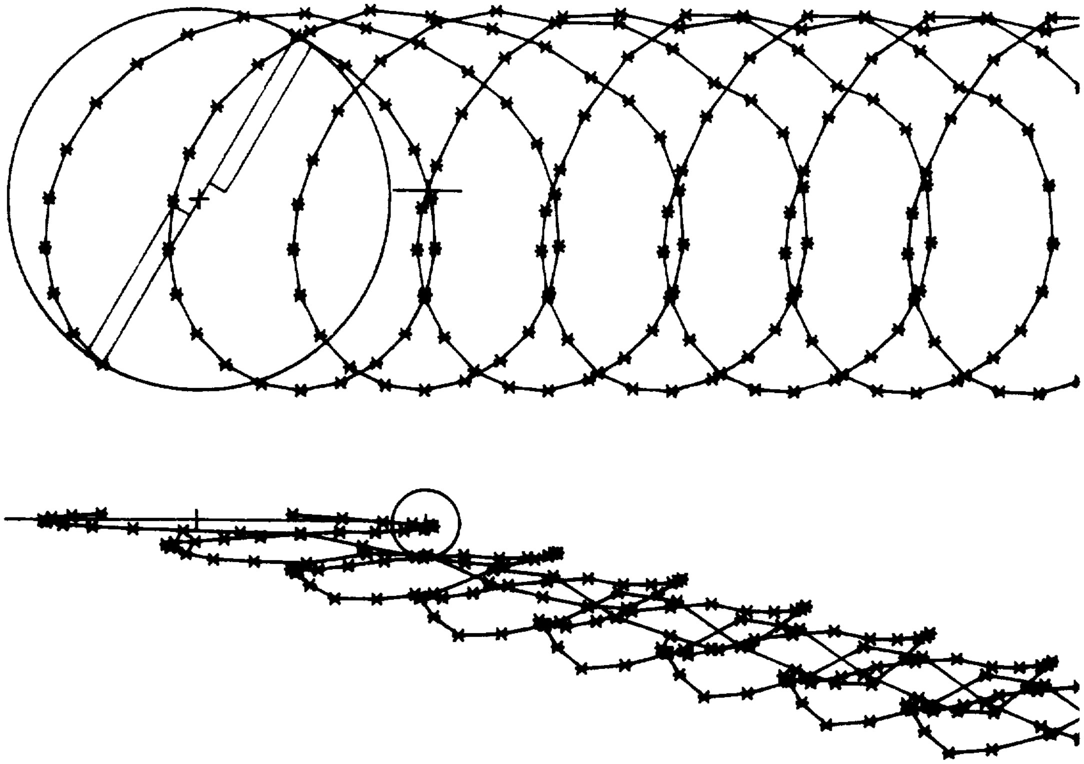

Figure 5.6a: (Continued) Main Rotor $\psi = 60^{\circ}$.

rotor blade span. It should be noted that interactions with vortices originating from other azimuthal angles or with some relatively "old" vortices are still possible. Such interactions had been observed in our calculations for the model scale UH-1, and are certainly possible for full scale helicopters operated in appropriate conditions.

Also the results indicate the lack of multiple interactions, i.e., no two vortex traces are found simultaneously on the tail rotor disk. This phenomenon has been observed in the model scale experiment by Balcerak (1976). But this phenomenon is again possible for full scale helicopters, providing the operating conditions and tail rotor location are suitable.

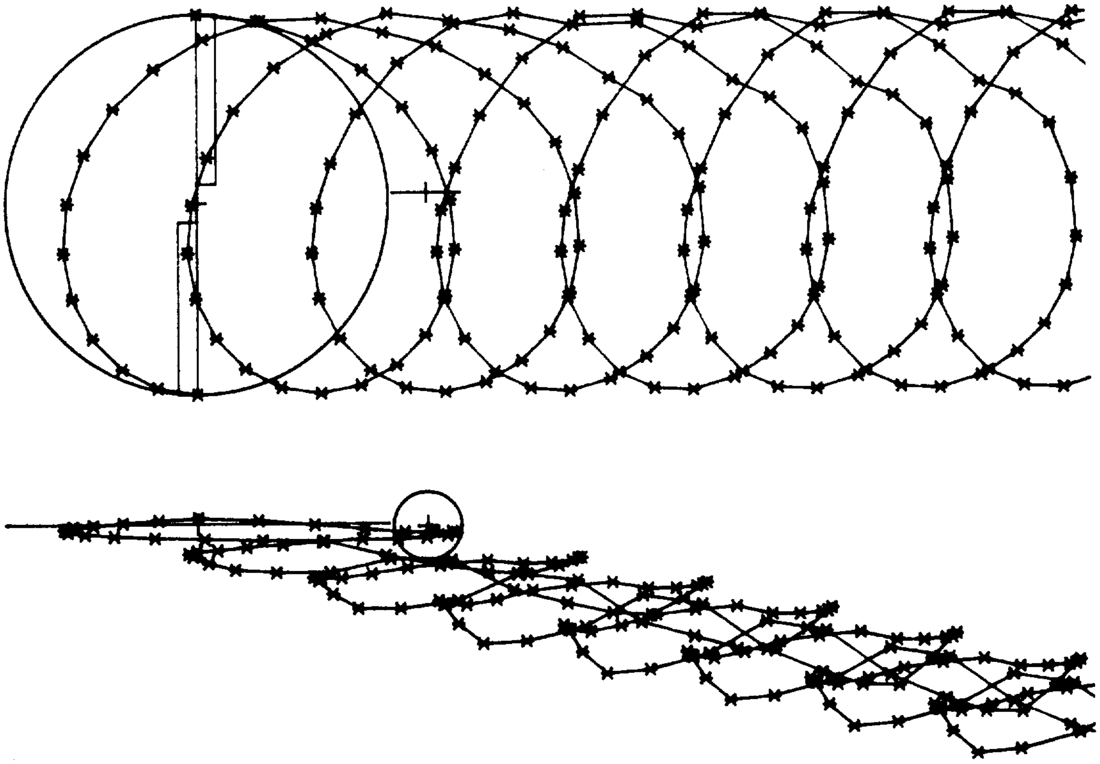

Figure 5.6b: (Continued) Main Rotor $\psi = 90^{\circ}$.

Our results also show that a certain vortex may be chopped by several tail rotor blades. It is quite possible that a certain vortex may "breakdown" locally after the first blade-vortex interaction, thus a subsequent interaction with the same vortex may be weaker. However, the free wake geometry calculations indicate that the main rotor tip vortex will generally be drifting through the tail rotor disk. Therefore, the subsequent interactions are actually the results of tail rotor blades chopping through a fresh piece of vortex. Thus, no effects of possible interactions with burst vortices have been included in the present study.

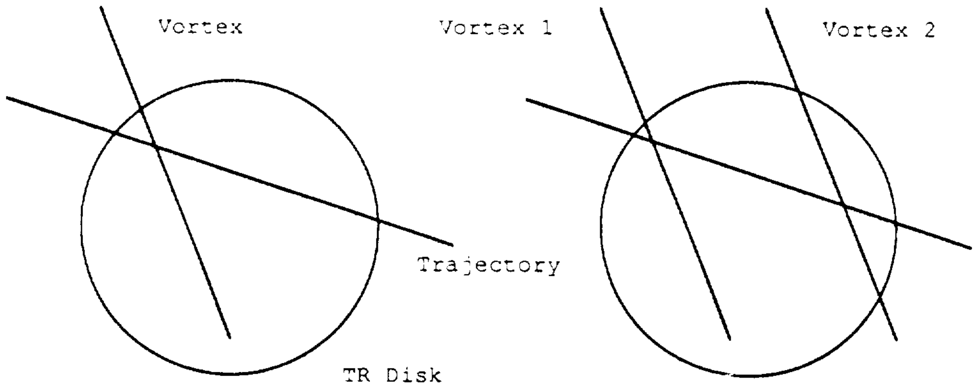

(a) Single Vortex Interaction

(b) Two Vortex Interactions - Single Trajectory

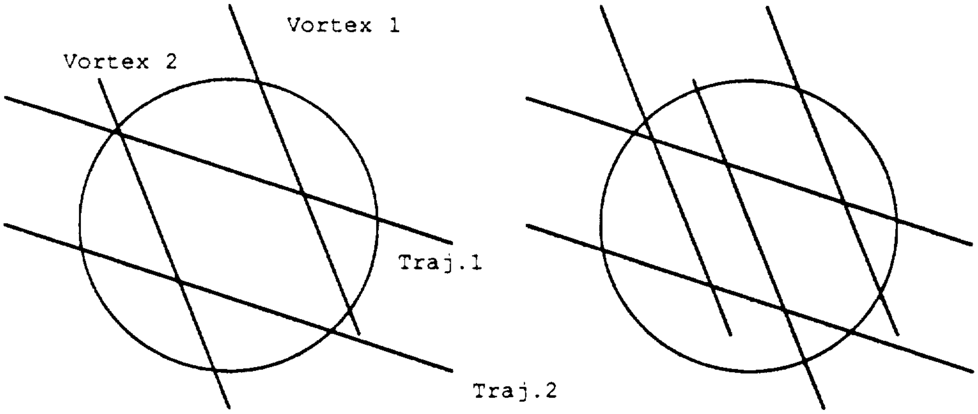

(c) Two Vortex Interactions - Two Trajectories

(d) Complex Interaction - Multiple Vortex/Trajectories

Figure 5.7: Possible Main Rotor Tip Vortex Trajectory Patterns on the Tail Rotor Disk.

5.3.2 Acoustic Signals from the Blade Vortex Interactions

Figure 5.10 shows the results for the tail rotor blade-main rotor tip vortex interaction noise signals for the 100 Knot case; horizontal tick marks in the figure are 0.1 seconds apart. Figure 5.11 shows the same interactions as in Figure 5.10 with a higher time resolution (tick marks are 0.01 seconds apart). Figures 5.12 and 5.13 show

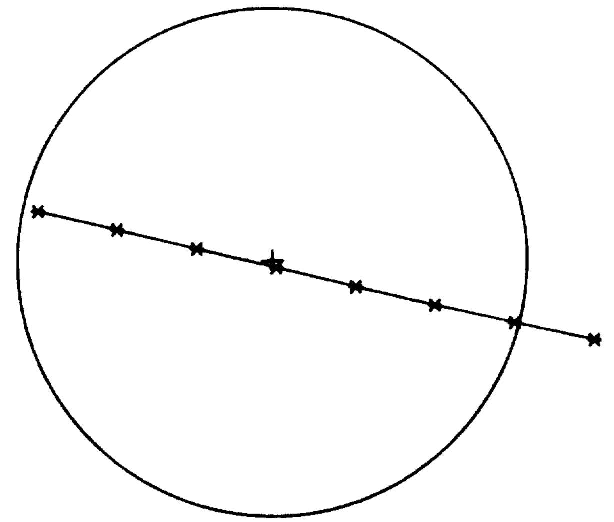

Figure 5.8: Main Rotor Tip Vortex Trajectory on Tail Rotor Disk, UH-1D Helicopter, 100 Knot Level Flight.

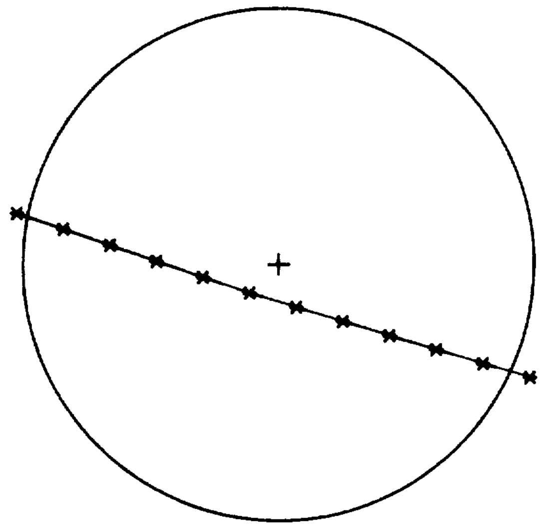

Figure 5.9: Main Rotor Tip Vortex Trajectory on Tail Rotor Disk, UH-1D Helicopter, 60 Knot Level Flight.

similar results for the 60 knot level flight case. One important aspect of the tail rotor blade-vortex interaction we see from these results is that the strength of the acoustic signal does not decrease when the helicopter is flying at slower speed. Moreover, the interaction seems to be more frequent in such case. It should be noted that the above calculations assume a bottom-forward rotating tail rotor.

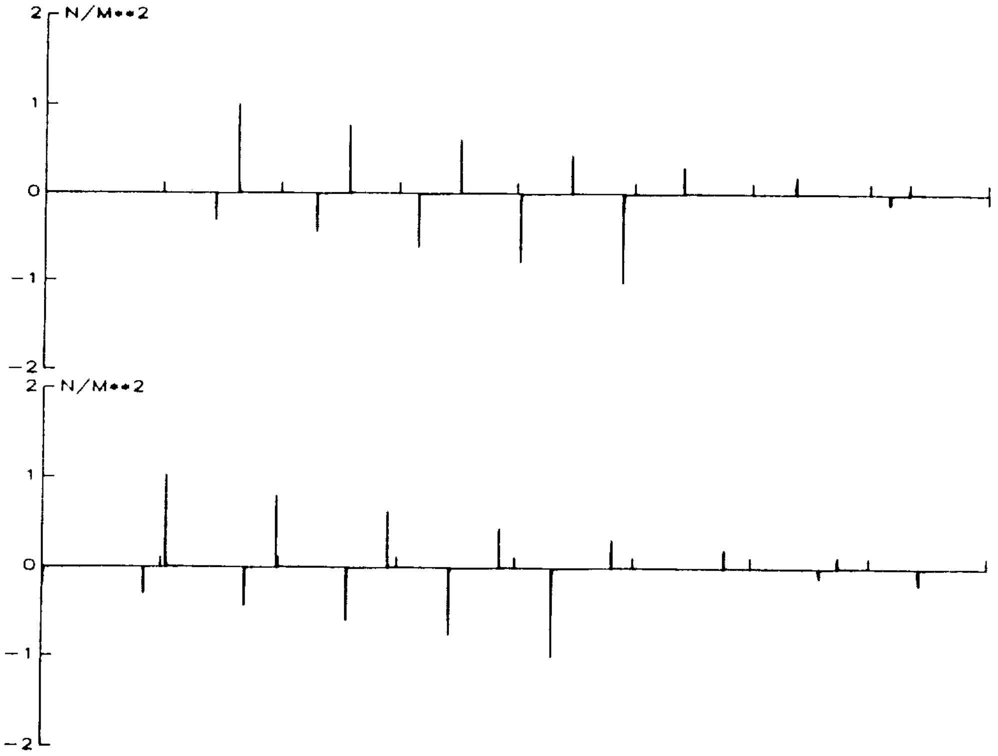

Figure 5.10: **Sound Pressure History for Tail Rotor Blade Vortex** Interactions, UH-1D, 100 Knots.

5.3.3 Comparison with Other Harmonic Noise Mechanisms

To determine the relative importance of the tail rotor blade-main rotor tip vortex interaction, results are compared to the tail rotor loading and to high speed thickness noises. The loading and thickness

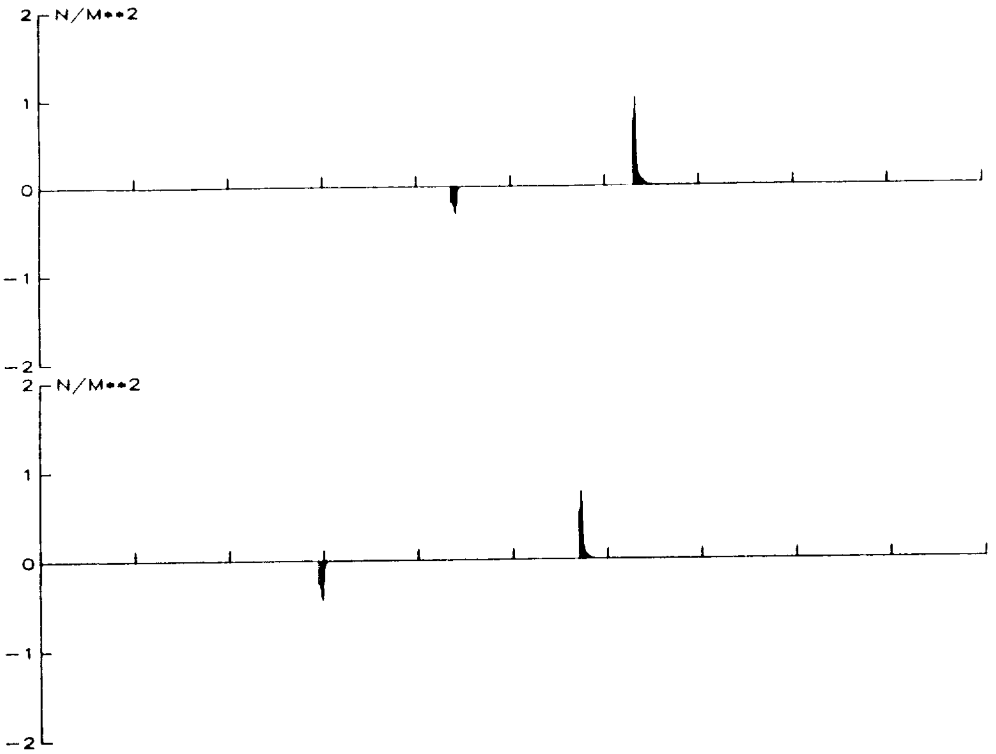

Figure 5.11: Sound Pressure History for Tail Rotor Blade Vortex Interactions, UH-1D, 100 Knots.

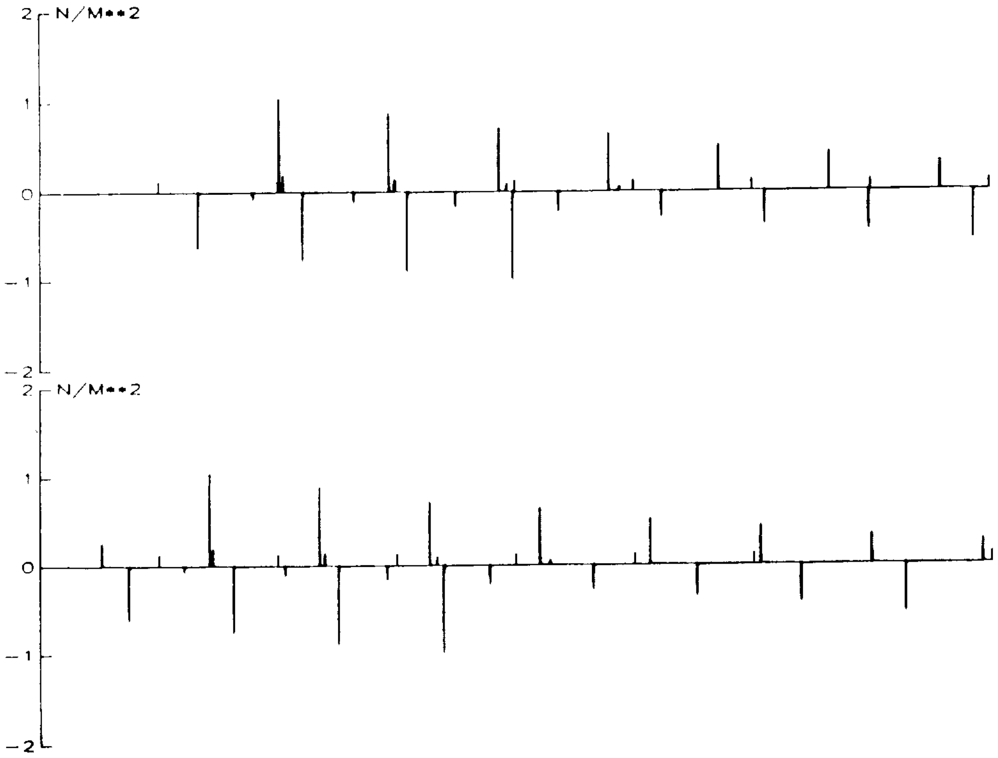

Figure 5.12: Sound Pressure History for Tail Rotor Blade Vortex Interactions, UH-1D, 60 Knots.

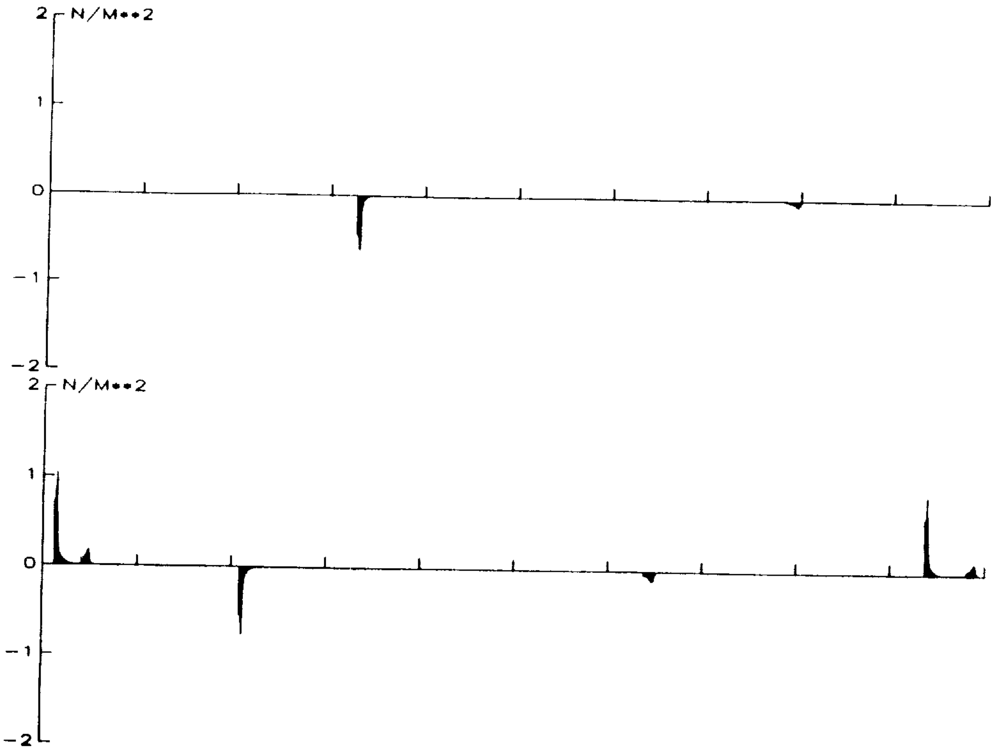

Figure 5.13: **Sound Pressure History for Tail Rotor Blade Vortex** Interactions, UH-1D, 60 Knots.

noises shown are obtained with a discrete frequency noise prediction program WOPWOP using Farassat's linear acoustic analysis (Farassat et al., 1980, 1983). The airloads on the tail rotor blades are obtained with approximate aerodynamic analysis. Figures 5.14 and 5.15 show the comparisons of loading and thickness noise with some representative blade-vortex interaction signals for the 100 knot case. Clearly the blade-vortex interaction signals are very important. These figures also show the detailed shape of a typical tail rotor blade-main rotor tip vortex interaction.

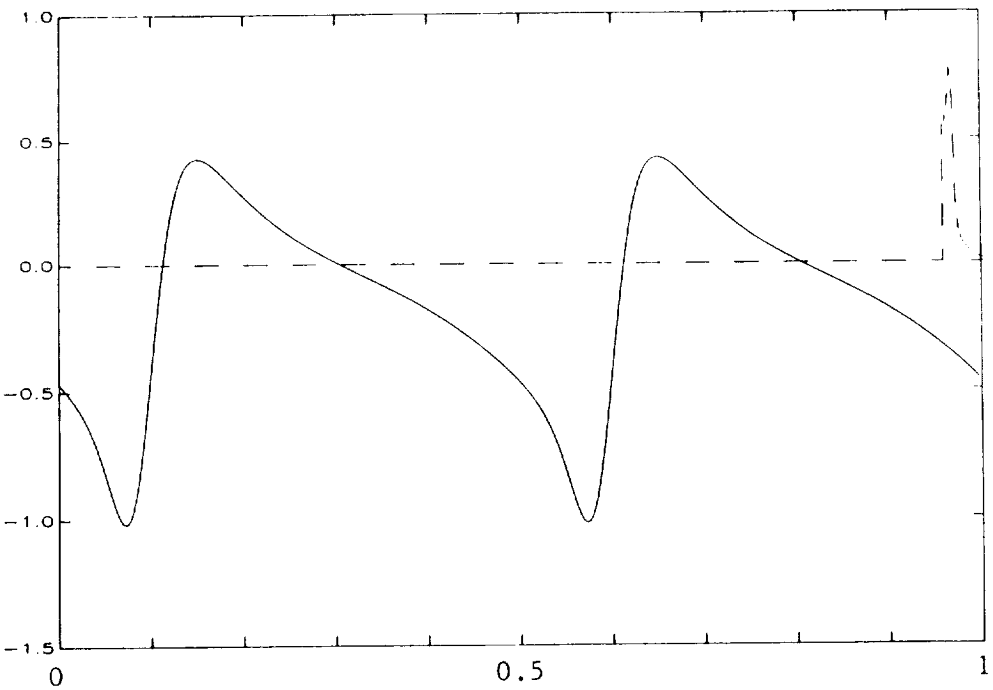

Figure 5.14: Comparison of Tail Rotor Blade Vortex Interaction Noise with Thickness/Loading Noise, UH-1D, 100 Knots.

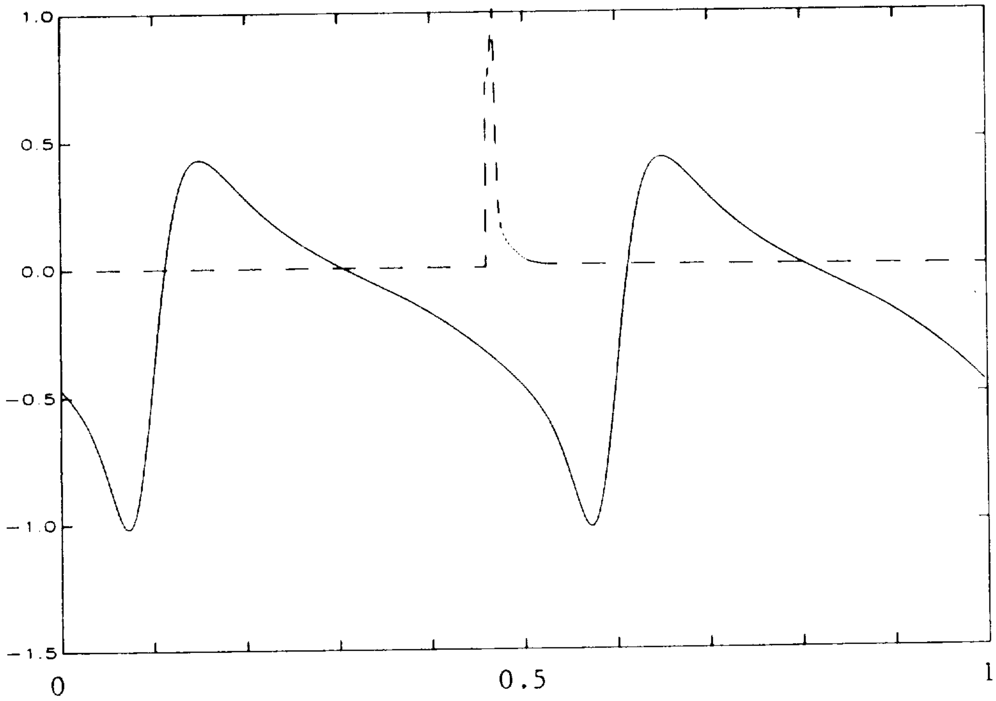

Figure 5.15: Comparison of Tail Rotor Blade Vortex Interaction Noise with Thickness/Loading Noise, UH-1D, 100 Knots.

5.3.4 Effects of Changing the Tail Rotor Location

As discussed previously, the vortex trajectory on the tail rotor disk is very important to the tail rotor blade-vortex interaction noise. The tail rotor location relative to the main rotor, and the helicopter operating conditions are two primary factors that determine the vortex trajectories on the tail rotor disk. For the cases shown so far, the interactions usually occurred at the retreating side of the tail rotor; this effectively reduces the incident velocity U, and therefore the strength of the interaction noise. To study the effect of tail rotor location on the blade-vortex interaction noise, we artificially lowered the UH-1D tail rotor by 0.5 m. This will cause the blade-vortex interactions to occur on the advancing side of the tail rotor, thus enhancing the strength of the interactions.

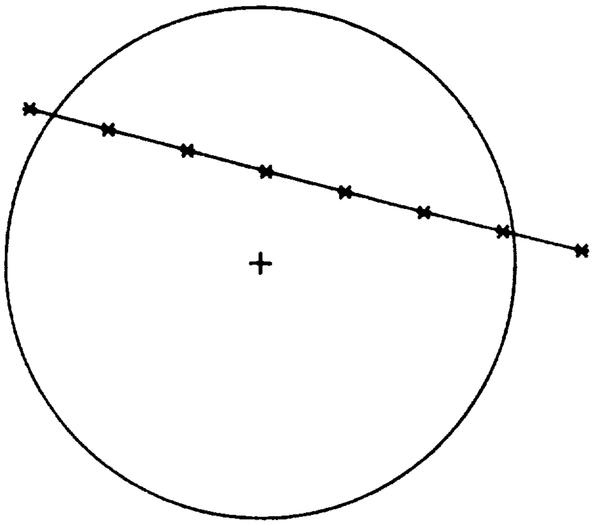

Figure 5.16: Main Rotor Tip Vortex Trajectory on Tail Rotor Disk, UH-1D Helicopter, 100 Knot Level Flight, Tail Rotor Lowered by 0.5 meters.

For the 100 knot level flight case, the main rotor tip vortex trajectory on the tail rotor disk is now shown in Figure 5.16. Notice that the path is higher than that shown in Figure 5.8 due to the lowered tail rotor. The acoustic pressure-time history of the resulting blade-vortex interaction is shown in Figure 5.17. Notice that there are considerable differences between the results shown in Figures 5.10 and 5.17. Since the vortex is passing through the advancing side of the tail rotor, the relative velocity between the tail rotor blade and the vortex element is generally higher, so the interaction signals have higher magnitude. Also, the interactions are more frequent than in the previous cases. Unquestionably, with this configuration (with lowered tail rotor), tail rotor noise would be higher than that from a standard tail rotor.

5.3.5 Comparison with Experiments

As mentioned previously, very few experiments have ever addressed the tail rotor noise problem. The most important experiment we have examined is that of Balcerak (1976). In his parametric studies of tail rotor noise mechanisms, he found that the noise increased as the main rotor wake passed the tail rotor disk. In the present study, we examine several of his cases. Presented here is a special case for which the tail rotor RPM is an integer multiplier of the main rotor RPM. In this case, the interaction will be periodic. The corresponding advance ratio is 0.2, and the model is an 1/16th scaled UH-1 series helicopter.

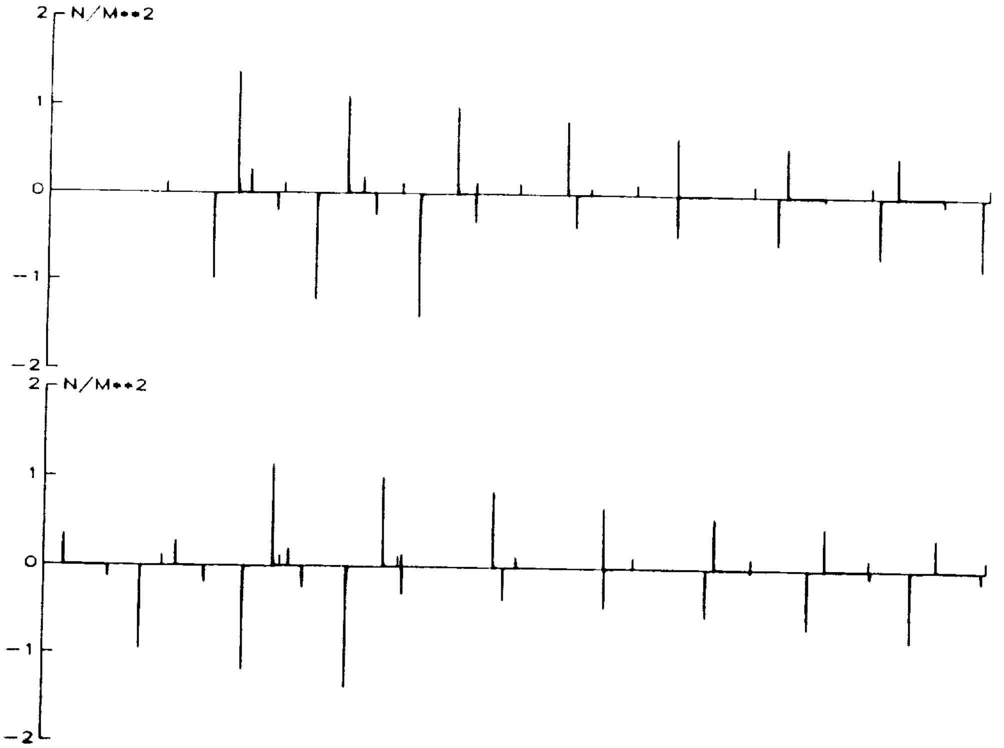

Figure 5.17: Sound Pressure History for Tail Rotor Blade Vortex Interaction, UH-1D, 100 Knots, Tail Rotor Lowered by 0.5 meters.

Figure 5.18 shows the free wake geometry analysis results; unlike the full scale cases, multiple interactions (with vortices originating from approximately 0^{o} and 180^{o}) do exist in this example as mentioned by Balcerak in his study. The 180^{o} vortices are also quite "old" (their wake age are about 540^{o}). Figure 5.19 shows the tip vortex trajectories on the tail rotor disk. The acoustic signals due to the blade-vortex interactions are shown in Figure 5.20. Figure 5.21 shows the acoustic pressure spectrum obtained from the above results along with the experimental results of Balcerak. (Notice that the calculated results shown do not include the loading and high speed thickness noise.)

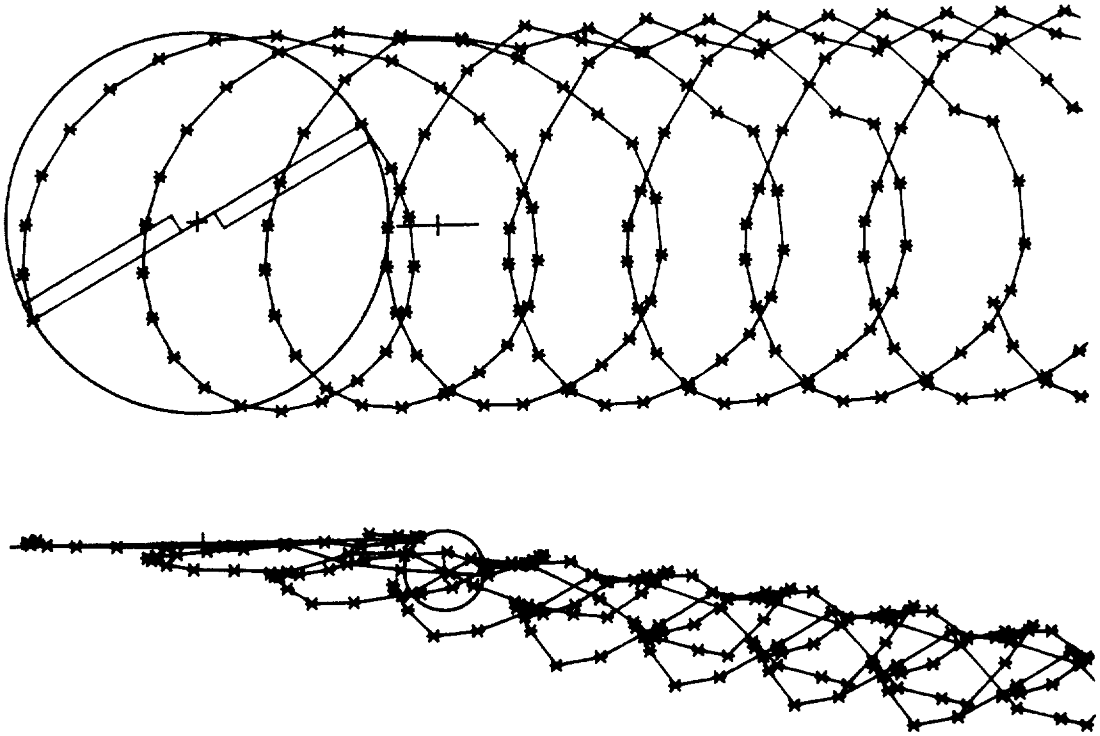

Figure 5.18: Model UH-1 Free Wake Geometry Analysis Results, Level Flight ($\mu = 0.2$), Main Rotor $\psi = 30^\circ$.

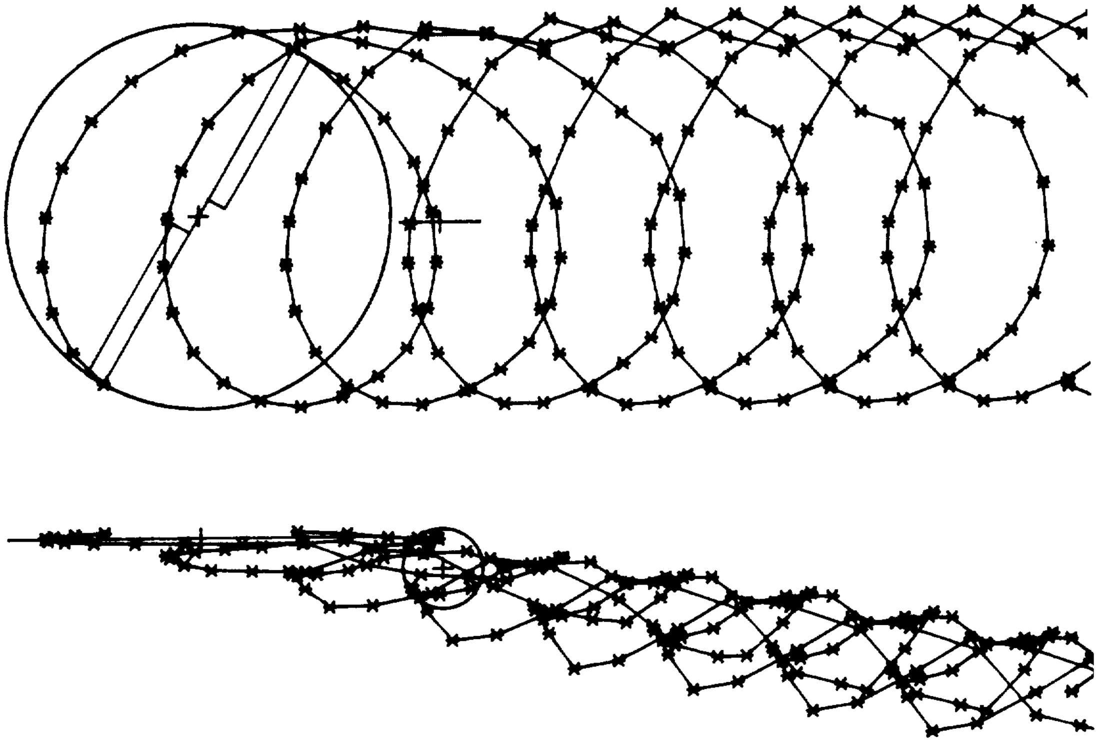

Figure 5.18a: (Continued) Main Rotor $\psi = 60^\circ$.

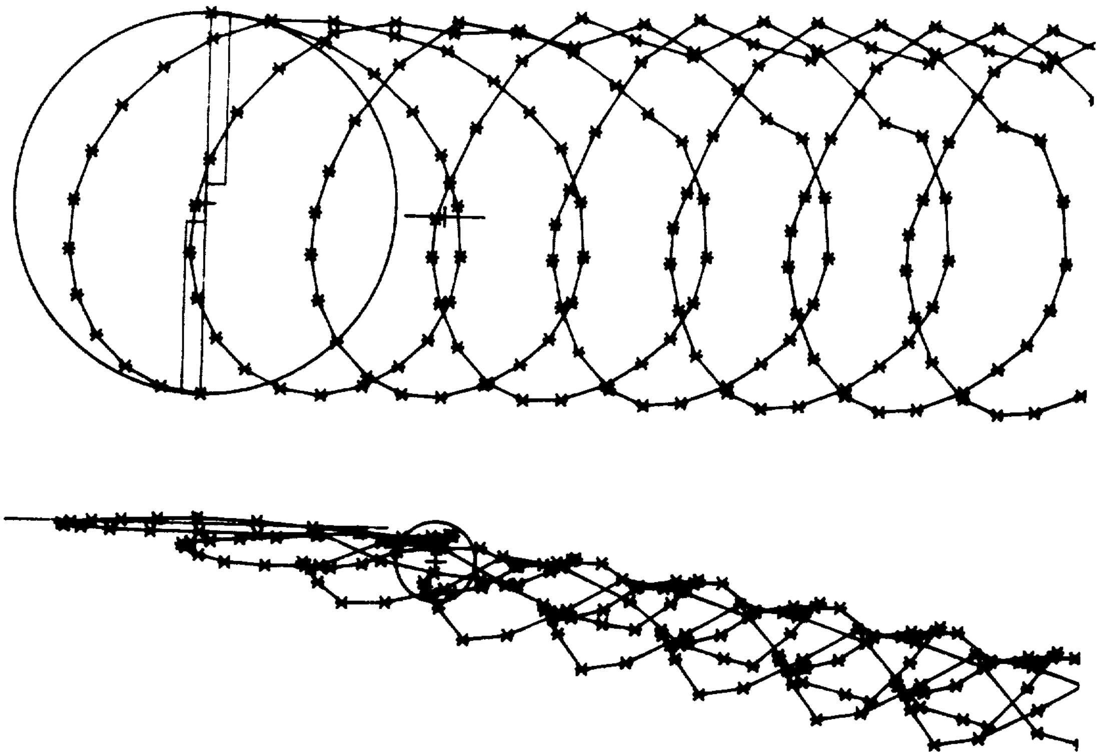

Figure 5.18b: (Continued) Main Rotor $\psi = 90^{\circ}$.

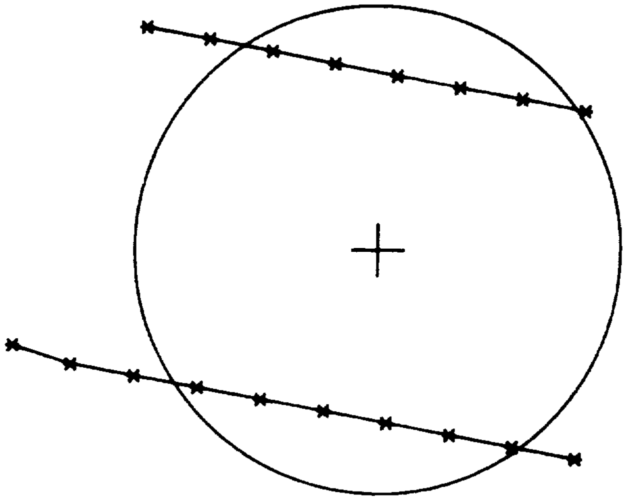

Figure 5.19: Main Rotor Tip Vortex Trajectory on Tail Rotor Disk, Model UH-1 Helicopter, $\mu = 0.2$.

Figure 5.20: Sound Pressure History for Tail Rotor Blade Vortex Interaction, Model UH-1, $\mu = 0.2$.

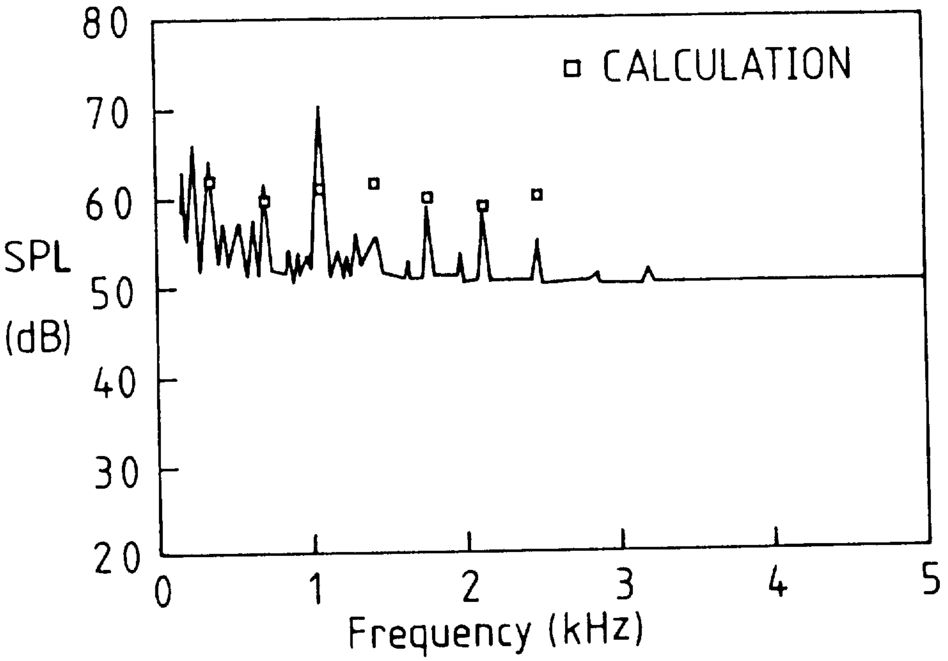

Figure 5.21: Comparison of Tail Rotor Blade Vortex Interaction Noise Spectrum and the Experimental Result of Balcerak (1976), Model UH-1, $\mu = 0.2$.

Chapter VI

CONCLUSIONS

The understanding of and the ability to predict broadband rotor noise are approaching a satisfactory state in many respects. The present study shows that the important broadband noise mechanisms are now understood well enough to be able to make predictions to within about 5 dB of experimental data. This understanding should enable designers to minimize broadband noise in the cases where it is a controlling factor in a design.

The calculations and comparisons made in the present study indicate that inflow turbulence induced lift fluctuations are the most important broadband noise sources at low frequencies. This radiation can be predicted down to the lowest blade passing frequency, including the smooth peaked spectral structure, by the method of Homicz and George (1974). For the higher frequencies, which are of more practical interest, the methods of George and Kim (1976) and of Amiet (1976) are just as satisfactory and are much easier to compute the method of Homicz and George. When the same inflow turbulence spectrum is used, both methods agree well with each other and with measurements over a full range of parameters, except at angles within about 10^{o} to 15^{o} of the rotor plane where other in-plane mechanisms are dominant.

The Karman spectrum, which has been implemented in both George and Kim's and Amiet's methods, is shown to be suitable for use in predicting the inflow turbulence noise from full-size rotors. However, the Dryden spectrum, which is only available in George and Kim's method, is shown to be more suitable to predict the inflow turbulence noise for indoor model rotor where small scale turbulence is involved. The accuracy of the prediction depends strongly upon the description of the inflow turbulence: the integral length scale, Λ, the turbulent intensity, w, and the turbulent spectral shape. Further research on turbulence properties is needed in the future.

Boundary layer trailing edge noise is now well understood. The analyses of Kim and George (1980) and of Schlinker and Amiet (1980) and the correlation of Fink (1978) all appeared to give results which agree reasonably well with experiments. This source often is the most important noise source at high frequencies on large rotors when inflow turbulence is weak. It increases significantly with angle of attack due to the increase of boundary layer thickness.

Tip vortex formation noise is satisfactorily predicted, although it does not dominate in any of the experiments to definitively establish the precise accuracy of the model of George et al. (1980, 1983b, 1984a). More experimental data is needed on flows and fluctuating pressure on different shapes of rotors and wing tips. Tip vortex noise is most important for rotors with square tips and wide chords at high angles of attack. This noise can be reduced significantly by detailed tip shape changes, but this is presently unexplored.

Turbulent vortex shedding noise from blunt trailing edges is now reasonably predicted. Generally speaking, the noise spectra due to turbulent vortex shedding from blunt trailing edges show a peak occurring at certain frequency range. The peak frequency depends upon the trailing edge thickness; a small trailing edge thickness will generate a high frequency peak and a thick trailing edge will result in a peak of lower frequencies. The level of the spectrum peak also depends on the thickness of trailing edge; peak level increases roughly to the third power of trailing edge thickness, thus a slightly blunted rotor trailing edge can contribute significantly to the overall noise. More measurements of surface pressure fluctuations near blunt trailing edges are needed to improve the accuracy of the prediction.

For helicopter tail rotor broadband noise, a number of approximate analyses of the interaction noise sources have been presented. The interaction noises are generally much greater than the isolated tail rotor noise. Inflow turbulence noise is the most important tail rotor broadband noise mechanism: the turbulent wakes of the main rotor and the fuselage are the most important sources of the tail rotor turbulent inflow, while the turbulent main rotor tip vortex is of less significance. Further studies are needed to determine the turbulent properties in the tail rotor inflow.

The present study has shown that fuselage, hub, and hub shaft wakes and engine exhaust may be important to harmonic noise if the tail rotor is fully immersed in the respective disturbed flows. In order to minimize noise, it is desirable to place the tail rotor where it will not be affected by any of the upstream disturbances. While the engine, fuselage, etc. flows may be avoided or reduced, the main rotor wake is so large that it tends to interact the tail rotor over a wide range of flight conditions. The flow disturbances in the main rotor wake (including both the overall downwash field of the main rotor mean wake and the main rotor tip vortex wake) are found to be the strongest tail rotor harmonic noise sources.

The interaction between the tail rotor blade and main rotor tip vortices is very important to harmonic noise. The noise generated depends strongly upon the helicopter operating conditions and on the tail rotor location. Major parameters governing this blade-vortex noise generation are the ingested vortex strength, the ingested vortex orientation relative to the blade, and the relative velocity of the ingested vortex to the tail rotor blade. The present study has shown that this noise mechanism is at least of the same order of magnitude as some of the strongest tail rotor noise sources such as high speed thickness noise. Future studies should consider a vortex chopped by an airfoil of finite span and the possibly major effect of the axial flow in the main rotor tip vortex.

BIBLIOGRAPHY

Ahmadi, A. R., "An Experimental Investigation of the Chopping of Helicopter Main Rotor Tip Vortices by the Tail Rotor," NASA CR-177338, September 1984a.

Ahmadi, A. R., "An Experimental Investigation of Blade Vortex Interaction at Normal Incidence," in Proceeding, Workshop on Blade-Vortex Interactions, NASA Ames Research Cencer, Moffet Field, California, October 1984b.

Ahtye, W. F., Miller, W. R., and Meecham, W. C., "Wing and Tip Noise Measured by Near- and Far-Field Cross-Correlation Techniques," AIAA-79-0667, AIAA 5th Aeroacoustics Conference, Seattle, Washington, March 1979.

Amiet, R. K., "Compressibility Effects in Unsteady Thin-Airfoil Theory," AIAA Journal, Vol. 12, No. 2, 1974, pp. 252-255.

Amiet, R. K., "Acoustic Radiation from an Airfoil in a Turbulent Stream," Journal of Sound and Vibration, Vol. 41, No. 4, 1975, pp. 407-420.

Amiet, R. K., "Noise Due to Turbulent Flow Past a Trailing Edge," Journal of Sound and Vibration, Vol. 47, No. 3, 1976, pp. 387-393.

Amiet, R. K., "Noise Produced by Turbulent Flow into a Propeller or Helicopter Rotor," AIAA-76-560, AIAA 3rd Aeroacoustic Conference, Palo Alto, California, July 1976b; also AIAA Journal, Vol. 15, No. 3, 1977, pp. 307-308.

Amiet, R. K., "Effect of Incident Surface Pressure Field on Noise Due to Turbulent Flow Past a Trailing Edge," Journal of Sound and Vibration, Vol. 57, 1978, pp. 305-306.

Amiet, R. K., "Airfoil Gust Response and the Sound Produced by Airfoil-Vortex Interaction," AIAA-84-2268, AIAA/NASA 9th Aeroacoustics Conference, Williamsburg, Virginia, October 15-17, 1984.

Amiet, R. K., "Airfoil Gust Response and the Sound Produced by Airfoil-Vortex Interaction," Journal of Sound and Vibration, Vol. 107, No. 3, 1986a, pp. 487-506.

Amiet, R. K., Simonich, J. C., and Schlinker, R. H., "Rotor Noise Due to Atmospheric Turbulence Ingestion, Part II - Aeroacoustic Results," AIAA-86-1903, AIAA 10th Aeroacoustic Conference, Seattle, Washington, July 1986b.

Aravamudan, K. S., Lee, A., and Harris, W. L., "An Experimental Study of High Frequency Noise from Model Rotors: Prediction and Reduction," Vertica, Vol. 3, No. 1, 1979a, pp. 47-63.

Aravamudan, K. J., and Harris, W. L., "Low Frequency Broadband Noise Generated by a Model Rotor," Journal of the Acoustical Society of America, Vol. 66, No. 2, 1979b, pp. 522-533.

Balcerak, J. C., "Parametric Study of the Noise Produced by the Interaction of the Main Rotor Wake and Tail Rotor," NASA CR-145001, 1976.

Barlow, W. H., McCluskey, W. J., and Ferris, H. W., "OH-6A Phase II Quiet Helicopter Program," U.S. Army, USAAMRDL TR-72-29, 1972.

Bartlett, G. E., and Vidal, R. J., "Experimental Investigation of Influence of Edge Shape on the Aerodynamic Characteristics of Low Aspect Ratio Wings at Low Speeds," Journal of Aeronautical Sciences, Vol. 22, 1955, pp. 517-533.

Bergland, G. D., and Dolan, M. T., "Fast Fourier Transform Algorithms," in Programs for Digital Signal Processing, IEEE, 1979.

Bies, D. A., "A Review of Flight and Wind Tunnel Measurements of Boundary Layer Pressure Fluctuations and Induced Structure Response," NASA CR-626, October 1966.

Biggers, J. C., and Orloff, K. L., "Laser Velocimeter Measurements of the Helicopter Rotor-Induced Flow Field," Journal of the American Helicopter Society, Vol. 20, No. 1, 1975, pp. 2-10.

Bossanyi, E. A., "Windmill Wake Turbulence Decay: A Preliminary Theoretical Model," SERI TR-635-1280, February 1983.

Brooks, T. F., and Hodgson, T. H., "Prediction and Comparison of Trailing Edge Noise Using Measured Surface Pressures," AIAA-80-0977, AIAA 6th Aeroacoustics Conference, Hartford, Connecticut, June 1980; also Journal of Sound and Vibration, Vol. 78, No. 1, 1981, pp. 69-117.

Brooks, T. F., "Trailing Edge Noise Prediction Using Amiet's Method," Journal of Sound and Vibration, Vol. 77, No. 3, 1981, pp. 437-439.

Brooks, T. F., Marcolini, M. A., and Pope, D. S., "Airfoil Trailing Edge Flow Measurements and Comparisons to Theory, Incorporating Open Wind Tunnel Corrections", AIAA-84-2266, AIAA/NASA 9th Aeroacoustics Conference, Williamsburg, Virginia, October 1984a.

Brooks, T. F., and Marcolini, M. A., "Airfoil Tip Vortex Formation Noise", AIAA-84-2308, AIAA/NASA 9th Aeroacoustics Conference, Williamsburg, Virginia, October 1984b.

Carrier, G. F., and Pearson, C. E., Partial Differential Equations, Academic Press, New York, 1976.

Chigier, N. A., and Corsiglia, V. R., "Tip Vortices - Velocity Distributions," NASA TM X-62087, 1971; also Preprint #522, 27th Annual National V/STOL Forum of the American Helicopter Society, May 1971.

Chou, S.-T., and George, A. R., "Effect of Angle of Attack on Rotor Trailing Edge Noise," Cornell University Fluid Dynamics and Aerodynamics Program Report FDA-83-03, 1983; also AIAA Journal, Vol. 22, No. 12, 1984, pp. 1921-1823.

Chou, S.-T., and George, A. R., "Effect of Blunt Trailing Edges on Rotor Broadband Noise," Cornell University Fluid Dynamics and Aerodynamics Program Report FDA-85-01, 1985; also AIAA Journal, Vol. 24, No. 8, 1986, 1380-1382.

Chou, S.-T., and George, A. R., "Progress in Helicopter Tail Rotor Noise Analysis," 42nd Annual Forum of the American Helicopter Society, Washington, D. C., June 1986; also AIAA-86-1900, AIAA 10th Aeroacoustic Conference, Seattle, Washington, July 1986.

Clark, D. R., and Maskew, B., "Study for Prediction of Rotor/Wake/Fuselage Interference, Part I: Technical Report," NASA CR-177340, 1985.

Corcos, G. M., "The Structure of the Turbulent Pressure Field in Boundary-Layer Flows," Journal of Fluid Mechanics, Vol. 18, 1964, pp. 353-378.

Cox, C. R., and Lynn, R. R., "A Study of the Origin and Means of Reducing Helicopter Noise," TCREC TR-62-73, U. S. Army Transportation Research Command, Fort Eustis, Virginia, 1962.

Curle, N., "The Influence of Solid Boundaries upon Aerodynamic Sound," Proceedings of the Royal Society of London, Series A, Vol. 231, 1955, pp. 505-514.

Deming, A. F., "Noise from Propellers with Symmetrical Sections of Zero Blade Angle, Part II," NACA TN-679, 1938.

Dommasch, D. O., Sherby, S. S., and Connolly, T. F., Airplane Aerodynamics, 4th Edition, Pitman Publishing, New York, 1967, Chapter 7.

Etkin, B., "Theory of the Flight of Airplanes in Isotropic Turbulence: Review and Extension," AGARD Report 372, 1961; also University of Toronto, Institute of Aerophysics Report No. 72, 1961.

Farassat, F., "Theory of Noise Generation from Moving Bodies with an Application to Helicopter Rotors," NASA TR R-541, 1975.

Farassat, F., and Succi, G. P., "A Review of Propeller Discrete Frequency Noise Prediction Technology with Emphasis on Two Current Methods for Time Domain Calculations," Journal of Sound and Vibration, Vol. 31, No. 3, 1980, pp. 399-419.

Farassat, F., and Succi, G. P., "The Prediction of Helicopter Rotor Discrete Frequency Noise," Vertica, Vol. 7, No. 4, 1983, pp. 309-320.

Farassat, F., "Prediction of Advanced Propeller Noise in the Time Domain," AIAA-84-2303, AIAA/NASA 9th Aeroacoustics Conference, Williamsburg, Virginia, October 15-17, 1984; also AIAA Journal, Vol. 24, No. 4, 1986, pp. 578-584.

Ffowcs Williams, J. E., and Hawkings, D. L., "Sound Generated by Turbulence and Surfaces in Arbitrary Motion," Philosophical Transactions of the Royal Society of London, Series A, Vol. 264, No. 1151, 1969a, pp. 321-342.

Ffowcs Williams, J. E., and Hawkings, D. L.: "Theory Relating to the Noise of Rotating Machinery," Journal of Sound and Vibration, Vol. 10, No. 1, 1969b, pp. 10-21.

Fink, M. R., "Minimum On-Axis Noise for a Propeller or Helicopter Rotor," Journal of Aircraft, Vol. 15, No. 10, 1978, pp. 700-702.

Fink, M. R., and Bailey, D. A., "Airframe Noise Reduction Studies and Clean Airframe Noise Investigation," NASA CR-159311, April 1980.

Fricke, F. R., and Stevenson, D. C., "Pressure Fluctuations in a Separated Flow Region," Journal of the Acoustical Society of America, Vol. 44, 1968, pp. 1198-1201.

Fricke, F. R., "Pressure Fluctuations in Separated Flows," Journal of Sound and Vibration, Vol. 17, 1971, pp. 113-123.

George, A. R., and Kim, Y. N., "High Frequency Broadband Rotor Noise," AIAA-76-561, AIAA 3rd Aeroacoustics Conference, Palo Alto, California, July 1976; also AIAA Journal, Vol. 15, No. 4, 1977, pp. 538-545.

George, A. R., "Helicopter Noise: State-of-the-Art," Journal of Aircraft, Vol. 15, No. 11, 1978, pp. 707-715.

George, A. R., Najjar, F. E., and Kim, Y. N., "Noise Due to Tip Vortex Formation on Lifting Rotors," AIAA-80-1010, AIAA 6th Aeroacoustic Conference, Hartford, Connecticut, June 1980.

George, A. R., and Chou, S.-T., "Comparison of Broadband Noise Mechanisms, Analyses, and Experiments on Helicopter Rotors, Propellers, and Wind Turbines," AIAA-83-0690, AIAA 8th Aeroacoustic Conference, Atlanta, Georgia, April 11-13, 1983a; also Journal of Aircraft, Vol. 21, No. 8, 1984, pp. 583-592.

George, A. R., Najjar, F. E., and Kim, Y. N., "Noise Due to Tip Vortex Formation on Lifting Rotors," Cornell University Fluid Dynamics and Aerodynamics Program Report FDA-83-02, April 1983b.

George, A. R., and Chang, S.-B., "Noise Due to Transonic Blade-Vortex Interactions," 39th Annual Forum of American Helicopter Society, St. Louis, Missouri, May 9-11, 1983c.

George, A. R., and Chou, S.-T., "Broadband Rotor Noise Analyses," NASA CR-3797, April 1984a.

George, A. R., and Chang, S.-B., "Flow Field and Acoustics of Two-Dimensional Transonic Blade-Vortex Interactions," AIAA-84-2309, AIAA/NASA 9th Aeroacoustics Conference, Williamsburg, Virginia, October 1984b.

George, A. R., and Chou, S.-T., "A Comparative Study of Tail Rotor Noise Mechanisms," 41st Annual Forum of the American Helicopter Society, Fort Worth, Texas, May 1985a; also Journal of the American Helicopter Society, Vol. 31, No. 4, 1986, pp. 36-42.

George, A. R., and Chou, S.-T., "Broadband Noise of Propellers and Rotors," Proceedings NOISE-CON 85 , Ohio State University, June 1985b.

George, A. R., and Lyrintzis, A. S., "Mid- and Far-Field Calculations of Blade-Vortex Interactions," AIAA-86-1954, AIAA 10th Aeroacoustic Conference, Seattle, Washington, July 1986.

Glegg, S. A. L., "Broadband Propeller Noise Prediction in the Plane of the Rotor," AIAA-86-1964, AIAA 10 th Aeroacoustic Conference, Seattle, Washington, July 1986. Graham, J. M. R., "Similarity Rules for Thin Aerofoils in Non-Stationary Subsonic Flows," Journal of Fluid Mechanics, Vol. 43, No. 4, 1970, pp. 753-766.

Gray, R. B., McMahon, H. M., Shenoy, K. R., and Hammer, M. L., "Surface Pressure Measurements at Two Tips of a Model Helicopter Rotor in Hover," NASA CR-3281, May 1980.

Gutin, L., "On the Sound Field of a Rotating Propeller," Physikalische Zeitschrift der Sowjetunion, Band 9, Heft 1, 1936, pp. 57-71 (in German); English translation, NACA TN-1195, 1948.

Hanson, D. B., and Fink, M. R., "The Importance of Quadrupole Sources in Prediction of Transonic Tip Speed Propeller Noise," Journal of Sound and Vibration, Vol. 62, No. 1, 1979, pp. 19-38.

Hawkings, D. L., "Theoretical Models of Helicopter Rotor Noise," in Helicopter Acoustics, NASA CP-2052, May 1978, pp. 89-108.

Hayden, R. E., "Noise from Interaction of Flow with Rigid Surfaces: A Review of Current Status of Prediction Techniques," NASA CR-2126, 1972.

Heyson, H. H., "Nomographic Solution of the Momentum Equation for VTOL-STOL Aircraft," NASA TN-D-814, 1961.

Homicz, G. F., and George, A. R., "Broadband and Discrete Frequency Radiation from Subsonic Rotors," Journal of Sound and Vibration, Vol. 36, No. 2, 1974, pp. 151-177.

Houbolt, J. C., "Atmospheric Turbulence," AIAA Journal, Vol. 11, No.4, 1973, pp. 421-437.

Howe, M. S., "A Review of the Theory of Trailing Edge Noise," Journal of Sound and Vibration, Vol. 61, 1978, pp. 437-465.

Hubbard, H. H., "Propeller-Noise Charts for Transport Airplanes," NACA TN-2968, 1953.

Hubbard, H. H., Shepherd, K. P., and Grosveld, F. W., "Sound Measurements of the MOD-2 Wind Turbine Generator," NASA CR-165752, July 1981.

Huber, H., and Polz, G., "Studies on Blade-to-Blade and Rotor-Fuselage-Tail Interferences," in Prediction of Aerodynamics of Rotorcraft, NATO AGARD Conference Proceedings CP-334, London, May 1982.

Humbad, N. G., and Harris, W. L., "Effects of Tip Geometry on Model Helicopter Rotor Low Frequency Broadband Noise," MIT FDRL Report 81-2, May 1981.

Huston, R. J., and Morris, C. E. K., Jr., "A Note on a Phenomenon Affecting Helicopter Directional Control in Rearward Flight," Journal of the American Helicopter Society, Vol. 15, No. 4, 1970, pp. 38-45.

Johnson, W., "A Comprehensive Analytical Model of Rotorcraft Aerodynamics and Dynamics, Part I, II, and III," NASA TM-81182, 81183, and 81184, 1980.

Johnson, W., "Development of a Comprehensive Analysis for Rotorcraft - I. Rotor Model and Wake Analysis," Vertica, Vol. 5, 1981, pp. 99-129.

Kaji, S., "Noncompact Source Effect on the Prediction of Tone Noise from a Fan Rotor," AIAA-75-446, March 1975.

Karman, Th. Von, and Sears, W. R., "Airfoil Theory for Non-Uniform Motion," Journal of Aeronautical Sciences, Vol. 5, No. 10, 1938, pp. 379-390.

Kendall, J. M., "Measurements of Noise Produced by Flow Past Lifting Surfaces," AIAA-78-239, 1978.

Kim, Y. N., and George, A. R., "Trailing Edge Noise from Hovering Rotors," Preprint 80-60, American Helicopter Society 36th Annual Forum, May 1980; also AIAA Journal, Vol. 20, No. 9, 1982, pp. 1167-1174.

Lamb, H., Hydrodynamics, 6th Edition, Cambridge University Press, England, 1932, p. 165.

Lehman, A. F., "Model Studies of Helicopter Tail Rotor Flow Patterns in and out of Ground Effect," USAAVLABS TR-71-12, April 1971.

Leverton, J. W., "The Noise Characteristics of a Large 'Clean' Rotor," Journal of Sound and Vibration, Vol. 27, No. 3, 1973, pp. 357-376.

Leverton, J. W., Pollard, J. S., and Wills, C. R., "Main Rotor Wake/Tail Rotor Interaction," Vertica, Vol. 1, 1977, pp. 213-224.

Leverton, J. W., "Reduction of Helicopter Noise by Use of a Quiet Tail Rotor," Paper #24, 6th European Rotorcraft and Powered Lift Aircraft Forum, September 16-19, 1980.

Levine, L. S., "An Analytic Investigation of Techniques to Reduce Tail Rotor Noise," NASA CR-145014, July 1976.

Lighthill, M. J., "On Sound Generated Aerodynamically I. General Theory," Proceedings of the Royal Society of London, Series A, Vol. 211, No. 564, 1952, pp. 564-587.

Lighthill, M. J., "On Sound Generated Aerodynamically II. Turbulence as a Source of Sound," Proceedings of the Royal Society of London, Series A, Vol. 222, No. 1148, 1954, pp. 1-32.

Lighthill, M. J., "The Bakerian Lecture, 1961. Sound Generated Aerodynamically," Proceedings of the Royal Society of London, Series A, Vol. 267, No. 1329, 1962, pp. 147-182.

Lowson, M. V., "The Sound Field for Singularities in Motion," Proceedings of the Royal Society of London, Series A, Vol. 286, 1965, pp. 559-572.

Lowson, M. V., and Ollerhead, J. B., "A Theoretical Study of Helicopter Noise," Journal of Sound and Vibration, Vol. 9, 1969, pp. 197-222.

Lowson, M. V., Whatmore, A., and Whitfield, C. E., "Source Mechanisms for Rotor Noise Radiation," Loughborough University of Technology, Department of Transport Technology, Report TT-7202, February 1972.

Lumley, J. L., and Panofsky, H. A., The Structure of Atmospheric Turbulence, Wiley, New York, 1964, pp. 135-137 and 167-175.

Lynn, R. R., Robinson, F. D., Batram N. N., and Duhon, J. M., "Tail Rotor Design, Part I: Aerodynamics," Journal of the American Helicopter Society, Vol. 15, No. 4, 1970, pp. 2-15.

Mabey, D. G., "Analysis and Correlation of Data on Pressure Fluctuations in Separated Flow," Journal of Aircraft, Vol. 9, 1972, pp. 642-645.

McCroskey, W. J., Yu, Y. H., and Smetana, F. O., Proceedings, Workshop on Blade-Vortex Interactions, NASA Ames Research Center, October, 1984.

Morse, P. M., Vibration and Sound, McGraw-Hill, New York, 1948.

Owen, P. R., "The Decay of a Turbulent Trailing Vortex," Aeronautical Quarterly, Vol. 21, 1970.

Paterson, R. W., Vogt, P. G., Fink, M. R., and Munch, C. L., "Vortex Noise of Isolated Airfoils," Journal of Aircraft, Vol. 10, 1973, pp. 296-302.

Paterson, R. W., Amiet, R. K., and Munch, C. L., "Isolated Airfoil Tip Vortex Interaction Noise," Journal of Aircraft, Vol. 12, No. 1, 1975, pp. 34-40.

Paterson, R. W., and Amiet, R. K., "Noise and Surface Pressure Response of an Airfoil to Incident Turbulence," Journal of Aircraft, Vol. 14, No. 8, 1977, pp. 729-736.

Paterson, R. W., and Amiet, R. K., "Noise of a Model Helicopter Rotor Due to Ingestion of Turbulence," NASA CR-3213, 1979.

Peckham, D. H., "Low-Speed Wind-Tunnel Tests on a Series of Uncambered Slender Pointed Wings with Sharp Edges," Great Britain A.R.C. Technical Report, R&M No. 3186, London, 1961.

Pegg, R. J., and Shidler, P. A., "Exploratory Wind Tunnel Investigation of the Effect of the Main Rotor Wake on Tail Rotor Noise," International Specialist Symposium on Helicopter Acoustics, NASA Langley Research Center, Hampton, Virginia, May 1978.

Pegg, R. J., "A Summary and Evaluation of Semi-Empirical Methods for the Prediction of Helicopter Rotor Noise," NASA TM-80200, December 1979.

Polz, G., and Quentin, J., "Separated Flow Around Helicopter Bodies," Paper # 48, 7th European Rotorcraft and Powered Lift Aircraft Forum, September 1981.

Powell, A. O., "On the Aerodynamic Noise of a Rigid Flat Plate Moving at Zero Incidence," Journal of the Acoustical Society of America, Vol. 31, December 1959, pp. 1649-1653.

Rayleigh, Lord, The Theory of Sound, 2nd Edition, MacMillan, London, 1896.

Revell, J. D., "Induced Drag Effect on Airframe Noise," in Progress in Astronautics and Aeronautics, Vol. 45, Aeroacoustics, I. R. Schwartz (ed.), MIT Press, 1976, pp. 221-235; also AIAA Paper 75-487, 1975.

Richards, E. J., and Fahy, F. J., "Turbulent Boundary Layer Pressure Fluctuations over Two-Dimensional Surfaces and Narrow Delta Wings," Acoustic Fatigue in Aerospace Structures, Syracuse University Press, Syracuse, 1965, pp. 39-62.

Schmitz, F. H., and Yu, Y. H., "Helicopter Impulsive Noise: Theoretical and Experimental Status," presented at International Symposium on Recent Advances in Aerodynamics and Aeroacoustics, Stanford University, August 1983.

Schlichting, H., Boundary Layer Theory, 7th Edition, McGraw Hill, New York, 1979, Chapter 24.

Schlinker, R. H., and Amiet, R. K., "Helicopter Rotor Trailing Edge Noise," AIAA-81-2001, October 1981; also NASA CR-3470.

Schlinker, R. H., and Brooks, T. F., "Progress in Rotor broadband Noise Research," Preprint # A-82-38-51D, 38th Annual Forum of the American Helicopter Society, Anaheim, California, May 4-7, 1982.

Schlinker, R. H., and Amiet, R. K., "Rotor-Vortex Interaction Noise," NASA CR-3744, October 1983.

Scully, M. P., "Computation of Helicopter Rotor Wake Geometry and its Influence on Rotor Harmonic Airloads," M.I.T. ASRL Report TR-178-1, March 1975.

Sharland, I. J., "Sources of Noise in Axial Flow Fans," Journal of Sound and Vibration, Vol. 1, No. 2, 1964, pp. 302-322.

Sheridan, P. F., and Smith, R. P., "Interactional Aerodynamics: A New Challenge to Helicopter Technology," 35th Annual Forum of the American Helicopter Society, 1979.

Sheridan, P. F., Hanker, E. J. Jr., and Bruce, B. B., "Investigation of Operational and Design Factors Resulting from Main Rotor and Tail Rotor Interactions," USAAVRADCOM TR-82-D-40, U.S. Army Research and Technology Laboratories, January 1984.

Shockey, G. A., Williamson, J. W. and Cox, C. R., "Helicopter Aerodynamics and Structure Loads Survey," 32nd Annual National V/STOL Forum of the American Helicopter Society, Washington, D. C., May 1976.

Simonich, J. C., Amiet, R. K., Schlinker, R. H., and Greitzer, E. M., "Helicopter Rotor Noise Due to Ingestion of Atmospheric Turbulence," NASA CR-3973, May 1986a.

Simonich, J. C., Amiet, R. K., Schlinker, R. H., and Greitzer, E. M., "Rotor Noise Due to Atmospheric Turbulence Ingestion, Part I - Fluid Mechanics," AIAA-86-1857, AIAA 10 th Aeroacoustics Conference, Seattle, Washington, July 1986b.

Srinivasan, G. R., McCroskey, W. J., and Kutler, P., "Numerical Simulation of the Interaction of a Vortex with a Stationary Airfoil in Transonic Flow," AIAA-84-0254, AIAA 22nd Aerospace Sciences Meeting, Reno, Nevada, January 1984.

Tangler, J. A., "Experimental Investigation of the Subwing Tip and its Vortex Structure," NASA CR-3058, November 1978.

Tennekes, H., and Lumley, J. L., A First Course in Turbulence, MIT Press, Cambridge, Massachusetts, 1972.

Townsend, A. A., The Structure of Turbulent Shear Flow, 2nd Edition, Cambridge, London, 1976, Chapter 6.

White, R. P., Jr., "The Status of Rotor Noise Technology - One Man's Opinion," in Helicopter Acoustics, NASA CP-2052, May 1978, pp. 723-780.

Widnall, S. E., "A Correlation of Vortex Noise Data from Helicopter Main Rotors," Journal of Aircraft, Vol. 5, No. 3, 1969, pp. 279-281.

Widnall, S. E., "Helicopter Noise Due to Blade-Vortex Interaction," Journal of the Acoustical Society of America, Vol. 50, No. 1, 1971, pp. 354-365.

Widnall, S. E.,and Wolf, T. L., "Effect of Tip Vortex Structure on Helicopter Noise Due to Blade-Vortex Interaction," Journal of Aircraft, Vol. 17, No. 10, 1980, pp. 705-711.

Wiesner, W.,and Kohler, G., "Tail Rotor Performance in Presence of Main Rotor, Ground, and Winds," Journal of the American Helicopter Society, Vol. 19, No. 3, 1974, pp. 2-9.

Wright, S. E., "Sound Radiation from a Lifting Rotor Generated by Asymmetric Disk Loading," Journal of Sound and Vibration, Vol. 9, No. 2, 1969, pp. 223-240.

Yu, J. C., and Joshi, M. C., "On Sound Radiation from the Trailing Edge of an Isolated Airfoil in an Uniform Flow," AIAA-79-0603, March, 1979.

Yu, Y. H., and Schmitz, F. H., "High-Speed Rotor Noise and Transonic Aerodynamics," AIAA-80-1009, AIAA 6th Aeroacoustic Conference, Hartford, Connecticut June 1980.

NASA
National Aeronautics and Space Administration

Report Documentation Page

1. Report No. NASA CR-177565	2. Government Accession No.	3. Recipient's Catalog No.

4. Title and Subtitle A Study of Rotor Broadband Noise Mechanisms and Helicopter Tail Rotor Noise	5. Report Date August 1990
	6. Performing Organization Code
7. Author(s) Shau-Tak Rudy Chou	8. Performing Organization Report No. A-90269
	10. Work Unit No. 505-61-51
9. Performing Organization Name and Address Sibley School of Mechanical and Aerospace Engineering Cornell University Ithaca, NY 14853-7501	11. Contract or Grant No. NAG2-379
12. Sponsoring Agency Name and Address National Aeronautics and Space Administration Washington, DC 20546-0001	13. Type of Report and Period Covered Contractor Report
	14. Sponsoring Agency Code

15. Supplementary Notes

Point of Contact: Marianne Mosher, Ames Research Center, MS T042
Moffett Field, CA 94035-1000
(415) 604-4560 or FTS 464-4560

16. Abstract

The rotor broadband noise mechanisms considered in the present study are (1) lift fluctuation due to turbulence ingestion, (2) boundary layer/trailing edge interaction, (3) tip vortex formation, and (4) turbulent vortex shedding from blunt trailing edge. Predictions show good agreement with available experimental data. The study shows that inflow turbulence is the most important broadband noise source for typical helicopters' main rotors at low- and mid-frequencies.

Due to the size difference, isolated helicopter tail rotor broadband noise is not important compared to the much louder main rotor broadband noise. However, the inflow turbulence noise from a tail rotor can be very significant because it is operating in a highly turbulent environment, ingesting wakes from upstream components of the helicopter. Our study indicates that the main rotor turbulent wake is the most important source of tail rotor broadband noise. The harmonic noise due to the main rotor mean wake is found to be very important. Finally, the tail rotor harmonic noise due to ingestion of main rotor tip vortices is studied.

17. Key Words (Suggested by Author(s)) Aerodynamic noise, Helicopter tail rotor, Broadband noise, Helicopters, Aircraft noise	18. Distribution Statement Unclassified–Unlimited Subject Category–71

19. Security Classif. (of this report) Unclassified	20. Security Classif. (of this page) Unclassified	21. No. of Pages 188	22. Price A09

NASA FORM 1626 OCT 86

For sale by the National Technical Information Service, Springfield, Virginia 22161